

Appearance of polished 18 karat gold surfaces: linking aesthetics to surface features

Thèse N° 7123

Présentée le 24 mai 2019

à la Faculté des sciences et techniques de l'ingénieur
Groupe SCI STI SM
Programme doctoral en science et génie des matériaux

pour l'obtention du grade de Docteur ès Sciences

par

Leili BATOOLI

Acceptée sur proposition du jury

Prof. D. Damjanovic, président du jury
Dr. S. Mischler, directeur de thèse
Dr J. Perret, rapporteur
Dr P. Blattner, rapporteur
Dr P. Schmutz, rapporteur

2019

To Ashraf and Ziaeddine for loving me to
life every single day of my existence;

To Paul, my dream come true;

And to Borna and Kyan, my most favorite
little humans.

“It might seem that nothing could be easier than to be conscious of one’s own sensation; and yet experience shows that for the discovery of subjective sensations some special talent is needed.”

Hermann Helmholtz 1821-1894

Acknowledgments

My first and foremost gratitude goes to my thesis director Dr. Stefano Mischler who provided me with the opportunity of perusing my PhD thesis in the Laboratory of Tribology and Interfacial Chemistry (TIC) at EPFL. Through the course of numerous scientific discussions, I have largely benefited from your extensive knowledge and insightful comments. Your guidance stands strong on pillars of trust, mutual respect, delegation of responsibility, availability and abundance of humor. Thank you for your supervision.

I would like to acknowledge Dr. Dragan Damjanovic, Dr. Patrik Schmutz, Dr. Julien Perret and Dr. Peter Blattner for accepting to be the jury members of this thesis. The discussions and the feedbacks were an important complement to the present document. I am particularly thankful to Dragan Damjanovic for having been a consistent point of reference and guidance throughout my entire studies at EPFL. You are the true definition of a teacher.

I am genuinely grateful to Patek Philippe for financial and technical support of the project. The current work would not have been made possible without the guidance and fruitful interactions with Dr. Julien Perret, Mr. Frédéric Maier, Mr. Alexandre Vandini and Mr. Pascal Cavicchiolo. It has been an honor and an absolute pleasure to conduct my PhD thesis in close collaboration with a company of such level of prestige and excellence. I have been profoundly inspired by the spirit of excellence and tradition in Patek Philippe.

My gratitude goes to the administrative team of materials department and doctoral school of EPFL or, as I would like to call them, the wonder women. Thank you Homeira, Danièle, Anne, Chrystelle, Sylvie and Sandra for amazing job. You are great.

I would like to thank all my old and new colleagues: Nicolas for all the charm he brings as he walks through the door, Shoufan for teaching me many cultural lessons, Alba for her kindness, Javier for how patient and attentive he is, Yue yue for always offering a helping hand, Fabio for our fashion, food and news exchanges, Vance for English lessons and finally Sandra for introducing me to the world of tribology. It has been a pleasure to work in your company. Additionally, I would like to acknowledge the great work of the students who helped me during this PhD work: Chloe, Minchuan, Jingwen and Mathilde.

My most sincere gratitude goes to our guest professors Anna and Alex for their valuable scientific input during numerous spontaneous discussions. You have taught me a lot about being a curious scientist, an inspirational team member and an exceptional human being. I am amazed by you and I deeply respect both of you. I am particularly grateful for your constant encouragements during my PhD studies and for the pleasure of getting to know the incredible Lara and Pau.

I heartfully thank the TIC girls Angela and Valentine, my outstanding friends and colleagues. You have made invaluable contributions to my academic and personal growth. Angela, you are among the strongest and most determined women I have ever met and yet, you have such a beautiful tenderness in your heart. Thank you for your consistent support through my PhD life. Valentine, you are talented, funny and kind-hearted. Your friendship, our never ending chit-chats and complaints, the lunches, the stories and laughters have been a precious sources of *bonne humeur* and courage for me particularly in the last year of the thesis. Thank you.

I would like to thank my first supervisor at EPFL. Mathieu Anthony, a PhD student at the time who played a significant role in introducing me to the Swiss academic world.

I would like to acknowledge some of the amazing friends that have made my academic journey in Switzerland more joyous: Elena, Zahra, Behnoush, Farhang, Lucie, Farnaz, Reza, Maryam, Masoumeh, Mina, Schahrazede, Eric and Moshe. Specially, I would like to express my gratitude to Sogol and Elahe. Thank you Sogol for having been the loving, supportive and simply wonderful best friend that you have been for the past two decades. A great share of my young ages is built around your sincere friendship. Elahe, I consider myself very lucky that you took me in as a friend in a time when I most needed one. You are honest, kind and wise; qualities that don't often gather in one person but ones that make you an amazing person and an incredible friend.

My deepest gratitude goes to Sheida. You are an extraordinary human being in every possible way. Over the years you have brought your outstanding support and encouragement, your moving sympathy and your selfless generosity to my life. Even though I always wonder if I deserve all the kindness you have in you, I consider you to be my true soulmate. Thank you for everything.

To my favorite noodles: they say it is hard to break the ice with the Swiss. The way I see it, you guys are gold hidden in the heart of a mountain. It takes a lot of digging to get to you but if one ever does get there, it is very much worth it. It is such a delight to have you as friends. Merci Tristan, Jeremy, (Norah), Valerie, Amalric, Simon, Minyeong.

My most sincere appreciation goes to Fabienne, Daniel and Maude. The people to whom I am not related by blood but only by love. I consider myself extremely lucky

to be a part of your family. You bring hope, joy and inspiration to my life. Your love and support in the past four years has been essential to this achievement. I would also like to warmly thank Pierette and William. I am deeply grateful to get to live the joy of having grandparents again.

This achievement also owes a lot to the wonderful people who have deeply inspired me in life: Hasan, Katayoun, Fakhri, Shapour, Nader, Jale and Aziz joon. I love you all.

My affectionate gratitude goes to my beloved family Maziar, Babak, Leila, Borna and Kyan. You are and will forever be an irreplaceable part of my identity. You are my roots and my future. Thank you for always being here for me. I widely rely on your love and support in all of the biggest steps of my life.

Thank you Paul simply for being who you are. Your passion, courage, humor and kindness light up my world. Your support has encouraged me through every single step of this long journey and your attentive presence highlights all the best and the hardest days of this PhD life. Thank you for never giving up on me. You are the best thing I have ever found in life.

And last but most importantly, I would like to express my eternal gratitude to my dearly loved parents Ashraf and Ziaeddine. You are my true heroes, my best friends, the bravest people that I know and my most solid supporters. Your love has shaped my heart and made me the person I am. I can't even begin to thank you for all you have done. Everything I am or will ever be, I owe it to you. I love you.

Abstract

Impeccable appearance of surfaces is a key constraint in high-end jewelry and watch manufacturing. Based on long tradition in the industry, appearance of products is assessed by trained individuals through visual inspection in designated intervals on the production line. Despite the high efficiency of the visual quality control in detecting aesthetic defects, it suffers from a major shortcoming. In many cases when the expert declares the appearance of an artifact to be unsatisfactory, she/he is unable to specify the surface defect that has caused the aesthetic imperfection. In other words, the visual control cannot provide a correlation between actual properties of the surfaces and the responsible manufacturing process to their aesthetic consequences. Addressing this industrial problem requires developing a methodology for assessing aesthetic defects on the polished surfaces based on an understanding of the surface phenomena.

This research work builds its approach towards the study of aesthetics of surfaces around an existing framework that proposes four parameters of color, gloss, translucency and texture as measurable surface properties, which can be linked to appearance. The current study allowed implementation of this general framework to the case study of polished gold surfaces by developing necessary application-related definitions and measurement techniques. Measurement techniques that were employed here granted the possibility for quantitative assessment of surface and near surface properties of ternary gold-silver-copper alloys in terms of topography, chemical composition, microstructure, mechanical properties and optical properties.

Based on findings of those measurements, two leading surface properties that could cause a defect in aesthetic appearance of polished gold surfaces were recognized to be roughness and chemical composition. Quantitative correlations could be drawn for 18 karat gold alloy between the magnitude of two well defined physical and chemical properties of the surface (surface roughness and near surface chemical composition) with color characteristics of the surface (through CIELAB L^* , a^* and b^* values) and reflection properties (through calculation of total integrated scattered light).

Finally, this work highlighted the significance of roughness evaluation at different length scales and also the importance of considering the chemical composition at the surface and near the surface. It was also shown that both of these parameters are modified during the common fabrication process of a watch or jewelry piece.

Keywords

18 karat gold alloys, Aesthetics of surfaces, Assessing appearance, Surface roughness, Surface composition, Polishing.

Résumé

L'esthétique des surfaces représente, dans le monde de la bijouterie et de l'horlogerie de luxe, l'un des principaux défis de fabrication. Basée sur une longue tradition et issue d'un savoir-faire acquis au fil des ans, la qualité des surfaces est vérifiée visuellement tout au long des lignes de production. Si cette méthode a fait ses preuves, celle-ci souffre cependant d'une limitation importante. En effet, dans la plupart des cas où un expert détecte un défaut esthétique, celui-ci ne peut pas spécifier quel défaut de surface l'engendre. Autrement dit, la méthode de contrôle visuel utilisée est incapable de lier les défauts esthétiques détectés aux propriétés de surface. Aborder un tel problème industriel requiert le développement d'une méthodologie qui évalue le lien entre les défauts esthétiques d'une surface polie et ses propriétés de surface, en se basant sur la compréhension des phénomènes physiques qui l'entourent.

Le travail de recherche présenté construit son approche sur la base des connaissances actuelles, en proposant quatre paramètres de mesures pour les propriétés de surface : la couleur, la brillance, la translucidité et la texture. Ces paramètres permettent de lier les propriétés de surface à son apparence. L'étude proposée permet l'utilisation de ces standards sur le cas d'étude d'une surface d'or polie grâce aux différentes techniques de mesures utilisées et aux définitions proposées. Les techniques de mesures employées permettent l'extraction des propriétés de surface pour des alliages ternaires d'argent, d'or et de cuivre. Ces mesures concernent les propriétés topographiques, mécaniques, optiques, de microstructure et de composition chimique.

En se basant sur l'ensemble des données collectées, deux propriétés de surfaces sont apparues comme des caractéristiques principales des défauts esthétiques dans notre cas d'application, à savoir la composition chimique et la rugosité. Une corrélation a pu être établie, dans le cas précis de l'or 18 carats, entre les deux propriétés physiques de surface définies (rugosité et composition chimique) et celle optique de couleur (CIELAB L^* , a^* et b^*) et de réflexion (intégrale de dispersion de lumière).

Finalement, ce travail met en évidence l'importance de la rugosité à différentes échelles et celle de la composition chimique de surface et en profondeur. L'étude a également permis de démontrer que ces deux paramètres changent tout au long des différentes étapes de fabrication des pièces de bijouterie ou d'horlogerie.

Mots-clés

Or 18 karat, Esthétique des surfaces, Mesure de l'apparence, Rugosité de surface, Composition de surface, Plissage.

Contents

Acknowledgments	i
Abstract	v
Résumé	vii
List of figures	x
List of tables	xvii
1 Introduction	1
1.1 Motivation	1
1.2 Thesis aim and structure	2
2 Assessing appearance: general background and state of the art	5
2.1 Introduction	6
2.2 Visual perception of surfaces	6
2.3 Appearance	7
2.4 NPL approach to assessing appearance of surfaces	9
2.4.1 Color	11
2.4.2 Gloss	15
2.4.3 Translucency	17
2.4.4 Texture	18
2.5 Effects of surface finish on appearance	19
2.5.1 Theoretical approach: light scattering from surfaces	19
2.5.2 Experimental links between surface finish and appearance	22
2.6 Summary and conclusions	25
3 Characterization of watch components	27
3.1 Introduction	28
3.2 Material	28
3.3 Methods	29
3.3.1 Topography and surface roughness	29
3.3.2 Chemical composition	32
3.3.3 Microstructure	34
3.3.4 Microhardness measurement	35
3.3.5 Reflectance and color measurements	35
3.4 Results	36

3.4.1	Surface topography and roughness	37
3.4.2	Chemical composition	43
3.4.3	Hardness measurement	53
3.4.4	Reflectance and color measurements	54
3.5	Summary and conclusions	57
4	Surface defects and their correlation to appearance	59
4.1	Introduction	60
4.2	Model samples: material, surface preparation and characteristics	60
4.2.1	Material	60
4.2.2	Surface preparation	61
4.3	Effect of surface roughness on aesthetic aspects of 4N gold alloy	62
4.4	Effect of polishing on chemical composition of the surface	68
4.5	Reflectance and color measurements	77
4.6	Quantitative correlation of reflectance and color to surface features . .	79
4.7	Summary and conclusions	84
5	Origin of defects	87
5.1	Introduction	88
5.2	Inhomogeneity in hardness and microstructure	88
5.3	Modified surface composition	93
5.3.1	Tribocorrosion: a side effect of polishing	93
5.3.2	Electrochemical copper dissolution	94
5.4	Surface porosity	101
5.5	Summary and conclusions	104
6	Revisiting the watch components	105
6.1	Introduction	106
6.2	Appearance of the polished surface	106
6.3	Reflectance measurement	107
6.4	Physical and chemical surface features	107
6.4.1	Surface topography	108
6.5	Chemical analysis	114
6.6	Summary and conclusions	117
7	Conclusions and perspectives	119
7.1	Conclusions	121
7.2	Perspectives	121
	Bibliography	123
	Curriculum Vitae	128

List of Figures

2.1	Schematic presentation of the process of visually perceiving an object. The building blocks of this process are the light source, the object and the visual receptor. The information received will be processed by our brain and interpreted by our experience.	7
2.2	The reflectivity of a number of metals as a function of energy and wavelength of the incident light (adapted from [1]).	12
2.3	3D CIELAB color space. Every color that is perceivable by human eye can be defined by three parameters of L^* , a^* and b^* [2].	13
2.4	CIELAB co-ordinates of various colored gold alloys. Figure is adapted from [3]	15
2.5	Different modes of reflection from surfaces: a)full specular reflection from a perfectly flat surface, b) ideal fully diffusing surface and c)typical reflection from a technical surface composed of a specular and a diffuse component	16
2.6	A translucent material that partially transmits light is placed between two extremes of opaque and transparent materials.	17
2.7	Light transmission through gold deposited thin films for a wavelength of 498 nm. The graph is adapted from [4].	18
2.8	(a) texture primitive, (b) Pattern generated by a line of primitives, (c) 2-dimensional texture pattern generated by an array of lines primitives. The primitive for a texture on surface could be any surface feature, periodic holes or dust particles or stains included (adapted from [5]).	19
2.9	AES atomic concentration depth profiles measure on polished surface of 17Au-10Ag-25Cu (a) before and (b) after oxidation at 150 degrees Celsius. This figure is adapted from [6].	23
2.10	Specular gloss values of ground polypropylene surfaces at incident angle of 60 degrees versus R_a roughness values (adapted from [3]).	24
3.1	Two watch dust cover pieces that have been characterized in this study. One that has been judged to be acceptable by visual experts in the industry and the other who has been rejected due to diagnosis of a defect specified as bright ring. The boundaries of this defect approximately lies between two dotted circles that have been marked on the surface.	29
3.2	The two profiles (a) and (b) have the same R_a values.	31
3.3	Schematics of auger spectroscopy combined with surface sputtering. Combining the two operations allows access to in-depth chemical composition of the samples.	34

3.4	Sample preparation steps to study the microstructure of watch pieces over the cross section.	35
3.5	Schematics of reflectance measurement set up: (a) diffuse reflectance measurement at 0 degree of incidence and (b) total reflectance measurement at 8 degree of incidence. Figure is adapted from [7].	36
3.6	Surface profiles are measured over half of the circular shape of the pieces. (a) and (b) show 3D surface profiles while (c) and (d) show a line profile across the diameter of flawless and defective pieces respectively.	37
3.7	Schematic markings of the locations where laser and 3D images are obtained.	38
3.11	SEM images of polished surface at different magnification of (a) and (b) the flawless piece and (c) and (d) the defective piece. The difference in microstructure between the two samples may result from a difference in their thermomechanical history during manufacturing.	40
3.12	SEM images of microstructure as seen from the top surface at the center of pieces for (a) flawless piece and (b) defective sample.	41
3.13	SEM images of examples of holes that can be found on polished surfaces of (a) and (b) flawless piece and (c) and (d) the defective sample. The holes that are found on the defective sample are typically bigger in size and they are detected with higher surface area coverage as well.	42
3.15	Intensity peaks of gold, silver, copper, carbon and oxygen for the watch component that was accepted by visual quality experts. The color code of positions marked on the piece correspond to the color of measurement curves. The oxygen peak is not background corrected.	44
3.16	Intensity peaks of gold, silver, copper, carbon and oxygen for the defective watch component. The color code of positions marked on the piece correspond to the color of measurement curves. The oxygen peak is not background corrected.	45
3.8	Optical images and 3D surface profiles are presented for the flawless and defective watch components measured in location 1 on the samples (near the edge of the flat bottom). a) and b) show optical image and 3D surface topography of flawless sample respectively while c) and d) show similar images of the defective piece.	47
3.9	Optical images and 3D surface profiles are presented for the flawless and defective watch components measured in location 2 on the samples (in the center of the flat bottom). a) and b) show optical image and 3D surface topography of flawless sample respectively while c) and d) show similar images of the defective piece.	48
3.10	Variable length scale analysis are performed for 710 μm long profiles obtained from the defective and the flawless piece: a) at location 1 near the edge of the flat bottom and b) at location 2 in the center.	49
3.14	Spectra of binding energies and characteristic peaks of elements that could be found on the surface.	50

3.17	Intensity profiles over a sputtered depth of 17.5 nm are plotted for a) flawless piece in the center b) defective watch piece in the center and c) defective watch piece in the defective zone (bright ring). In all cases a sharp increase in gold signal is visible after first sputtering interval. The signals of all the contaminants fall to zero in the same period. All the points in all graphs are measured data points.	51
3.18	Atomic concentration for the three alloying elements are calculated over a depth of 17.5 nm for a) flawless piece in the center, b) defective watch piece in the center and c) defective watch piece in the defective zone. Two measurements are performed and plotted in every location. In all cases, a sharp increase in gold signal is visible after first sputtering interval. The signals of all the contaminants fall to zero in the same period. All the points in all graphs are measured data points.	52
3.19	SEM images are presented together with chemical map of surface contamination that are obtained using Auger Electron Spectroscopy for a) flawless piece at the center of the watch dust cover and b) the defective piece again at the center.	53
3.20	Examples of the indent that Vickers microhardness measurements leave on the surfaces of watch pieces are shown in these images by means of a) optical imaging, b) SEM imaging from the top surface and c) line profile extracted from 3D measurement.	54
3.21	Microhardness of watch dust covers measured on a line across the interior diameter of the samples. Two set of data for visually good and defective pieces are presented. Both pieces show remarkable scattering in measured micro hardness but the scatter is larger for the flawless piece.	55
3.22	Reflection measurement for visible spectrum for flawless and defective samples (a) total reflectance at 8 degree of incidence and (b) diffuse reflectance at 0 degrees of incidence.	56
3.23	Two reflectance measurements in visible spectrum on different positions of flawless sample. A difference in intensity and slope of the curves is observed showing the large uncertainty associated with the measurement of large curved samples.	57
4.1	SEM pictures taken at the cross section of as received 4N gold alloy model samples (a) at 250X and (b) 500X.	62
4.2	SEM images of surface of 4N gold disks at a) 1st sampling, b) 2nd sampling and c) 3rd sampling. The scratches from polishing are evident at the first step of polishing. The surface appears drastically smoother on the second step. Surprisingly, on the 3rd step grain contrast appears on the very smooth polished surface. d) shows the surface at sampling 3 at lower magnification where several grains are clearly visible.	65
4.3	3D surface profiles of 4N gold disks obtained with laser scanning confocal microscope at magnification of 50X for a) 1st sampling, b) 2nd sampling and c) 3rd sampling.	66
4.4	Optical images of 4N gold disks obtained with laser scanning confocal microscope at magnification of 50X for a) 1st sampling, b) 2nd sampling and c) 3rd sampling.	67

4.5	Variable length scale analysis on a profile extracted from each one of the total 9 samples and results are plotted in double logarithmic scale.	68
4.6	Probability density function of surface height are plotted for surfaces at a) 1st 1, b) 2nd and c) 3rd step of sampling. For the first and second sampling the distribution is continuous and nearly Gaussian while for the third sampling with the surface texture of plateaus, a step-like distribution of surface heights is observed.	71
4.7	XPS peaks for the three alloying elements and the contaminants at the three stages of sampling.	72
4.8	Intensity of signals for the alloying elements are plotted as well as carbon and oxygen for a) first sampling, b) second sampling and c) third sampling. C and O are found on the top surface of the samples due to contamination created by polishing process. At the outer surface where these contaminants are present, all three signals metals have lower intensities. An overnight pause in the measurement for sampling one at 9 nm of sputtering and for sampling three at 11 nm of sputtering has caused a drop in gold signal as well as a jump in copper signal. The rest of elements remain unaffected.	73
4.9	Atomic concentration of three alloying elements as a function of sputtered depth for sampling one. Three repetitions of the measurement and three points are presented to show reproducibility and homogeneity of results. An overnight pause in measurement has caused the sudden drop for gold and jump for copper at 9 nm while silver remains unaffected. This might be caused by surface diffusion of copper.	74
4.10	Atomic concentration of three alloying elements as a function of sputtered depth for sampling two. Three repetitions of the measurement at three different points are presented to show reproducibility and homogeneity of results.	75
4.11	Atomic concentration of three alloying elements as a function of sputtered depth for sampling 3. Repetition of the measurement at three points on the same sample are presented to show reproducibility and homogeneity of results.	76
4.12	Atomic concentration of the three samples over the first 10 nm in depth are overlapped. The color code from lighter to darker colors correspond to sampling 1 to 3 respectively. It can be seen that remarkable difference exists between gold and copper profiles while silver has a similar atomic concentration in all three cases.	77
4.13	Reflectance is measured using a commercial spectrophotometer over the wavelength of 400 to 800 nm. The results are presented as a percentage compared to a reference sample. This reference sample is calibrated at 100% of reflectance before each set of measurements. One measurements is plotted on three samples after each step of polishing.	78
4.14	a^* and b^* color coordinates for nine samples in three surface roughness states. Color references for 3N, 4N and 5N alloys are plotted for comparison. Going further in polishing process shifts the color towards the alloy with lower copper to silver ratio.	79

4.15	Correlations between L^* and roughness parameters R_a and R_q at two length scales of analysis. 20 μm corresponds to the length scale below which all the surfaces are smooth and 710 μm corresponds to the length of the roughness profile. In all four cases a linear correlation exists between roughness and L^* for sampling 1 and 2 with Gaussian distribution of PDF. However, sampling 3 with a step-like PDF does not follow this relationship.	81
4.16	a^* is plotted against atomic concentration of copper averaged over 5 nm of the depth profile and b^* is plotted versus similar values of gold for three samples that have been studied by AES. A linear relationship was found in both cases	82
4.17	Measured TIS values at wavelength of 700 μm are plotted against both R_q and R_q^2	83
4.18	Measured TIS at incident wavelength of 700 nm is plotted versus TIS calculated through Equation 2.8.	83
5.1	SEM images of microstructure of a punched disk as raw material before entering the process of fabrication. Grain structure had a similar dispersion in size at different locations on the cross section	89
5.2	Average of three hardness measurements are marked at different positions on the surface. A slight gradient towards higher hardness is seen by moving from the edges towards the center of the piece.	90
5.3	Microstructure of a final product is shown at different locations on the cross section. The flat end of the image corresponds to the center of the dust cover and the other end of the image corresponds to the edge of the piece.	91
5.4	A 5N 18 karat watch component extracted from the production line after most steps of mechanical deformation: a) diffuse reflectance measurement shows similar contrast all over the cross section. High diffuse reflectance on the outline of the sample happens at the interface between the resin that the piece is mounted in. b) microstructure of the piece is imaged using the laser confocal microscope.	92
5.5	The combination of mechanical loading and relative movement of two surfaces in presence of a slurry means that polishing is potentially a tribocorrosion system.	94
5.6	Schematic representation of how polishing as a tribocorrosion process induces a chemically modified layer on the surface of Au-Ag-Cu alloy. a) The homogeneous bulk composition before polishing, b) exposure to potentially reactive environment causes oxidation of Cu on the surface, c) the oxide layer is removed by abrasion and due to gradient in composition, Cu atoms migrate from few nanometers below the surface to the top surface and d) at the end of polishing the surface is composed of a sandwich of thin oxide layer, chemically modified thin film on top of the bulk material.	95
5.7	Schematic presentation of the electrochemical cell used in this study. Details of electrodes and the solution are marked in the image.	95

5.8	Polarization curve for the 18 K gold alloy in $1MNa_2SO_4+0.02MH_2SO_4$ solution.	96
5.9	Intensity signals for in-depth profiles of a) E01 and b) E03.	97
5.10	Intensity signals for in-depth profiles of a) E01 and b) E03.	98
5.11	Depth profiles of the two samples are overlapped in the first 15 nanometers.	99
5.12	Total reflectance measurements for 2 samples with forced copper dissolution and 1 sample with cathodic surface cleaning. At lower wavelengths, all three samples have similar reflectance. However, E03 has slightly lower reflectance intensity at higher wavelengths.	100
5.13	Color values for disks E01, E02 and E03. For purpose of comparison, standard colors of 3N-5N 18 karat gold alloy with different proportions of copper to silver are plotted as well.	100
5.14	SEM image of the wear track after before heat treatment at various magnifications of (a) 250, b) 1000, c) 5000 and d) 10,000. The surface of the wear track is very smooth.	102
5.15	SEM image of the wear track after heat treatment at various magnifications of: (a) 250 times, b) 1000, c) 5000 and d) 10,000. Remarkable amount of porosity appears only inside the wear track and only after the heat treatment.	103
5.16	a) SEM image of an indentation performed with a Vickers testing instrument inside the wear track after heat treatment and b) a zoom in on the area that is marked on the indent. The image illustrates that the pores created after the heat treatment could be partially closed by further mechanical deformation.	104
6.1	Schematics of a watch cover that has been analyzed by a visual expert. Areas marked in light gold color are judged to be stained by the expert.	106
6.2	The line marked on the schematics show the location where diffuse radiance is locally measured using the multi-angle setup.	107
6.3	Radiance measured at illumination angle of 15 degrees and measurement angle of 0 compared to the normal of the surface. 0 radiance represents no reflection at the given angle and 1 means that the surface diffuses light as much as the white diffuse reference sample that is used for calibration. The defective watch components (D1 and D2) have remarkably higher diffuse reflectance compared to flawless pieces (F1 and F2).	108
6.4	a) Optical and b) laser intensity images obtained by laser confocal microscope. The three strips from top to bottom correspond to the three areas marked on the schematics of the dust-cover from right to left.	110
6.5	Locations 1 and 2 where measurements were performed are marked on the schematics of the sample. Location 1 is inside defective area while location 2 is on the flawless area.	111
6.6	Variable length scale analysis were performed on two profiles that have been obtained in location 1 inside the defective zone and in location 2 in the center of the piece. The results plotted in double logarithmic scale show similar R_q in lower scales but roughness in defective exceeds the one of the good area.	111

6.7	Images are obtained by stitching several SEM images at magnification of 5000 times. The locations where the images are taken are marked with corresponding letters on the schematics of the piece.	112
6.8	Examples of holes that can be found at different locations on the surface.	113
6.9	Signal intensities in AES analysis for the three alloying elements and carbon and oxygen that can be found on the surface as contaminants at a) location 1 and b) location 2 of the 3N dust cover.	115
6.10	In-depth atomic concentrations obtained by AES analysis a) at location 1 inside the defective zone and b) at location 2 of the 3N dust cover. . .	116
6.11	Three profiles obtained at each location are overlapped. It can be seen that the results are reproducible and the small differences observed between two locations in below surface composition are present in all measurements.	117

List of Tables

2.1	Composition of different ternary gold-silver-copper alloys and their relevant standard color indices	15
3.1	Kinetic energies of AES peaks and sensitivity factors that were used for calculating atomic concentration are listed (extracted from [8]).	34
3.2	Roughness values averaged over three line measurements are presented for two locations (as marked in Figure 3.7) on the surface for each piece.	39
3.3	Binding energies of three alloying elements and their oxides [9].	43
4.1	Composition of the model samples used in the current study.	60
4.2	Several roughness parameters measured for three surfaces. In each case 9 measurements are averaged.	64
5.1	Roughness values averaged over three measurement lines are presented for three samples before and after the electrochemical tests.	96
6.1	L^* values for R_q roughnesses measured at two different length scales using correlations found in Chapter 4 Section 4.6.	109
6.2	Gold and copper atomic percentage averaged over the first 5 nm of the depth profiles for three measurements in each location.	114
6.3	Calculated a^* and b^* based on compositions averaged in the first 5nm of the depth profiles at two locations on the watch dust cover	115

Nomenclature

$0N - 5N$	German DIN 8238 standard color indices for different compositions of Au-Ag-Cu ternary system
\bar{z}	Average value of surface heights (nm)
ΔE^*	Vectorial color distance between two color coordinates
λ	Wavelength of light (nm)
ρ	Ratio of reflected light from a rough surface compared to the one of a smooth surface
σ	Standard deviation of surface heights (nm)
θ_i	Incident angle of light
θ_s	Scattering angle of light
a^*	Green-red color component in CIELAB color space
ARS	Angle resolved scattering function
b^*	Blue-yellow color component in CIELAB color space
d	Average of the two diagonals of the Vickers imprint (mm)
H_ν	Vickers hardness (HV) ($kgfmm^{-2}$)
k	Attenuation index of light
L	Evaluation length of the topographic profile
L^*	Lightness in CIELAB color system
N	Complex refractive index
n	Refractive index of the material
P	Applied load (N)
PSD	Two-dimensional power spectral density function
Q	Angle dependent polarization reflectance
R	Percentage of reflected light
R_a	Arithmetic average of the absolute values of the profile height deviations from the mean line (nm)

R_q Root mean square average of the profile heights (nm)
 TIS Total integrated scattering

Chapter 1

Introduction

1.1 Motivation

Surface quality of goods addresses a wide range of domains from functionality and lifetime of devices to customer's perception of product quality. Accordingly, considerable interest exists in numerous industries in reaching both a nearly perfect surface finish and a flawless appearance. In luxury industry, specifically in jewelry and watch making, aesthetic appeal of a product is highly regarded because it is a testimony of the quality and the fineness of artifacts.

To this date, high-end jewelry and watch manufacturing remains an artisanal craft to a great extent. Based on long tradition in the trade, many steps of production involve highly individual-dependent craftwork. This method of fabrication can lay products of superior quality compared to those manufactured through more automatized paths. The reason behind it is that in this case, duration, extensions and even necessity of every single step of production can be adapted to individual working pieces by benefiting from the intelligence of the operator. The downside of such method of fabrication is its high dependency on individual qualitative judgment that makes implementing quantitative measures very difficult.

In addition to the execution, the success of every production step is also often assessed through dedicated intervals of visual inspection by skilled individuals. That is, a trained expert would decide whether the quality of the work done is satisfactory or acceptable for the concerning step or not. If yes, the piece can move forward in the manufacturing process. But if a defect is detected and judged as unacceptable by the expert, even if this defect is the slightest aesthetic imperfection, the piece will be either sent back to repeat some previously performed steps or it will be fully discarded despite having been through several costly production steps.

The ability of trained experts in visually detecting defects is astonishing. However, in many cases it is not possible for them to diagnose the nature of the imperfection. They would instead define the type of the defect based on an internally developed standard

terminology including stain, scratch, bright point, etc. and describe the intensity as little, average or strong. Also in many circumstances, they are unable to pinpoint the cause of this imperfection and its source in process of manufacturing. Such an event is particularly inconvenient when a defect of unrecognizable source is detected at the end of a long and costly process of manufacturing and causes the piece to be scrapped.

The industrial problem, which this thesis is based on, has arisen during the visual inspection of timepieces at the very last step of production. Here, the expert analyses the polished gold surface of watch components at the end of the manufacturing process with naked eyes under a spotlight at an approximate distance of 30 cm. In this inspection, she/he occasionally detects some inhomogeneity in appearance. The particular defect of interest is one that is labeled as a stain that can appear in different shapes and with different intensities. The expert here is not able to identify the physical surface characteristic(s) that create(s) this faulty appearance. Additionally, the origin of this, seemingly random, occurrence remains unknown.

Based on the problem stated above, there is a need for developing a methodology that can first assess an aesthetic defect and second link it to well defined properties of the surface. Assessing aesthetics requires providing definitions and measurement techniques that can be correlated to sensory feeling of visual perception. Additionally, finding the link between an aesthetic defect and properties of the surface requires understanding and measurement of surface features.

1.2 Thesis aim and structure

This applied research thesis stands at the interface of surface science and domain of aesthetic appearance.

This study was designed to address the industrial problem of aesthetic defects on mirror polished 18 karat gold surfaces and their origin. Accordingly, the objective of the current work is to develop an insight to appearance of mirror polished gold surfaces, provide methodologies for measuring appearance and also correlating this appearance to measurable surface properties. In other words, it aims at answering four following questions:

1. How can the aesthetic appearance of a surface be rationalized and linked to the properties of the surface?
2. What are the surface features that control visual perception of mirror polished gold surfaces?
3. To which extent these features affect the appearance?
4. When are these features generated in the relevant process of fabricating a gold jewelry or watch component?

To fulfill this objective, the present dissertation is structured around 7 chapters including the current chapter. Since understanding basic concepts of visual perception, appearance of surfaces and visual quality control are central to this work, **Chapter 2** begins by laying out a brief overview of these topics. The chapter will then continue to introduce an existing framework on assessing appearance through visually relevant optical properties of the surface. As this work is focused on aesthetics of polished surfaces, the chapter will be finished by presenting what is already known about aesthetic consequences of polishing.

In order to determine physical and chemical surface properties of polished gold surfaces that are relevant to their appearance, **Chapter 3** is dedicated to characterization of industrial surfaces. The goal is, first exploring adapted characterization methods and then employing those appropriate methods to search for surface imperfections that could potentially cause defects in appearance. The methods and the obtained results are described in details. Here, a set of defects that could appear on the industrial samples were determined. However, it is not yet clear which of those are directly, or indirectly, responsible for the aesthetic imperfection.

To better understand the role that each of these surface imperfections play in determining specific aspects of appearance, they were recreated in a controlled manner. Subsequently, we identify individual correlation between the imperfection and some visually relevant optical properties. To achieve this goal, **Chapter 4** shifts the focus from industrial pieces to moizationdel samples that are manipulated in the laboratory instead of the production line. Next, quantitative correlations are made between surface defects and reflection and color as aspects of appearance.

Chapter 5 looks into the process of fabrication of the pieces to identify the origin of surface defects both in the final step of surface finish and earlier steps of production. The results can help the relevant industry to take necessary precautionary measures to avoid the occurrence of the defects in the first place.

Chapter 6 is designed to bring back the well established methodologies and know-how developed during this work back to the initial industrial problem. For this final step, a brand-new piece is taken out of manufacturing which has been visually judged by a trained expert. This piece will be quantitatively analyzed by the methodology developed in this thesis. The comparison between the two approaches show cases that the provided toolkit is able to quantify an aesthetic defect.

And finally **Chapter 7** closes this dissertation by general discussions, conclusions and perspectives.

Chapter 2

Assessing appearance: general background and state of the art

For a high-end watch or jewelry product aesthetic imperfections are intolerable and yet, they occasionally appear on surfaces. In order to prevent them from happening, we need to first discover what an aesthetic defect is and how it translates to properties of a technical surface. Here, we review the literature on measurable aspects of appearance and how process of fabrication and surface finish can modify those aspects and consequently appearance of surfaces. We conclude that a global study that provides an understanding of all the modifications that are induced on the surface as a result of fabrication steps and their correlation to appearance is needed.

2.1 Introduction

Visual perception of an object is a critical factor in customer's choice. Accordingly, in many industries it is of high importance to create an appearance that is perceived as aesthetically appealing. This specially applies to products with high aesthetic value such as luxury watches and jewelry. However, understanding the way we perceive aesthetic aspects of a surface remains very complex and quantification of visual properties of an object is very challenging. In an effort to address such complex issues, this chapter will lay down the necessary background for understanding basic concepts of visual perception of surfaces, appearance and visual assessment of aesthetics. A framework will then be introduced that can be used for assessing appearance of surfaces.

2.2 Visual perception of surfaces

Our experience of seeing is effortless, and yet the mechanisms that underlie visual perception are endlessly complex. Philosophers, psychologists and scientists have been fascinated by the topic of visual perception for hundreds of years as a natural phenomenon and also as a source of knowledge. Yet, despite this long history of attention, many fundamental questions remain about the visual experience and the process that produces it [10].

Humans are remarkably good at visually perceiving objects and surfaces. In everyday life, we encounter a remarkable variation of materials and we succeed to distinguish them by sight almost without making any errors. We are even able to classify many materials by judging their properties only through our visual system. This facility of determining complex materials properties of even unfamiliar objects only through visual inspection is evidence of how rich and complex the visual phenomenology is. Nevertheless, we are not able to see all the physical and functional properties of materials. Some examples of these properties include but are not limited to: density, thermal conductivity or toxicity. This fact has a very important implication in the study of appearance i.e. in order to understand what makes the appearance of a surface it is essential to recognize defining characteristics of a surface. In addition, it is of particular importance to pinpoint among those physical attributes, the ones that contribute to our observation.

Process of visually perceiving an object is composed of three main components. The first component is a light source emitting an electromagnetic radiation (light). These radiated waves then need to interact with the object under study (the second component). Depending on the physical and chemical properties of the object and its surface characteristics, the interaction can occur in many different modes such as absorption, transmission and reflection or a combination of all. The result of this interaction then needs to reach human eye (the third component) and the segment of it that lies in the visible wavelength will be processed and visualized by our brain. The interpretation

of this image and the response of individuals to it is the human perception and it depends on psychological characteristics of every individual. Figure 2.1 schematically presents this process. The last two steps of this process as presented in the figure are image formation in brain following the reaction of light with receptor cells of the eye and individual human perception are topics of neuroscience and psychology respectively. The focus of the current study is the appearance of surfaces that is created by the outcome of light/matter interaction as received by the human eye (the first three steps in Figure 2.1). The next section will define appearance in more details and from there on, this work will be dealing with appearance of surfaces.

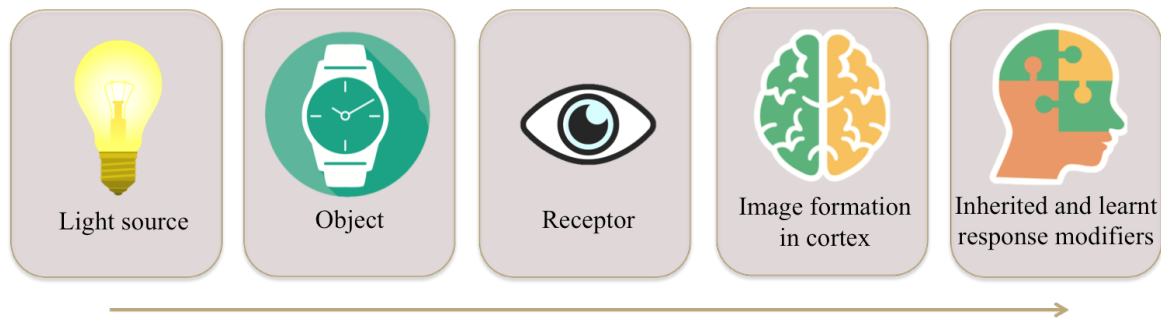


Figure 2.1: Schematic presentation of the process of visually perceiving an object. The building blocks of this process are the light source, the object and the visual receptor. The information received will be processed by our brain and interpreted by our experience.

2.3 Appearance

According to ASTM standard terminology, appearance is the aspect of visual experience by which things are recognized [11]. The description of appearance of an object is however multifaceted; it may include many aspects such as shape, size, texture, gloss and any other apparent quality that the object exhibits. Assessing appearance of an object as a whole is an extremely complex matter. One of the involved complications is that appearance implies a judgment: does this jewelry look appealing? is this surface finish adequate for the job? Thus relevant quantitative assessment of appearance must help with answering such questions [12]. Such complications reflect themselves in visual quality control of surfaces in industries specially in visual quality control of appearance of polished surfaces.

Mechanical polishing is the most widely used method for achieving mirror-like metal surfaces in majority of industries. Where mechanical polishing is performed manually, the quality of surface finish is controlled by visual inspection [13]. The goal of visual inspection is either to detect and eliminate functional anomalies of the product or to ensure that the expected visual characteristics are met or as well a combination of both. In our case we are interested in aesthetic defects that can be spotted by visual

inspection. By performing visual inspection, the expert must also decide if the product complies with expectations or not. In this light, the process of visual inspection can be broken down to at least two steps as proposed by Drury's two-component inspection model: searching and deciding [14].

There are several parameters that affect both of those steps of searching and deciding and thus the performance of the visual inspector including the ones listed and described by See [15]:

- Task factors (product complexity, standard for comparison, defect type, defect location, inspection aids, etc)
- Environmental factors (lightening, workplace design, etc)
- Individual factors (visual acuity, experience, vigilance, personality, etc)
- Organizational factors (training, instructions, management support, etc)
- And finally social factors (such as pressure, isolation and communication)

Where assessing aesthetic aspects are concerned, the process of decision making heavily depends on visual perception of the expert.

Contextual appearance

An aesthetic defect can be considered a visible contrast or deviation either from a surrounding surface or from a standard sample. Baudet et al [16] proposed that an expert could discard a product if she/he finds the sample to have an unacceptable deviation from an ideal sample or surface. They defined three types of such deviations :

- Deviation from a reference in terms of characteristics such as color and texture between the product and a model product.
- Deviation from intent of the designer defined as differences between different components of a whole.
- Local deviations where distinctions are perceived on the the same part.

Nevertheless, as deviations from a perfect surface at some scale are inevitable through fabrication process, judging the level of this deviation that is tolerable remains a task for the expert to perform based on her/his own experienced judgment. The level of tolerability for deviation also depends on the product of concern. For a polished gold watch component for example, local deviations in appearance of a piece create aesthetic defects and are often considered unacceptable.

This small tolerance for local deviations underlines the importance of a phenomenon known as contextual or contrast perception. This means that perceived visual properties do not solely depend on absolute properties of the stimulus. The perception depends instead on comparison of such properties to the surrounding area or so called contextual stimuli [17]. As a very simple example, the perception of a surface lightness is widely affected by the color of the background surrounding it so that a gray patch would look darker on a white background than on a black background (this is called

brightness contrast). Another example is the phenomenon known as chromatic contrast. A classical showcase of this phenomenon is a uniform patch that looks yellow on a dark background but appears greenish when viewed on a red surrounding [18]. This means that contrast between colors affects the appearance of a single color. The list of such examples is long but the short conclusion concerning the current study is that color perception is essentially a contextual phenomenon that depends on the sensory information which has come before and also the ones that emerge simultaneously from the surroundings [19]. In addition to the example mentioned here, several other perceived properties depend on surrounding stimuli as well.

On the whole, despite the fact that a well trained panel of experts provides the best judgment of appearance that we could currently obtain by any method and the fact that visual quality control is critical in many industrial application, it has been repeatedly observed that human inspectors are imperfect ([15] and [20]). Some studies are dedicated to estimating errors in visual quality control [21] and many others to optimizing the output of this technique by either defining the environment and method of inspection or by giving guidelines on decision making and expressing the judgment ([22], [23] and [24]) as well as broad range of studies that try to replace human visual inspection by automatized methods and computer image processing ([25], [26], [27] and [28] to name a few). However, those topics are beyond the scope of the present work. Rather than the process of visual judgment itself, this study is focused on the input as well as the output of this process or in other words causes of aesthetic anomalies and contributions they make to the appearance.

Typically every industry provides the visual experts with a set of terminology and frequently a scaling method for evaluation and reporting of the defaults. Some of the common terminology for describing an aesthetic default include but are not limited to: mark, heterogeneity, pollution or distortion [16]. While these terms may shed a light to the appearance of a piece, they offer little insight to the actual surface properties. The other downside of visual assessment is that the description even when presented through a system of ranking, are qualitative and also subjective. Meanwhile, the main shortcoming that motivates us in this work is the fact that for aesthetic defects that are more complicated than simple defects such as a scratch, the visual expert is unable to describe the imperfection in terms of physical or chemical properties of the surface. She/he is also unable to root the defect back in the process of production. Therefore, no intervention can be made in order to avoid defects from appearing in the first place. An approach that can quantitatively assess appearance of surfaces could be a way to address some of these challenges associated with visual assessment of appearance.

2.4 NPL approach to assessing appearance of surfaces

Quantitative assessment of visual perception is an example of soft metrology. Soft metrology is the science of developing techniques and/or mathematical models that

can objectively quantify properties of material that are otherwise determined by human senses (such as sight, touch, smell etc.). The goal is to identify measurement scales that provide physical objective measurements that can predict human's subjective response [12]. Additionally a strategy for appearance measurement should ideally include measurements which are possible to make and are capable of describing the total appearance of an object.

A broadly accepted method that has been developed in the field of soft metrology for characterization of visual properties of surfaces was suggested by Hutchings [29] in the context of food appearance. This approach has been later on generalized and documented under a report called "A framework for the measurement of visual appearance" by National Physics Laboratory (NPL) in Britain [5]. After a detailed discussion on the complexity of topic of appearance and visual perception, they propose that appearance of the surface can be studied in the light of optical properties of the surface. They suggest four surface properties that could possibly be measured and correlated to the appearance. These properties: color, gloss, translucency and surface texture. They recognize as well that these measures can be interdependent and affect one another. Each one of these parameters will be thoroughly discussed in sections 2.4.1 to 2.4.4 but before getting to that we will review the assessment techniques that have been proposed by NPL.

The four parameters proposed by NPL represent useful categories for measurements particularly in the sense that measurement techniques already exist for some of them. However, the indications given by NPL are rather general and in order to use them to specific applications, definitions need to be clarified and quantification methods need to be explored.

For color measurement they mention color assessment by human eye and visual comparison to standard samples. However, they conclude that measurement of spectral reflectance and application of CIE colorimetric parameters is a robust approach for the industry.

The most common way of measuring gloss is measuring light reflected from the surface at fixed angles. This method requires an instrument called gloss meter. A more complete gloss measurement method would be one that measures such reflection at all viewing angles. This method is called goniphotometry. In order to compare the data obtained by goniphotometry from different samples, a scale should be defined. For an average surface, the obtained data is composed of a diffuse reflectance plus a gloss peak. NPL suggests that the height of this peak could be considered as the scale for comparison of samples. However they also say that it does not give a significantly better correlation with visual assessment of gloss than does a simple measurement from a gloss meter [5].

For measuring translucency in bulk material, NPL does not propose a robust solution. Although measurement techniques exist for measuring the amount of light that passes

through a liquid or a thin film, phenomenon of surface translucency in bulk opaque material is not considered.

Texture and its measurement is a more complex topic both because it is more difficult to define and also because physical and apparent texture are not necessarily the same. They suggests that physical texture can potentially be assessed using a topography measurement instrument such as an stylus profilometer and that the apparent texture can possibly be assessed using camera images and image processing. They suggest that the idea of establishing a series of ‘standard’ textures for a set of real materials could be useful to help establish a measurement system and a measurement scale.

2.4.1 Color

It is usually assumed that the color of an object is due to partial absorption of incident light during the process of reflection. In metals however, this occurs in an indirect way. For an insulating material the percentage of reflected light, R for a beam of light at normal incidence angle is given by the following equation:

$$R = 100 \frac{(n-1)^2}{(n+1)^2} \quad (2.1)$$

Where n is refractive index of the material. For a typical glass, R has a value of about 4% so most of the light is transmitted. However, unlike insulators or semiconductors, vicinity of energy bands in metals gives the conduction electrons to respond to electromagnetic waves of almost any frequencies. Meaning that when light falls on a metal surface, the absorption is so strong that it can only penetrate to a depth of few hundreds of atoms i.e. less than a wavelength for metals is visible [4]. Simultaneously, as these conduction electrons are rather freely accelerated backwards and forwards, they radiate electromagnetic energy. Therefore, most of the incident light that has interacted with these electrons is re-emitted backwards giving rise to strong reflection [30]. Mathematical translation of this phenomenon is embodied in replacing refractive index n by the complex refractive index N defined as:

$$N = n + ik \quad (2.2)$$

Where i is the imaginary number $\sqrt{-1}$ and k is the attenuation index (also called extinction coefficient). The percent of reflectivity thus becomes:

$$R = 100 \frac{(n-1)^2 + k^2}{(n+1)^2 + k^2} \quad (2.3)$$

For silver under sodium D light for example, the values $n=0.18$ and $k=3.6$, give rise to reflectivity of 95%. Nagib et. al. [31] experimentally derived the optical constants of gold by ellipsometry methods using a laser with wavelength of 632.8 nm and found n and k to be equal to 0.2703 and 9.0559 respectively. This means a reflectivity of 98%

for gold.

The mechanism that causes the characteristic color of gold has been explained through different approaches by different physicists. In the Nasseau's classical reference book of colors [1], he explains that for metals, intense absorption is accompanied by very strong reflection. The metallic shine is thus a result of this very high reflectivity. The variation of color among metals is essentially due to variation of k with the wavelength. Silver has slightly reduced reflectivity at the extreme violet end of visible light spectrum, which makes it appear slightly warmer in color compared to stainless steel. While copper and gold which do not absorb efficiently at blue end of spectrum and hence do not reflect as much in this region causing their reddish and yellow colors [1]. Reflectivity of some metals as a function of wavelength and energy of incident light is given Figure2.2.

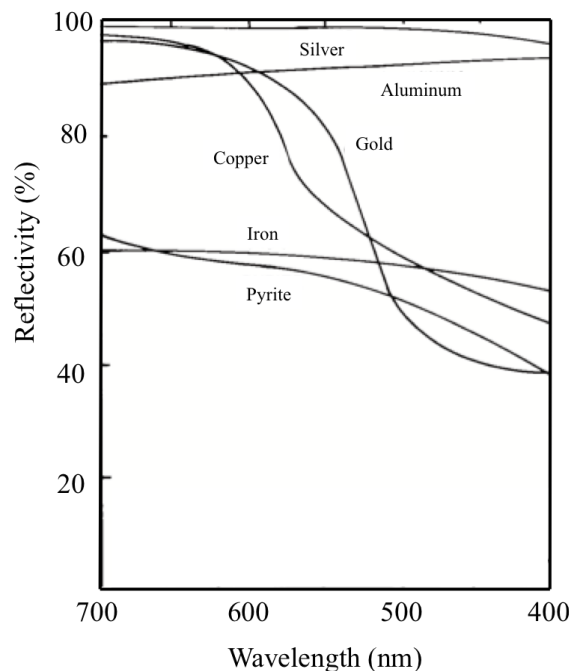


Figure 2.2: The reflectivity of a number of metals as a function of energy and wavelength of the incident light (adapted from [1]).

Some other authors explain color of metals using the band theory saying that the reason some metals show characteristic colors is that they have energy gap between the Fermi level and the top of d-band that corresponds to the energy of a photon in visible range which they say is the case for gold and copper [32].

While gold and copper remain the only metals with intrinsic chromatic colors, metals with achromatic colors (colors that lack hues such as white, gray and black) can create different hues by interference. For example, colored stainless steel can be produced by thermally, chemically or electrochemically encouraging an oxide film on the surface. Changing the thickness of this film can create brown, blue, golden blue, gold and

purple colors in order [33] and [34]. However, all those colors are formed as a result of interference of light reflected at the steel/oxide surface with that reflected at the oxide/air interface.

CIELAB color metric

Human eye can distinguish around ten million colors [1]. The difficulties and inconsistencies in color perception and specification among observers has been a driving force for industries to use standardized colorimetric tools [35]. A colorimeter is generally any tool that characterizes color samples to provide an objective measure of color characteristics. The need for precise assessment of colors has led to creation of several color measurement systems. CIE $L^*a^*b^*$ (CIELAB) is a color space specified by the International Commission on Illumination that describes all the colors visible to the human eye. There are several pros to using the CIELAB system the main one being a quantitative color description. What is more, the units given by this metric have a meaningful relationship with the perception of color differences by the human eye. These parameters are also independent of the measurement instrument which make the results obtained with different apparatus comparable.

CIELAB system is a three-dimensional space that defines colors by three co-ordinates including lightness L^* , a^* and b^* . The L^* values ranges from 0 for black to 100 for white. Intermediate L^* values represent the degree of luminescence. Positive a^* values correspond to red colors, and higher positive values of a^* mean more intensity (saturation) in red. Negative a^* values represent green colors. And finally, positive b^* values are associated with yellow colors and negative values with blue [36]. These three dimensions and the space they form are represented in Figure 2.3.

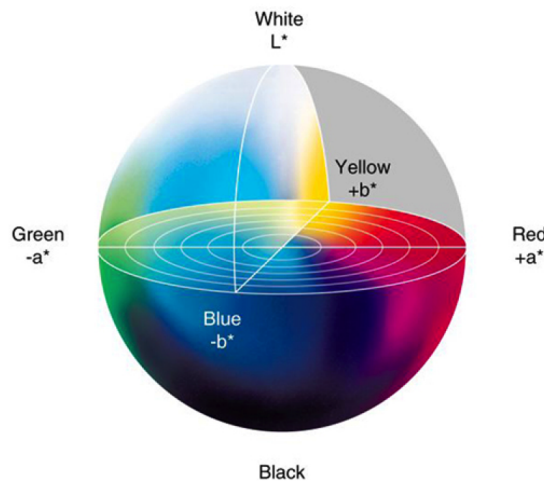


Figure 2.3: 3D CIELAB color space. Every color that is perceivable by human eye can be defined by three parameters of L^* , a^* and b^* [2].

What is often of more interest to industry is not the absolute color of a sample but the relative ‘color-difference’ between a reference sample and a test sample or inhom-

geneity of color on different locations on the same sample. In the CIE color metrics, the relative position of two colors located on a color map can be simply expressed as a single parameter, ΔE^* , which is the vectorial color distance between two color coordinates of L_1^* , a_1^* and b_1^* , and L_2^* , a_2^* and b_2^* and is given by:

$$\Delta E^* = [(L_1^* - L_2^*)^2 + (a_1^* - a_2^*)^2 + (b_1^* - b_2^*)^2]^{\frac{1}{2}} \quad (2.4)$$

According to CIE 15:2004 report by international commission on illumination, distances in CIELAB color space represent close approximation of the perceived difference of color between two objects. They emphasize however that viewing conditions should be in lights similar to the one of the daylight and the background color of the two objects has too be similar for this correlation to apply [37]. Other researchers have as well verified visually meaningful and rigorous correlation between measured color differences by CIELAB system and response of human observer [38]. The color difference that is just noticeable by humans has been calculated to be equal to a CIE ΔE^* of 2.3 [39].

Gold colors

Pure gold has a rich yellow color. Yet, alloying gold with other elements provide the opportunity of achieving a multitude of hues and colors. In ternary system of Au-Ag-Cu alone, color variations of yellow, red and green can be obtained by different ratio of the components. Copper adds a reddish tint and silver contributes to alloy lightness by adding a greenish tint.

The change of color by alloying can be explained through band theory. In general, studying the band structure of alloys is a difficult endeavor as translational symmetry is lost in a disordered alloy. However, in case of gold-silver-copper alloy where all the constituents have similar band structures (they have five fully-occupied d-bands below a half-filled s-band), the explanation can be simplified to the following: alloying with silver shifts the d-bands down in energy translating into a wider gap and thus a higher energy absorbed from the incident light and increase of reflection for all red, yellow and green regions of the spectrum. Alloying with copper though shifts the d-bands up and narrows the energy gap [3]. Accordingly, numerous shades between yellow of gold, white of silver and red of copper can be achieved by manipulating the percentage of these three components in the alloy.

Figure 2.4 shows examples of a variety of colors that can be achieved by alloying gold. 0N to 5N are German DIN 8238 standard color indices for different compositions of Au-Ag-Cu ternary system. Table 4.1 shows the chemical composition of each of these alloys by weight percentage. However, copper and silver are not the only elements that can change the color of gold. Some other examples of colored gold alloys include:

- Red gold: binary Au-Cu alloy
- Blue gold: either made by alloying gold with iron or with indium
- Purple gold: made by addition of aluminum

- Black gold: gold-cobalt alloy

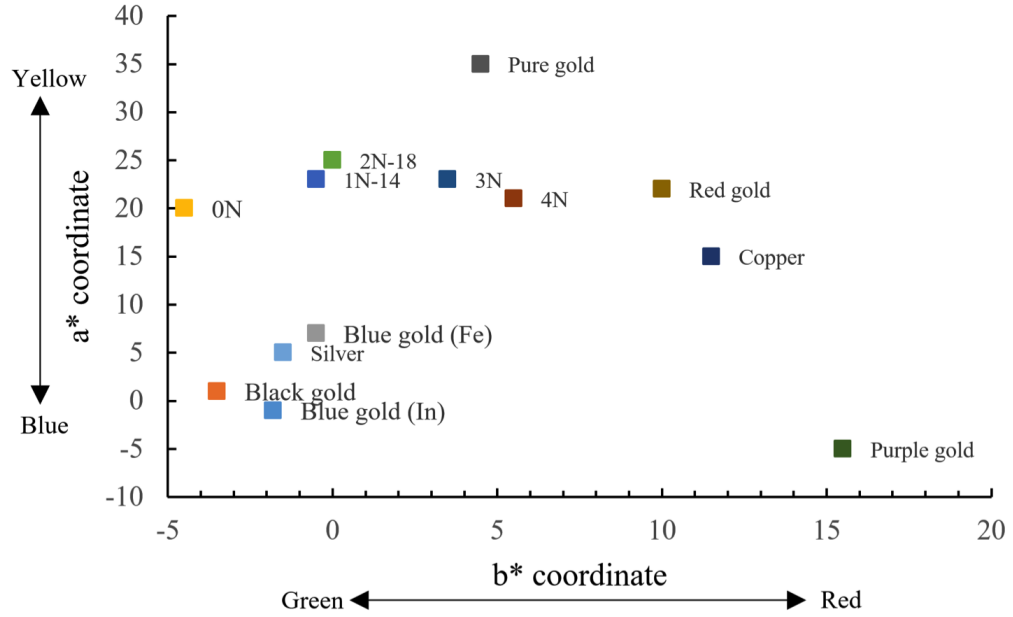


Figure 2.4: CIELAB co-ordinates of various colored gold alloys. Figure is adapted from [3]

Table 2.1: Composition of different ternary gold-silver-copper alloys and their relevant standard color indices

Color indice	Chemical composition (wt%)		
	Au	Ag	Cu
0 N	585	300 to 340	75 to 115
1 N	585	240 to 265	150 to 175
2 N	750	150 to 160	90 to 100
3 N	750	120 to 130	120 to 130
4 N	750	85 to 95	155 to 165
5 N	750	45 to 55	195 to 205

2.4.2 Gloss

Gloss is associated with the way that an object reflects light; particularly the power of a surface to reflect light specularly. Specular reflection is the phenomenon that makes a surface appear somewhat like a mirror. On an ideal perfectly flat surface, the reflected beam lies in the plane of incidence at an identical angle to the incidence angle but on the opposite side of the surface normal (as shown in Figure 2.5 (a)). In contrast a diffuser would scatter the incident light at all angles. An ideal diffuser is schematically shown in Figure 2.5 (b) and it would exhibit Lambertian reflection, meaning that it would have equal luminescence when viewed from all angles lying in the half-space adjacent to the surface. A real world technical surface however typically has a behavior similar to what is shown schematically in Figure 2.5 (c) which would

mean a combination of a specular and a diffuse component. For a smoothly polished surface, the specular component would be dominant.

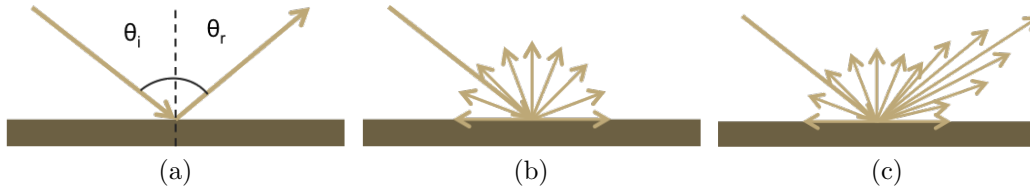


Figure 2.5: Different modes of reflection from surfaces: a) full specular reflection from a perfectly flat surface, b) ideal fully diffusing surface and c) typical reflection from a technical surface composed of a specular and a diffuse component

Gloss appearance is often studied independent of color however the two can affect visual perception of one another [5]. The manner to characterize the gloss perception and the definition of gloss scales yet is a very open study object [12]. The earliest studies of gloss assumed that gloss could entirely be defined as the amount of specular reflectance of light compared to the amount of diffusely reflected light. However, later on Hunter considered the perception of gloss in human vision to be a gestalt (corresponding to no single property of the surface, but formed by an appraisal of the whole seen) [40]. He outlined six types of perceptual gloss including specular gloss, sheen, contrast gloss, haze, distinctness-of-reflected-image and absence-of-surface-texture gloss all of which are described in details in reference [41].

In this classical work that has been the base of many scientific works since 1937, Hunter mentions that this classification has been made upon scientific observation but is not a final and complete method capable of fully describing the phenomenon of gloss perception. As an example, he points out that some of the aspects appearance associated with the degree of polishing of a surface are hard to describe with this terminology. Also, among all the above-mentioned categories, only number 1 and 3 are related to measurable entities (the specularly reflected light and the diffused light) [42]. Therefore, instrumental gloss measurement is mainly focused on measuring specular and diffuse reflectance from the surfaces.

In the field of general appearance assessment, measurement methods that can be used to more globally characterize the visually relevant characteristics of a surface are commonly used [43]. Using a commercial spectrophotometer, one can measure total and diffuse reflectance of surfaces over visible wave-length of light. In this work, choose to study total reflectance measurement as the method to the light reflection from such surfaces will be assessed. Total reflectance refers to the sum of specularly reflected light and the diffuse component. Since the surfaces under study in the current work are finely polished and smooth surfaces that reflect light mostly specularly, the diffuse component is very small compared to the specular and therefore total reflection will largely present the specular surface reflection.

2.4.3 Translucency

Translucency is the property by which the light can penetrate and disperse into and/or through a material [29]. In other words, a translucent material simultaneously transmits, reflects and scatters light and has an appearance that is in between the two extremes of completely transparent and completely opaque materials. This phenomenon is schematically presented in Figure 2.6. Within the concept of total appearance, translucency has an important role as appearance of an object. A translucent object can appear different in color due to the way it interacts with the light that is the relationship between the light transmitted, the light reflected and the light scattered by the object.

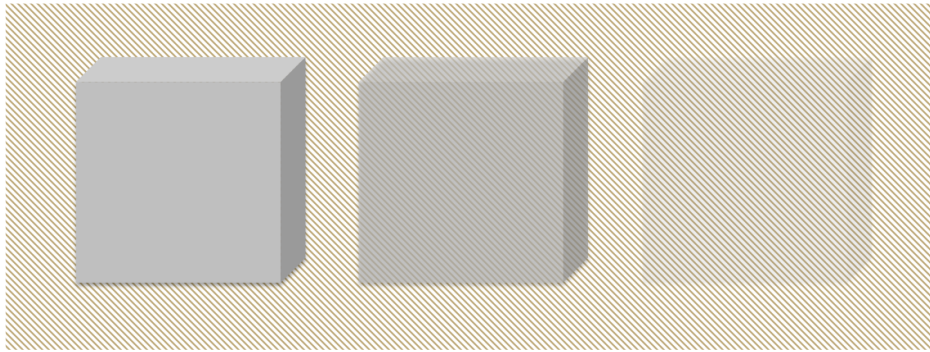


Figure 2.6: A translucent material that partially transmits light is placed between two extremes of opaque and transparent materials.

As explained earlier, typical penetration depth of light into metals is less than a wavelength and as a result bulk metals generally appear opaque. Therefore, the role of translucency is often ignored in appearance of bulk metals and it is assumed that the color is given only by the reflection of light [44]. Meanwhile, some studies have shown translucency in gold thin films. As an example, Furrer studied the penetration of visible light through thin films of gold of different thicknesses created by Physical Vapor Deposition (PVD) on a glass substrate [45]. She tested gold thicknesses of 16, 18, 60, 109, 189 and 291 nm. Gold layers of above 100 nm thick had an opaque appearance while up to 60 nm they appeared translucent. Although evident structural differences exist between bulk gold compared to a PVD deposited thin-film, this simple experiment is yet evidence of penetration of visible light into gold. Consequently, we suggest that the first few nano meters of a bulk gold material can be considered as a translucent layer that affects appearance of the metal.

This experimental results are in agreement with previous theoretical calculations presented by Leobich [4]. They also stated that thin film gold deposits transmit a remarkable amount of visible light at thicknesses below 40 nm. As seen in Figure 2.7, their results also showed that gold becomes fully opaque only at a thickness of 100 nm. Accordingly below this thickness, the gold films are translucent to a degree. This implies that visible light can penetrate few nanometers into the surface of an object in bulk gold and therefore properties of this surface layer, and not only the outer most

surface, can affect the total appearance of the object.

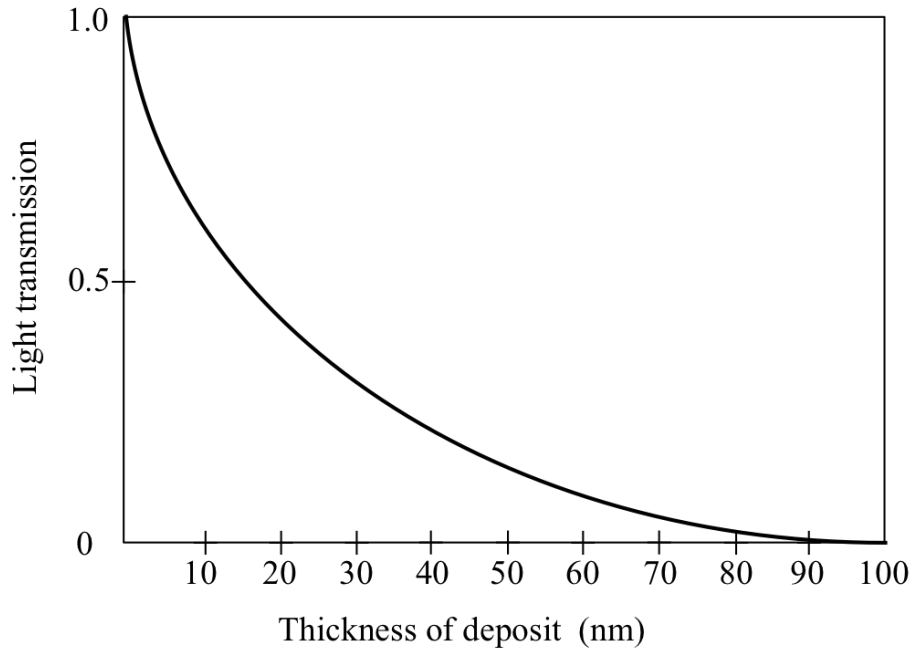


Figure 2.7: Light transmission through gold deposited thin films for a wavelength of 498 nm. The graph is adapted from [4].

2.4.4 Texture

The fourth category of surface properties to be assessed in study of surface appearance is texture. A human response to texture can be associated to the terms such as fine, coarse, grained or smooth. While texture can also be described as a variation in tone (intensity or lightness) and structure [5]. In all those cases, the words are attempting to describe a physical, topological or optical variation such as non-uniformity in tone or color. Texture is also dependent on changes in rotation, viewing distance, scale and illumination angle. However, in many cases texture is invariant to parameters such as illumination intensity. This is in contrast to color that has inverse sensitivity to the parameters mentioned here [46]. Texture is typically used to describe appearance of objects such as woven fabric, wood, granite and so on that have a clear local structure and are rarely used for describing material that have a flat appearance to the eyes [47].

The building blocks of texture can be considered as texture elements i.e. those elements of the physical surface that are perceived to be different. Texture can then be described by the number and types of primitives (also known as textons or texels) and by their relative spatial relationships (see Figure 2.8).

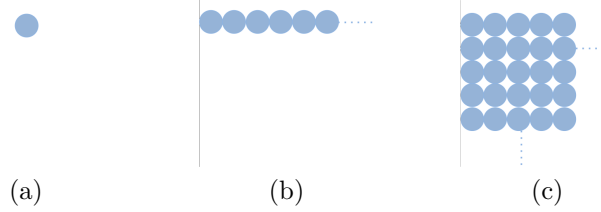


Figure 2.8: (a) texture primitive, (b) Pattern generated by a line of primitives, (c) 2-dimensional texture pattern generated by an array of lines primitives. The primitive for a texture on surface could be any surface feature, periodic holes or dust particles or stains included (adapted from [5]).

2.5 Effects of surface finish on appearance

Fine mechanical polishing is a very commonly used surface finish method. It is performed by rubbing a working piece against either an abrasive counter part in presence of lubricants or a smooth counter part with an abrasive slurry spread between the two. The aim of polishing is often achieving low surface roughness and/or bright surfaces appearance. Therefore, the term polished surface as described in ASM handbook refers to "a surface that reflects light brightly and that produces a clear image of distant objects in the manner expected of a mirror" [48].

A low surface roughness is desirable in many application for the range of beneficial contributions that it makes. Some examples could be found in food industry where most of surfaces are smoothly polished (Mechanically or electrochemically) to help with maintaining a high state of surface cleanliness [49]. Another example could be in the field of biomedical applications for dental restoration materials where surface roughness and texture have dramatic influence on plaque accumulation and in vivo wear behavior of material [50]. In many other applications however, the leading reason behind mechanical polishing and smoothing the surface is improving aesthetics.

Studies on the correlation between surface roughness and appearance, in particular brightness or gloss, are diverse in their approach. Some researchers tackle the question in terms of psychology of appearance [51], some focus on developing theories based on optics and physics of light-matter interaction (Such as [52], [53] and [54]) and many other study computer simulated surfaces [55], [56] and [57]. In the pages that will follow, we will introduce two fundamental works on theory of light scattering as a result of surface roughness and then discuss the experimental works that have been done on real surfaces.

2.5.1 Theoretical approach: light scattering from surfaces

After world war II, scattering of electromagnetic waves from rough surfaces was a topic of interest in developing radar technology and therefore lunched several scientific

researches on the topic [58]. In 21st century, scattering of light as a result of surface roughness in optical tools such as mirrors and lenses remains an attractive field of study. There have been a remarkable number of attempts in modeling the reflection from rough surfaces. However, historical theories on surface scattering specially those developed by Rayleigh-Rice [53] as early as 1951 and the one published later by Beckmann and Spizzichino in 1963 [54] are still commonly used basis for predicting the relationship between surface roughness and light scattering behavior [59].

The starting point for scattering theories that study the link between surface roughness and light scattering are Maxwell's equation. Rayleigh-Rice theory or Vector Perturbation theory considers reflectance of electromagnetic waves from a surface with small roughness's (or in Rice's words: "a surface which is almost, but not quite, flat") with random distribution of z heights [53]. This theory suggests the following relationship between Angle Resolved Scattering (ARS) and the 2-dimensional Power Spectral Density function (PSD). The former is defined as the power scattered into a small solid angle, normalized to that solid angle and the incident power. While PSD is the squared modulus of the Fourier transformation of the surface topography. The relationship between the two is given by the following:

$$ARS(\theta_i) = \frac{16\pi^2}{\lambda^4} \gamma_i \gamma_s^2 \theta_s Q PSD(f) \quad (2.5)$$

Where $\gamma_i = \cos \theta_i$ and $\gamma_s = \cos \theta_s$ with θ_i and θ_s being the incident and scattering angles respectively. Q is the angle dependent polarization reflectance. It is an optical factor that depends on dielectric function and the illumination and detection conditions (such as angles of incidence and scattering, polarization, etc.). For the Rayleigh-Rice theory to be valid, several conditions need to be met [58]:

- The illumination resembles a plane wave.
- The detector is sufficiently far away.
- Lateral size of surface features are larger than the wavelength of illuminating light.
- Wavelength of illumination light is much larger than topography heights so that secondary reflections are neglected.

While in practical conditions of visual perception and surface roughness not all these criterion are obeyed.

Beckmann gives a theory for specular and diffuse reflection of electromagnetic waves. His approach commonly known as Beckmann-Kirchhoff is valid for rougher surfaces and takes assumptions of neglecting effects of mutual interactions of surface roughness (such as shadowing and multiple scattering) as well as assuming a paraxial small angle (that limits applications to wide angle scattering and large angles of incidence). His theory suggests that specular reflection is determined by probability distribution of roughness heights while the diffuse reflection is dependent on surface slopes [60]. For

a Gaussian surface, his solution for specular reflection takes a simple form and mean reflected amplitude is given by:

$$\langle \rho \rangle = \exp\left(-\frac{1}{2}\left(\frac{4\pi\sigma \cos \theta_i}{\lambda}\right)^2\right) \quad (2.6)$$

Where ρ is the ratio of reflected light of a rough surface to one that would be reflected by smooth surface, σ is the standard deviation of heights, θ_i is the incident angle of light and λ is the wavelength of the incident radiation. The angle dependency of diffusely reflected light though takes a more complicated shape. While specular reflection depends on height distribution of surface roughness, the angle dependency of diffusely reflected light depends on the distribution of surface slopes.

In development of this model, it has been assumed that the surface is a perfect conductor. However, Beckmann and Spizzichino mention that surface roughness has a bigger effect on the spatial spread of scattered light compared to electrical properties of the surface [61]. Another assumption made here is that the radius of curvature of surface features should be large compared to the wavelength of light. Meaning that their approximation would not apply if surface has features with sharp edges or points [61].

Bennett [52] defined a parameter named total integrated scatter (TIS for short) that gives the ratio of diffuse reflection over total reflection as shown in Equation 2.7. For smooth surfaces and at normal angle of incidence, this parameter can be related to root mean square (rms) roughness through simplified Equation 2.8 [62] where σ is rms roughness and λ is the wavelength of incident light.

$$TIS = \frac{\text{diffuse reflection}}{\text{specular} + \text{diffuse reflection}} \quad (2.7)$$

$$TIS = \left(\frac{4\pi\sigma}{\lambda}\right)^2 \quad (2.8)$$

Meanwhile, several authors such as Harvey et al. [63] argue that the total root mean squared (rms) roughness in this equation must be replaced with so called relevant band-limited rms roughness that takes into account the "spacial frequency band limits of the roughness that is relevant to the particular scattering application". That is because every roughness measurement method is limited to a certain spacial frequency both by investigated surface area and the resolution of the instrument itself [64]. So a measured roughness value cannot directly be used but it should be corrected to band-width limited rms roughness for the particular application as well as the technique used. Therefore, the accuracy of such complicated calculations will depend on the quality of surface metrology inputs and the inherit limits of homogeneity and isotropy of the surface as well as spread of surface defects.

Other than the difficulties of obtaining suitable roughness parameters for accurate calculations of reflectance, the variety of assumptions that are made in order to simplify the solutions (some of which were mentioned earlier), can also make application of modeling techniques to predict behavior of technical surfaces very difficult. Therefore, in many cases it is more desirable to perform direct reflectance measurements instead or at least in addition to modeling [64]. Additionally, such direct measurements can provide information with a more clear link to appearance.

The current work is focused on the study of relationship between surface parameters of mirror-polished gold surfaces to their reflection properties. As the name suggests, these surfaces are highly polished very smooth surfaces with very low surface roughness values. Mirror like appearance that reflects a very clear image of the surrounding objects is evidence of high specular reflection as opposed to low diffused scattering from these surfaces. Accordingly, in the current study of these technical surfaces, we will make the approximation that total reflection is mostly a result of specular reflection and therefore we will not be considering the angle dependency of diffuse scattering such as the one that could be calculated by the above discussed models. Instead we will follow an experimental approach involving direct measurement of total reflectance from surfaces as a result of physical modifications to roughness. The next section will therefore discuss the existing literature on experimental approaches that are based on reflectance measurements.

2.5.2 Experimental links between surface finish and appearance

Among the experimental works, author could only find one that links surface modifications introduced by polishing to the appearance of the ternary gold-silver-copper alloy. In this study Wells et. al. [6] state that formation tarnish on precious metal alloys can occur during cleaning by some products. The removal of this tarnish layer by polishing should then be considered as a chemical-mechanical removal of material and the effect of this process on appearance should be studied. They study the chemical modifications of the surface followed by accelerated oxidation. They used 18K gold coupons with the composition of 75Au-10Ag-15Cu and studied the surface composition of mirror polished surfaces. They compared AES depth profiles of polished surfaces before (as received) and after heating and oxidizing at 150 degrees Celsius under oxygen flow. They report that as received samples show enrichment of gold in the surface and that changes in surface composition are enhanced by oxidation process. They conclude that this composition change with oxidation is the cause of distinct red-brown tarnish appearance. They assume that at ambient temperature, oxidation of copper will not be as significant as in elevated temperatures and therefore consequences of copper oxidation on appearance of 18 karat gold would be minimal at room temperature.

The results reported in this work is vivid example of a phenomenon known as surface

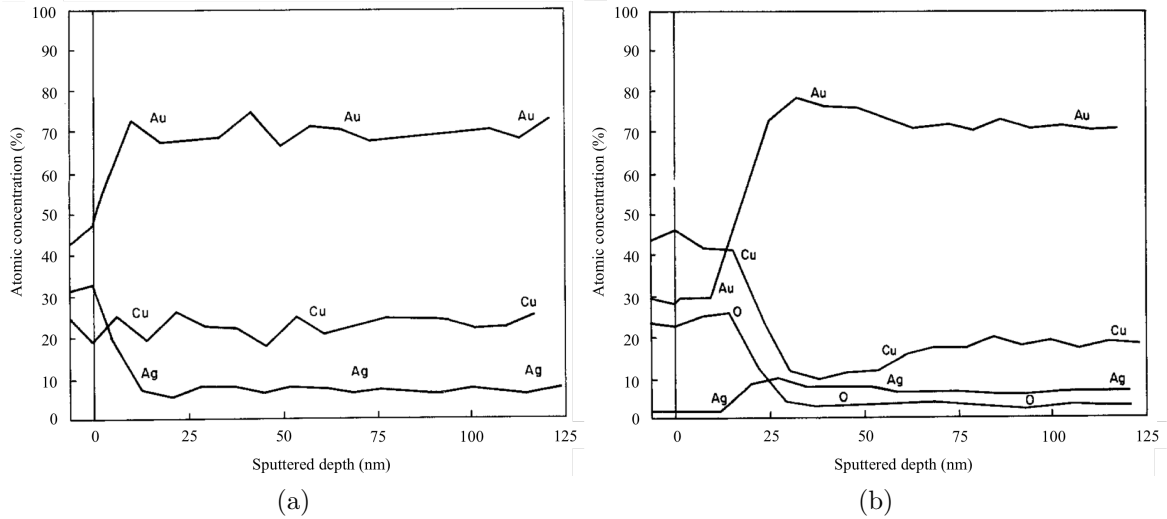


Figure 2.9: AES atomic concentration depth profiles measure on polished surface of 17Au-10Ag-25Cu (a) before and (b) after oxidation at 150 degrees Celsius. This figure is adapted from [6].

segregation. Surface segregation refers to a situation where composition of topmost surface of an alloy is different from the one of the bulk. The leading causes of surface segregation in an alloy are listed by Somorjai as the following [65]:

1. Minimizing surface free energy: for a solution, surface free energy can be minimized by segregation of the constituent that has the lower surface tension. As metals have high surface tension (compared to organic surfaces for example), this surface enrichment is likely to happen.
2. The size effect of alloying compounds: alloying elements with a radii that is remarkable different from that of the matrix introduce strain in the crystal lattice. This strain can act as a motor providing energy for segregation of these misfitting atoms on the surface in order to reduce surface free energy. However, in cases of very stable compounds that have high energy lattices, the bulk composition can pin the surface and keep it identical to the bulk because the energy needed to modify surface composition is too high.
3. Formation of compounds: chemical reaction with gases or impurities: if an alloying element forms chemical bonds with gases or impurities (such as oxygen, carbon, sulfur or calcium), the compound can accumulate on the surface. In this way a binary alloy can turn into a three component system with a different composition on the surface.

While the first and second driving forces are intrinsic to the alloy properties, the third one can come from the process of fabrication and surface finish. Process of fabrication of a product or even only the surface finish, exposes the surface to different active environments and various temperatures. These factors can modify the surface of an alloy and its chemical composition and therefore contribute to creating a composition gap between bulk and surface. In the case of an alloy such as jewelry gold that contains

a very noble metal together with a active metal such as copper, the most active metal is prone to chemical reaction and formation of compounds.

A study by Nelson [66] on surface composition of gold-silver alloys also gives an example of such surface segregation. He measured surface composition of two mirror polished Au-Ag alloys that contained 30.5 % and 64.7 % of gold by low-energy ion-scattering spectroscopy and found only 15.5 % and 42 % gold on the surface in respective order.

This potential gap between surface composition and bulk composition is though neglected in some other works. An example is a study by Yonehara et al. [67] on the relationship between surface roughness, glossiness and color. They modify the surface roughness of samples made of several alloys either based on aluminum for achromatic colored metals or copper for chromatic colored metals. They correlated L^* and the color tint to R_a (calculated with cut-off length). They concluded that lightness increases with increase in roughness of all their samples. They also correlate roughness values of colored alloys to color without considering the surface chemical composition and suggest that smoothing the surface causes a bluish tint.

Van Gorp et al. [68] studied the effect of grinding non-conductive polypropylene surfaces against a range of SiC papers on their roughness and brightness. They measured specular gloss with a three-angle glossmeter and report it as a percentage compared to a calibrated black mirror as reference sample. They demonstrate the increasing trend in specular gloss (brightness) by the decrease in R_a values. Although the roughness parameter under study here is R_a and not rms, it is evident that in these experimental results, the relationship between specular gloss and roughness is not exponential as theoretically expected from 2.8.

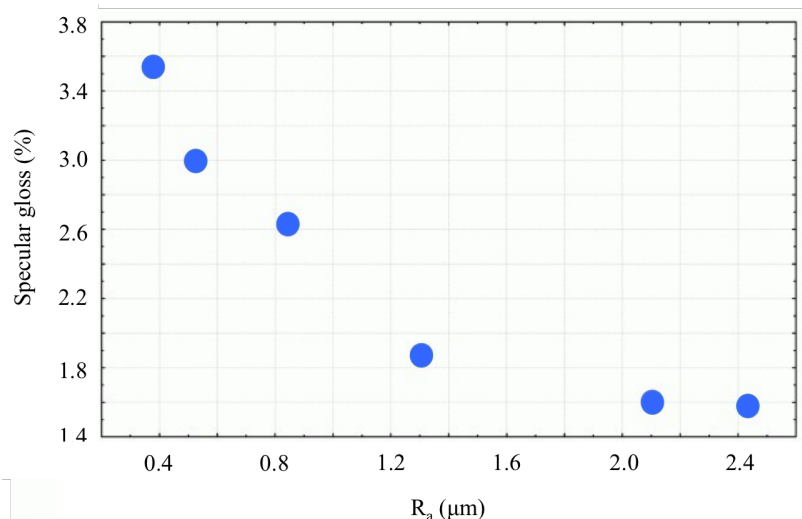


Figure 2.10: Specular gloss values of ground polypropylene surfaces at incident angle of 60 degrees versus R_a roughness values (adapted from [3]).

If we consider continues contact with human skin as a form of polishing process, we

can include the study of Fredj et. al. [69] who looked at the problem of discoloration in several commercial copper alloys as a result of contact with hand skin and sweat. They used a hand baton that was in non-continuous contact with human palm for two years and checked degradation of shiny appearance for copper and four of its alloys: copper (at 99.9% purity), cartridge brass, bronze, copper nickel and nickel silver. After the test period, they assessed the visual appearance of the five samples and found out that the first three were exhibiting a dull surface while the last two remain bright. Chemical analysis showed similar thickness and composition of surface oxide layer. However, the surfaces had different degree of porosity typically in sizes from 0.1 to 1 micrometer. They concluded that the diffuse light reflection caused by surface roughness and porosity was responsible for the non-glossy (mat) appearance.

2.6 Summary and conclusions

Aesthetic aspects of a luxury product are key in customer appeal. Meanwhile, understanding the fundamentals of how humans visually perceive objects and the factors that make an object aesthetically appealing remain challenging topics. Topic of appearance is the part of the domain of visual perception that involves the outcome of light/matter interaction that reaches our eyes. Analyzing appearance is the pathway to the goal of this work that is linking surface features to visual perception

The framework proposed by National Physics Laboratory (NPL) is a valid starting point for assessing appearance. In this framework four parameters of gloss, color, translucency and texture are proposed as measurable properties to assess appearance. Despite the suggestions of the framework for measurement methods, the definitions and the choice of measurements techniques for most of these parameters need to be advanced. Also the quantitative links between these properties and aspects of appearance are not provided. Consequently, the current study aims at developing a toolkit of measurement techniques that are tailored for application in polished jewelry gold surfaces. It also seeks to provide quantitative correlations between surface features and aspects of appearance.

The literature on quantitative appearance of surfaces is limited and it fails to present a global image that considers a combination of all involved factors. Consequently, a global link is missing for the concerned industry between appearance (or imperfections in appearance) of mirror polished surfaces to the relevant surface features generated during process of manufacturing and surface finish. Accordingly, in the current work the multifaceted consequences of preparation steps (particularly mechanical polishing) on appearance of a mirror-polished watch or jewelry component made of 18 karat gold alloy will be studied.

The next chapter will begin by studying industrially produced gold polished surfaces to discover the kind of surface features that are induced on a technical surface of a

product from the industry.

Chapter 3

Characterization of watch components

In this chapter, polished surface of two watch components in 5N jewelry gold are characterized. The goal of this characterization is to identify potential sources of aesthetic defects. Two samples that have been judged by experts in the company are compared. One of the pieces has successfully passed the visual judgment and the other has failed and not been accepted. Several physical and chemical surface properties are studied and following imperfections were recognized: variations in surface roughness, presence of porosity, surface contamination, inhomogeneity in microstructure and hardness and finally differences in color and reflection.

3.1 Introduction

As discussed in Chapter 1, appearance of a surface can be evaluated through assessing four groups of characteristics including color, gloss, translucency and texture. This chapter will be looking at physical and chemical surface properties that could potentially affect these parameters and therefore appearance of polished gold surfaces.

In order to find surface properties or defects related to defective appearance in watch and jewelry components, two pieces will be studied and compared one of which has a defective appearance and the other has a flawless appearance. The chapter starts by introducing the material under study and then explain all the characterization methods that have been chosen and were used for analysis. Finally, results of these characterizations are presented and discussed.

3.2 Material

Watch dust cover is an extreme example of upmost surface quality. It is an external component of a watch that is used in certain models as a closure on the backside of the watch case. While open, it can reveal the movement of the watch and while closed it provides a discrete protection. The reason why the dust cover is an extreme showcase of the level of visual quality that can be obtained by polishing is that it is composed of a large circular flat bottom (typically around 30 mm in diameter) with concave edges. The curved edges make mechanical polishing of the flat interior surface very challenging and the large mirror polished surface makes the smallest defect in appearance clearly visible to the eyes as there is no form, texture or pattern to mask it. Therefore, this piece has been chosen as the reference industrial sample for the study of appearance of a mirror polished 18K gold surfaces for watch components.

Two such samples have been studied and compared here. Both pieces are made of 18 karat rose gold alloy containing 75wt% gold, 4.5wt% silver and 20.5wt% copper. Accordingly the atomic fractions of the three alloying elements are the following: 51.1%Au, 5.6%Ag and 43.3%Cu. These pieces have been examined by quality controllers at the production line. One of them has consequently been judged as flawless and the other is judged to be defective. The kind of defect is described as a stain so called bright ring that appears in the approximate location schematically marked between two dashed circles in Figure 3.1.

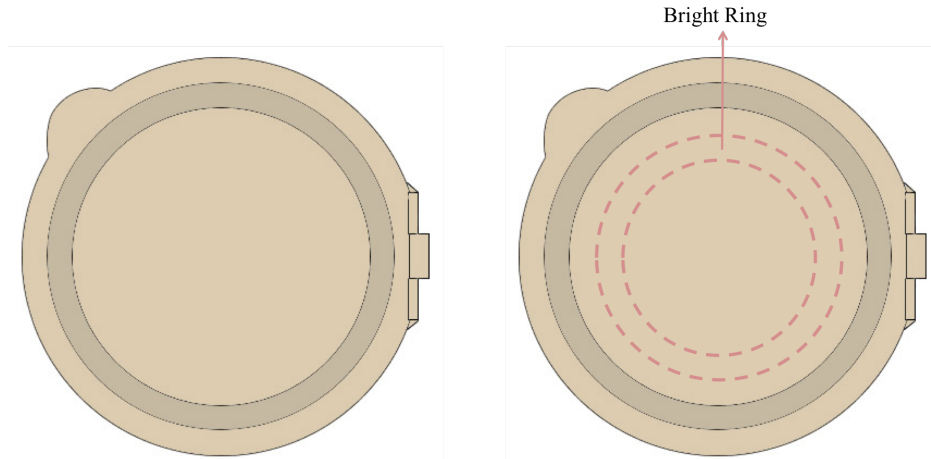


Figure 3.1: Two watch dust cover pieces that have been characterized in this study. One that has been judged to be acceptable by visual experts in the industry and the other who has been rejected due to diagnosis of a defect specified as bright ring. The boundaries of this defect approximately lies between two dotted circles that have been marked on the surface.

3.3 Methods

The next step of the work has been making the choice of characterization methods to study the as-received status of these samples. The goal is to identify features that could appear on the surface or right below it and potentially affect the appearance. In this study the following aspects of the surfaces were studied:

- Surface topography
- Chemical composition
- Microhardness
- Reflection and color

For characterizing each of these properties, the instrument that was used and the measurement protocol are presented in paragraphs that follow and the results of the analyses will be discussed in Section 3.4.

3.3.1 Topography and surface roughness

3D topography measurements

Profilometry is a technique for morphological study of a surface. Two non-contact instruments were used in this study to analyze the shape and surface topography of the watch covers. The first one is an Altisurf 520 white light interferometer by Altimet with a vertical resolution of 22 nm and a motorized table that is suitable for measurement over large areas. This instrument has been used to study the shape of

the piece rather than small scale topography.

White light interferometry is a non-contact method of surface topography measurement. It takes advantage of constructive and destructive wave interference principle to estimate the height distribution of surface points. The light emitted by the source is divided into two reference and measurement beams. The former passes directly through a reference mirror and the latter is guided towards the surface where it gets reflected back to the reference mirror. From here, both beams will arrive to the CCD image sensor where they form an interference pattern. From the interference pattern, the travel distance of light and therefore the height of the surface points can be calculated.

Meanwhile, surface topography and roughness parameters were measured using a Keyence VK-X250 3D laser scanning confocal microscope with higher spatial resolution compared to the Altisurf white light interferometer. The Keyence laser scanning confocal microscope has a white light source and a short-wavelength laser source and can be used to produce three types of images. The first type is a conventional optical microscopy image produced using the light source. The laser beam is used for producing laser intensity images and 3D surface topography images. The principal of measurement with the laser is the following: first a range for measurement in height (Z) is defined. Then at a fixed height, the laser beam scans the area within the field of view of an X-Y optical scanning system. Next, the objective moves one step in Z and the X-Y scan is repeated. This process is reciprocated to cover the whole defined range of Z and the results are compiled in one image. During this process, both the reflected laser light data and color information data are recorded for each individual pixel. The color data obtained from focused positions is used to create a color image showing the height differences (3D surface topography) [70].

Roughness measurement

A 2D surface profile is essentially a line profile of surface heights that can be measured using the profilometer introduced previously. Considering that $z(x)$ is the height of any point on a line, average value of z over a distance of L can be calculated using the following equation:

$$\bar{z} = \lim_{L \rightarrow \infty} \frac{1}{L} \int_{-\frac{L}{2}}^{\frac{L}{2}} z(x) dx \quad (3.1)$$

Roughness of the surface can be defined as deviations from this average value. The most commonly used roughness value in industry is arithmetic average roughness R_a and is given by Equation 3.2.

$$R_a = \lim_{L \rightarrow \infty} \frac{1}{L} \int_{-\frac{L}{2}}^{\frac{L}{2}} |z(x) - \bar{z}| dx \quad (3.2)$$

Another very common surface height average is the root mean square (rms) roughness or R_q which is as well defined as deviations of surface height from the average (mean) surface:

$$R_q = \left(\lim_{L \rightarrow \infty} \frac{1}{L} \int_{-\frac{L}{2}}^{\frac{L}{2}} [z(x) - \bar{z}]^2 dx \right)^{\frac{1}{2}} \quad (3.3)$$

These definitions assume that length L is infinite. Obviously this cannot be the case in a measurement. In a typical roughness measurement there can be features with spatial frequencies larger than the length of the measurement. Therefore, it is important in each practical case to measure a long enough profile to contain the spatial frequencies of interest. The lower end of length spectrum would depend on the inherent limit of measurement technique that is used as well as the distance between two measurement points.

It must also be noted that tilt or curvature in the surface affects the roughness values that are calculated by Equations 3.2 and 3.3. In addition to the question of shape, there are other complications about expressing surface roughness in only one value. A simple and well-known example of such complications is illustrated in Figure 3.2 where two different profiles present the same R_a value. In summary, surface roughness parameters such as R_a and R_q are very convenient factors specially in industrial context as they are easy to measure and understand. However, due to several imitations (some of which were stated here) expressing one such value to describe the topography and the roughness of surfaces would in be insufficient. All the calculations for roughness parameters that will be later on reported, are performed by the profilometers' software and the values can be directly extracted.



Figure 3.2: The two profiles (a) and (b) have the same R_a values.

Surface roughness also much depends on the length-scale at which the roughness is studied. Features scaling from atomic size to the entire size of a sample affect roughness values. Taking into account the length-scale of surface roughness, provides a better understanding of surface topography and surface texture. A method called variable length scale analysis (VLS) was developed by Chauvy et al. for quantifying length-scale dependence of surface roughness [71]. This method is composed of the five following steps:

1. Choosing a length interval along the x-axis, starting with a small segment of the profile length.
2. Performing a linear least square fit on the selected interval and calculating the roughness value.

3. Moving the interval point by point through the entire length of the profile and repeating step 2 for every interval position.
4. Calculating average roughness value and standard deviation for the all the interval positions.
5. Repeating steps 2-4 for increasing interval lengths

In this study VLS method was applied to the roughness profiles using a software named Scale crawler V3.11 developed by Chauvy.

Scanning Electron Microscopy (SEM)

A Zeiss Merlin microscope was used. SEM images are taken at a voltage of 3 kv with a secondary electron detector at a typical working distance of 6 mm (5.9 -6.2 mm) with aperture size of 20 μm .

3.3.2 Chemical composition

Chemical analysis were performed using two measurement methods namely X-Ray Photoelectron Spectroscopy (XPS) and Auger Electron Spectroscopy (AES). Both devices take advantage of characteristic electron binding energy of atoms to detect their presence on the surface. As chemical analysis is core to this work, these two methods will be introduced in more details.

X-ray photoelectron spectroscopy (XPS)

X-ray photoelectron spectroscopy is able to provide elemental and chemical status information of all elements from lithium to uranium at the outer 5-10 nm of a solid surface. At its core, a XPS setup has three main composing elements including an X-ray source, a chamber (typically under vacuum) and an electron energy analyzer. The basic principal of the measurement is irradiating a sample with X-Ray waves of a specific energy to excite electrons from the surface of the material. As a result, some electrons are ejected from the sample surface. A detector filters these electrons by energy and records the intensity of the signal. Resulting energy spectra presents peaks that correspond to the electronic structure of atoms that are present at the surface of the sample.

As previously mentioned, interpretation of a XPS data also provides information about chemical state of the material because binding energies of electrons are affected by the chemical status of the elements (meaning the surrounding of an atom). If an atom A is bound to a strongly electron withdrawing atom B, core electrons of atom A will have increased binding energies. This means that binding energy will increase when the chemical state number increases. In contrast, core electrons of atom B will have

decreased binding energies.

In the current work, XPS analysis has been performed using a PHI Versa Probe II scanning XPS microprobe (Physical Instruments AG, Germany). Measurements were carried out using a monochromatic Al $K\alpha$ X-ray source with 24.8 W power and a beam size of 100 μm in diameter. Binding energies were calibrated by setting the carbon 1s peak energy at 284.8 eV.

While XPS provides valuable insight into chemical composition and bonding status components, this information are measured and averaged over a rather large window of 100 by 100 microns. Moving on to AES analysis with a measurement spot size of 10 by 10 nm, can give more detailed and localized information. Moreover, AES analysis is more sensitive to certain elements.

Auger Electron Spectroscopy (AES)

Auger electron spectroscopy is a surface-sensitive analysis technique. This technique takes advantage of Auger electrons that are emitted from a surface when it is excited by an incident high energy electron beam. These Auger electrons have characteristic energies that appear as peaks in intensity over the spectrum of energy that is scanned. Escape depths of these electrons are only less than 5 nm and thus this technique is very surface sensitive.

A secondary electron detector and an ion gun provides two very important additional advantages. First one is the possibility of high resolution imaging of the surface and mapping the surface composition over this image to obtain very local information about composition. The second privilege with such instrument is that chemical analysis steps can be altered with steps of surface sputtering using the ion gun. This process allows access to in-depth chemical composition of the material. The process of chemical depth profiling is schematically outlined in Figure 3.3. It shows that after every step of chemical measurement, the sample is bombarded with ions that remove atoms from the surface at a rate that can be calibrated depending on the energy and current of the ion gun.

The instrument used in this study was a PHI 680 scanning Auger microscope (Physical Instruments AG, Germany) equipped with a scanning electron microscope and an argon ion gun. The measurements were done at a voltage of 10 kV and a current of 10 nA for the electron gun and a voltage of 1 kv and 500 nA for the ion gun with a spot size of 4 mm by 4 mm. Profiles are measured on points and the spot size of the measurement is less than 35 nm. The sputter rate at these settings was calibrated to be equal to 0.5 nm/min for physical vapor deposited gold coating on silicon wafer.

The kinetic energies of the peaks and sensitivity factors that were used for calculation

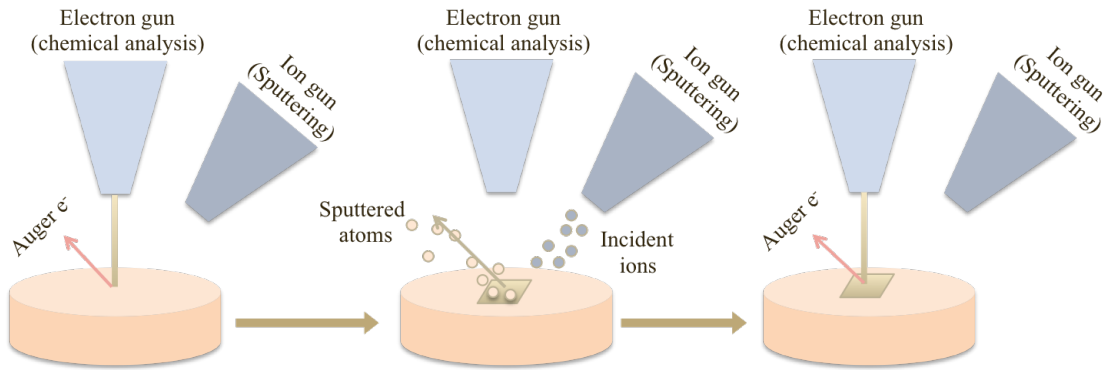


Figure 3.3: Schematics of auger spectroscopy combined with surface sputtering. Combining the two operations allows access to in-depth chemical composition of the samples.

of atomic concentrations are listed in Table 3.1.

Table 3.1: Kinetic energies of AES peaks and sensitivity factors that were used for calculating atomic concentration are listed (extracted from [8]).

Peak	Kinetic energy (ev)	Sensitivity factor
Au MNN	74	1.9
Ag MNN	359	1.85
Cu LMM	922	1.25
C KLL	275	-
O KLL	510	-
S KLL	153	-

3.3.3 Microstructure

Fabrication of dust covers starts with sheets of gold alloy that are punched into disks. The process that these disks follow afterwards to turn into a watch component is long and is composed of several steps with high-degree of mechanical deformation (such as cold stamping), several cycles of heat treatment, many steps of machining and material removal and finally mechanical mirror polishing of the surfaces by hand. During this process of fabrication, properties such as hardness, malleability, stiffness and toughness play key role in how conveniently a piece of raw metal can be shaped into the final product. Microstructure of the metal obviously has a significant role in determining all those material properties. For obtaining reliable and reproducible results, specially in forming and polishing procedures, dispersion of grain sizes and the uniformity of the microstructure (and therefore potentially uniform mechanical properties) across a piece are desirable.

Because the shape of a dust cover (except for some features at the very external edges) is symmetrical, the process of fabrication of the piece is as well symmetrical around the central axis of the piece. Therefore, for the study of microstructure the dust cover

has been cut in two perpendicular diameters and the cross section of only one quarter will be studied (over the radius). Figure 3.4 schematically shows sample preparation method. The cut quarter of the disk is embedded in Durofast epoxy resin by Struers using hot mounting. The obtained cross-section is then polished with grade 4000 grinding paper followed by mirror polishing performed on nap with 1 micrometer liquid diamond suspension (LDP by Presi LTD). Polishing the sample with an extra step of 0.03 micrometers colloidal silica particles in water (by Presi) reveals the microstructure of the gold alloy.

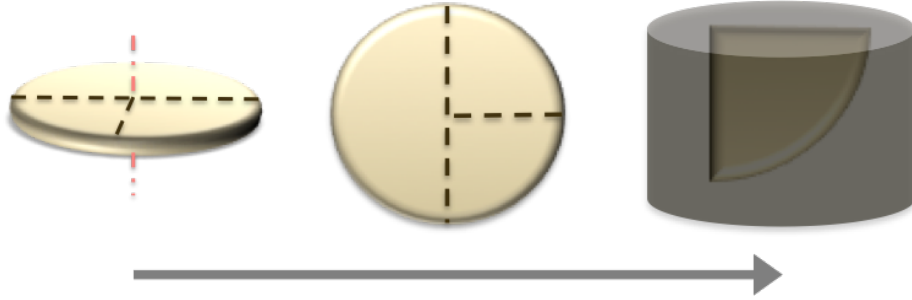


Figure 3.4: Sample preparation steps to study the microstructure of watch pieces over the cross section.

3.3.4 Microhardness measurement

The hardness was measured using a Leitz Vickers micro hardness tester. Applied load was 100 g and the hardness values were calculated by measuring the diameters of the indent using Keyence profilometer and by implementing the following equation:

$$H_v = \frac{1.8544P}{d^2} \quad (3.4)$$

Where P represents the applied load in kg and d is the average of the two diagonals of the imprint in mm and therefore, H_v is in kg/mm^2 .

3.3.5 Reflectance and color measurements

Spectrophotometry is the quantitative measurement of the reflection or transmission properties of a material as a function of wavelength. Accordingly, the two main composing elements of a spectrophotometer are a spectrometer for producing light with adjustable wavelength (often in the range of UV to Visible light), and a photometer for measuring the intensity of light. In this study, measurements are performed for the light wavelength between 400 nm and 700 nm (the visible range) using a Shimadzu UV-VIS reflectometer with integrated sphere in configurations shown in Figure 3.5. Two measurements at 0 and 8 degrees have been performed. The measurement angles of the instrument are fixed and limited to the two above-mentioned values and

to switch between the two, it is necessary to move sample from one opening on the sphere to the other. The window of measurement at all times is 2 mm by 3 mm which is the minimum size to have a high enough signal to noise ratio.

The first measurement is performed at 0 degree where the sample is placed in front of the incident light window and reflected light is concentrated on the detector using the collection sphere coated by barium sulfate. The obtained value is the relative reflectance of the sample compared to the reflectance of the reference standard white board as perfect diffuser, which is calibrated to 100% reflectance. This step of calibration is performed before every set of measurements. In this setup, when incident light makes an angle of 0° with respect to normal to the sample surface, specularly reflected light exits the integrating sphere and is therefore, not collected. As a result, at 0 degree of incident only diffusely reflected light is measured while at 8 degree of incidence light, the sum of specular and diffused reflectance will be measured. Even though measuring a diffuse or specular components separately can provide very interesting information about the gloss of an object, in real world application our visual perception would be a simultaneous combination of the two. Therefore, in future sections of this work, total reflection would be more commonly discussed.

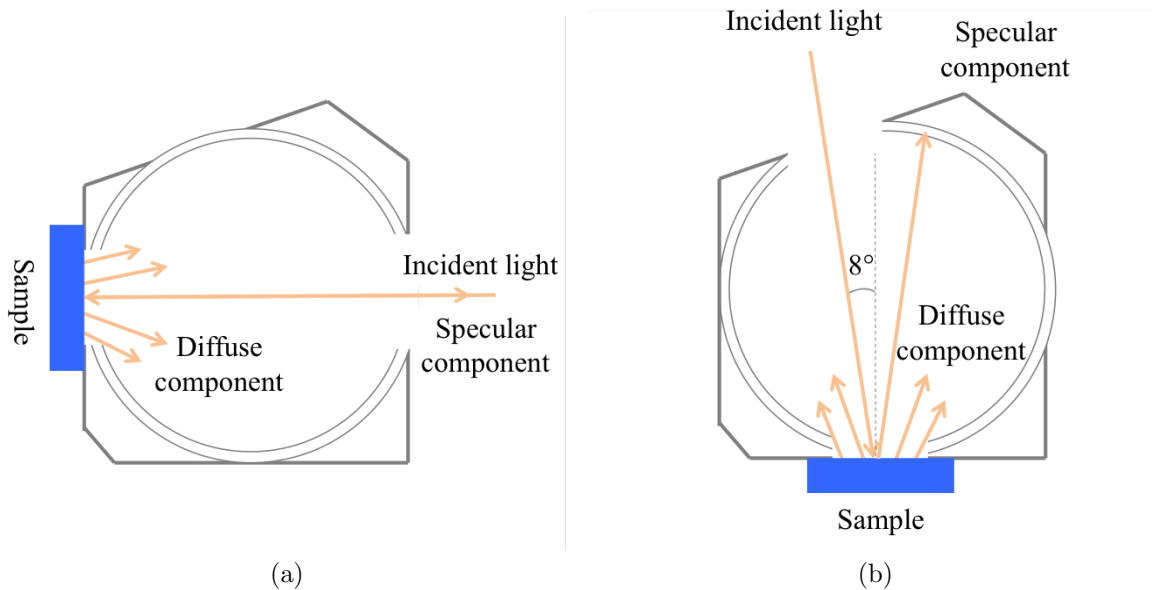


Figure 3.5: Schematics of reflectance measurement set up: (a) diffuse reflectance measurement at 0 degree of incidence and (b) total reflectance measurement at 8 degree of incidence. Figure is adapted from [7].

3.4 Results

In this section, outcomes of all the measurements methods described previously will be presented and discussed in respective order.

3.4.1 Surface topography and roughness

Figure 3.6 shows the results of measurements with Altisurf interferometer on the good and the bad piece. 3D measurement of the piece is run over the half circle and a line profile has been extracted over the diameter. From 3D images shown in Figure 3.6 (a) and (b), it is evident that despite what appears to naked eyes, flat bottom of the samples are not completely flat. This deviation from flat surface occurs both in the good watch cover and the bad one. However, it is more pronounced in the defective piece. On each piece, 2D profiles show two different slopes from the center towards the edges. The variation in height though is quite small being equal to approximately $70\text{ }\mu\text{m}$ for the good piece and $85\text{ }\mu\text{m}$ for the bad piece over a length of 30 millimeters.

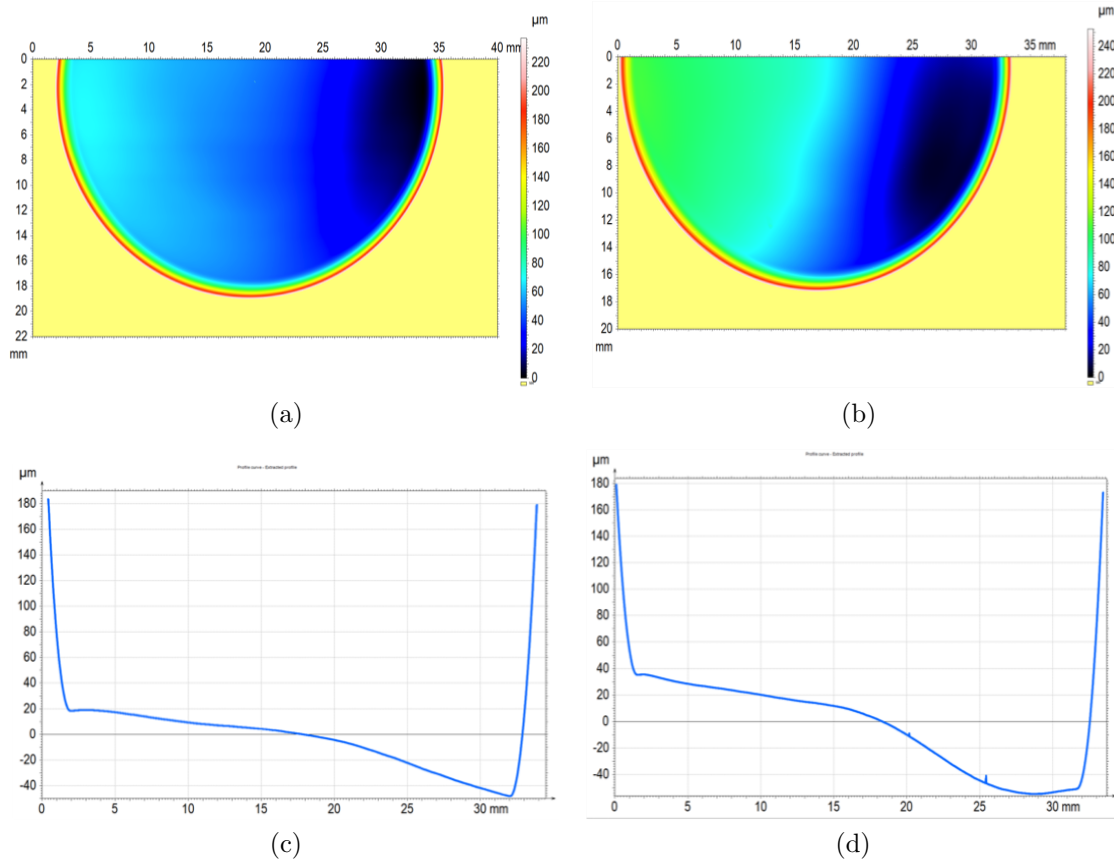


Figure 3.6: Surface profiles are measured over half of the circular shape of the pieces. (a) and (b) show 3D surface profiles while (c) and (d) show a line profile across the diameter of flawless and defective pieces respectively.

For more focused local analysis with higher resolution, the laser scanning confocal microscope was used. Figure 3.8 shows optical images and 3D surface topographies that were obtained at magnification of 50X on the flat bottom of samples for the good and the bad piece. Measurement results are shown for two locations that are marked in Figure 3.7 as location 1 and 2. Laser images were also obtained and used for calculating surface area fraction of holes on the surface. The surface area fraction of the black spots for the bad piece is 0.2% compared to 0.03% for the good piece. The surface area fraction is calculated by finding a threshold in the gray-scale of the images that corresponds to the dark spots. In the next step image is binarized into black and

white for values that are below and above this threshold using VK Analyzer which is a dedicated software of the profilometer. Finally, the surface area fraction can be calculated by dividing the number of pixels that represent the dark spots over the total.

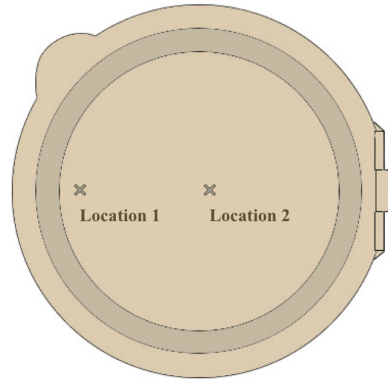


Figure 3.7: Schematic markings of the locations where laser and 3D images are obtained.

On the 3D images it can be seen that most of these spots appear in dark color in height scale and therefore, correspond to holes. Figure 3.9 shows the same measurements done in the center of the watch cover (location 2 as marked on Figure 3.7). The results are very close to the ones already discussed. The surface area fraction of holes were measured to be 0.12 % for the bad piece and 0.02 % for the good one.

If these holes are considered as black holes that do not reflect any light, it could be contemplated that the percentage of loss in lightness of a surface with holes would be equal to surface coverage of holes. That would mean that the highest detected amount of holes would result in a loss of 0.2 % in lightness and therefore giving rise to a $\Delta E^* = 0.002$. This value is far below visible ΔE as mentioned in literature (2.3). The effect on other NPL parameters (gloss, texture and translucency) is at present more difficult to assess. Our experimental scattering on reflectance measurements are larger than 0.2% and therefore it appears that holes should not play a crucial role in scattering of light. The effect of holes on texture is already included in the roughness measurements. And there is no obvious reason that holes affect translucency of the bulk material. Therefore we conclude that the amount of holes present on the relevant surfaces does not create a visible defect in appearance.

R_a and R_q values are extracted from the 3D topography measurements and the results are shown in Table 3.2. Line roughnesses are measured over a length of 285 micrometers with a distance of $0.280 \mu\text{m}$ between every two points with values averaged over three measurements. Defective sample shows higher roughness values towards the edges while both samples have similar roughnesses in the central location.

Table 3.2: Roughness values averaged over three line measurements are presented for two locations (as marked in Figure 3.7) on the surface for each piece.

	Location 1		Location 2	
	R_a	R_q	R_a	R_q
Flawless piece	16 nm	18 nm	15 nm	18 nm
Defective piece	20 nm	23 nm	14 nm	18 nm

Variable length-scale analysis

Variable length-scale analysis (VLS) was performed on profiles obtained with Keyence instruments that are $710\text{ }\mu\text{m}$ in length and the distance between every two measurement points are $0.567\text{ }\mu\text{m}$. Results are presented in Figure 3.10 in double logarithmic scale. The lines show the average roughness value and the bars represent the standard deviation in the measurement. It can be seen that at location 1 near the edge of the sample, the two samples have similar roughness profiles over different length scales with defective piece having slightly lower values. However, in location 2 at the center of pieces, defective piece has higher roughness values at all scales.

Scanning Electron Microscopy (SEM)

SEM images of polished surfaces are shown for both pieces in Figure 3.11. At magnification of 1000 times, both surfaces are very smooth and almost featureless. Few scratches start to appear only at higher magnification images. Meanwhile, Figure 3.12 shows SEM images of microstructure of the two pieces on the top surface in the center of the pieces. Figure 3.13 presents examples of holes that were previously recognized by laser imaging in a close up. SEM studies also confirmed that the holes can more frequently be found on the surface of defective piece compared to the acceptable one. It also shows that the holes are bigger in size for the defective sample. Yet, the total surface area fraction remains very low.

Figure 3.13 (c) and (d) show very clearly the peculiar shape of these holes. It appears that some materials are smeared into the holes. Polishing scratches can also be partially traced on this material. The surface shown in Figure 3.13 (d) appears to be one such hole that is buried below the surface. Top surface has created a step by partly sinking into the hole but it has not fully collapse and has stayed attached on the borders to surrounding surface.

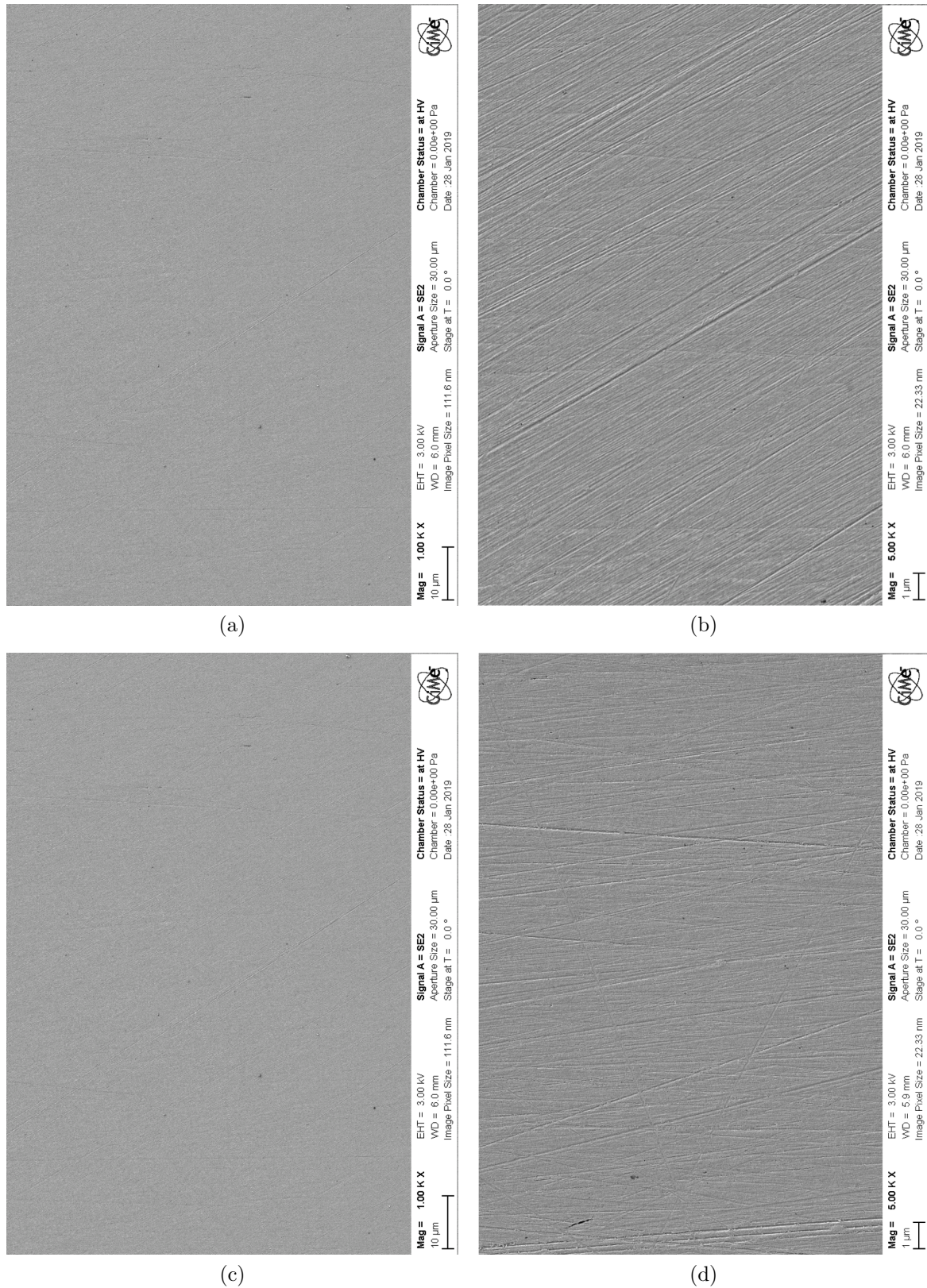
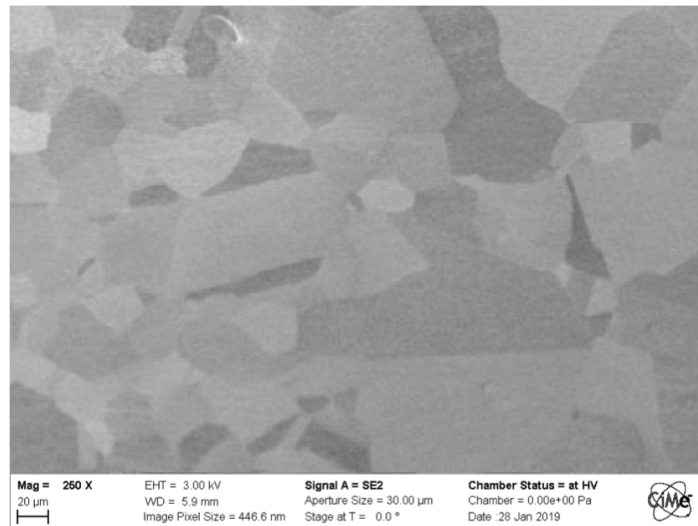
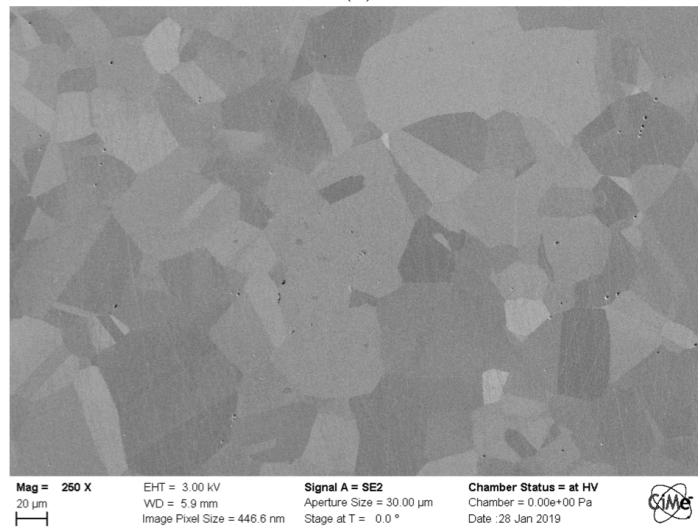


Figure 3.11: SEM images of polished surface at different magnification of (a) and (b) the flawless piece and (c) and (d) the defective piece. The difference in microstructure between the two samples may result from a difference in their thermomechanical history during manufacturing.



(a)



(b)

Figure 3.12: SEM images of microstructure as seen from the top surface at the center of pieces for (a) flawless piece and (b) defective sample.

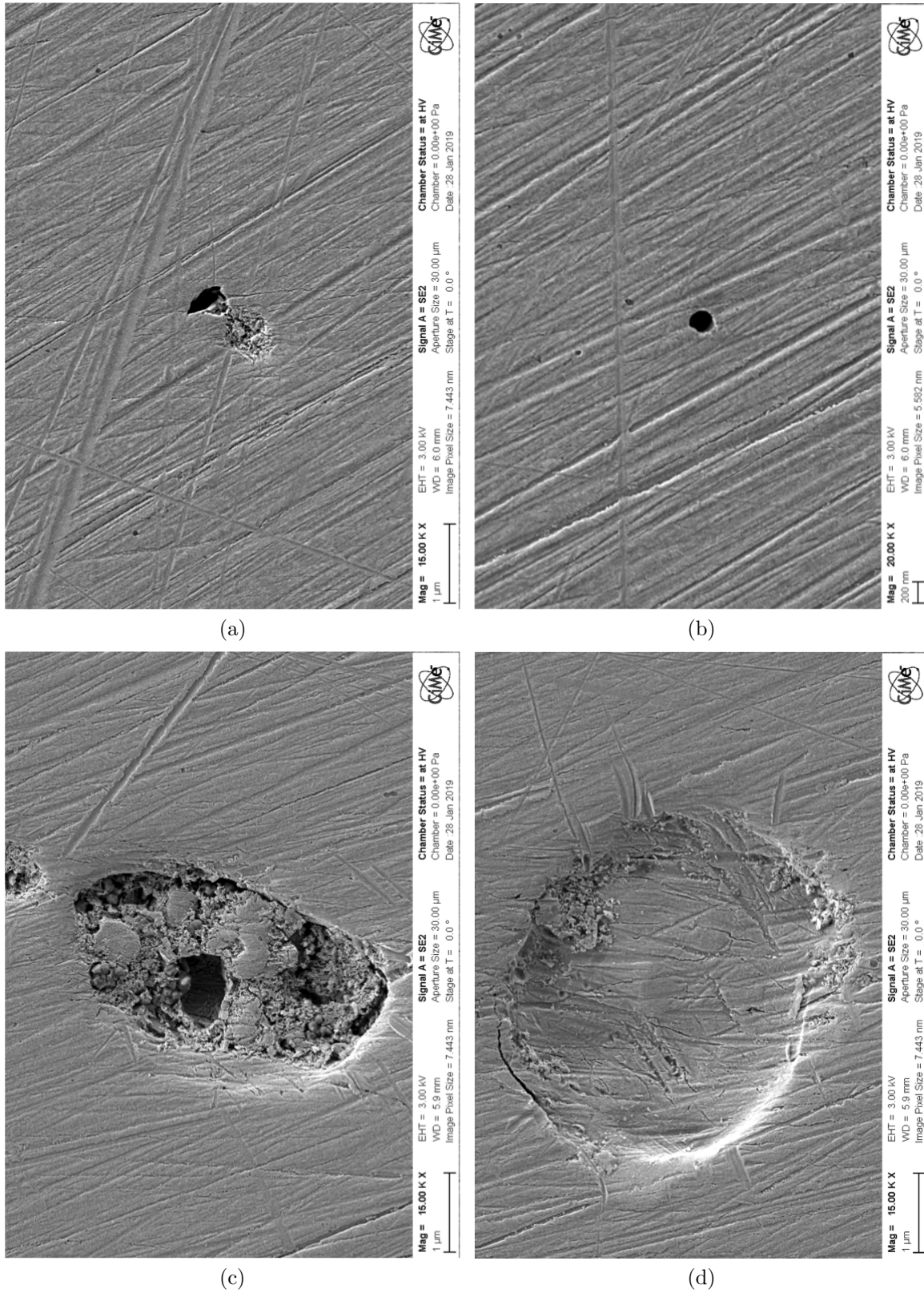


Figure 3.13: SEM images of examples of holes that can be found on polished surfaces of (a) and (b) flawless piece and (c) and (d) the defective sample. The holes that are found on the defective sample are typically bigger in size and they are detected with higher surface area coverage as well.

3.4.2 Chemical composition

X-Ray Photoelectron Spectroscopy (XPS)

In the initial survey performed on the watch dust covers both on accepted (or flawless) and rejected (or defective) pieces. A spectra of intensity signals over the scanned range of binding energies is shown in Figure 3.14 and binding energies of the metals in their elemental and oxide states are listed in Table 3.3. In addition to the three main composing metals of the alloy, carbon and oxygen were also spotted on the surface. These two elements are generally attributed to organic surface contamination. To check homogeneity of the surface, XPS measurements are performed on three spots on each sample. Figure 3.15 shows intensity peaks for the above mentioned elements present on the surface of the flawless piece. Color of the curves correspond to the locations where the measurement was done and this is indicated on the schematics of the piece.

Table 3.3: Binding energies of three alloying elements and their oxides [9].

Peak	Binding energy (ev)
$Au\ 4f_{7/2}$	84
$Ag\ 3d_{5/2}$	368.3
$Ag\ in\ AgO\ 3d_{5/2}$	367.4
$Ag\ in\ Ag_2O\ 3d_{5/2}$	367.8
$Cu\ 2p_{3/2}$	932.7
$Cu\ in\ CuO\ 2p_{3/2}$	933.6
$Cu\ in\ Cu_2O\ 2p_{3/2}$	932.5

It is observed that gold and silver present sharp peaks at the binding energies that correspond well to their metallic form. However, for copper, carbon and oxygen a shoulder is visible next to the sharp peak. Such shoulder is indication of presence of these elements in a different chemical compound form.

Similar measurements have been performed on the defective sample and results are presented in Figure 3.16. Three points are chosen in such way that they represent chemical composition at the edge of the bright ring, inside the bright ring and near the center of the sample. Here again, the same phenomenon as evident with copper, carbon and oxygen peaks. It is interesting to note that the different degrees of oxidation of copper seen in Figure 3.15 has apparently no influence on the appreciation of the expert of the visual quality.

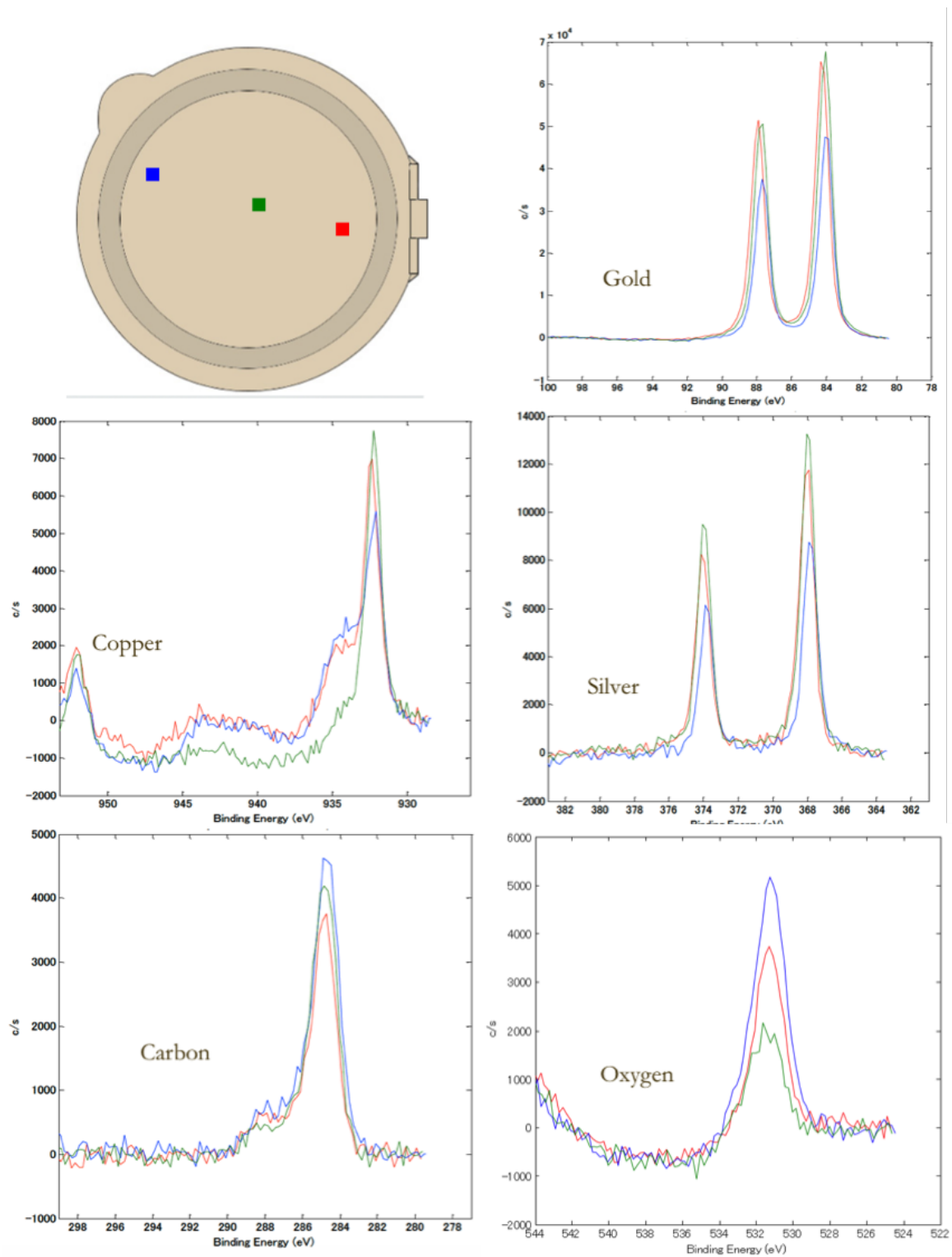


Figure 3.15: Intensity peaks of gold, silver, copper, carbon and oxygen for the watch component that was accepted by visual quality experts. The color code of positions marked on the piece correspond to the color of measurement curves. The oxygen peak is not background corrected.

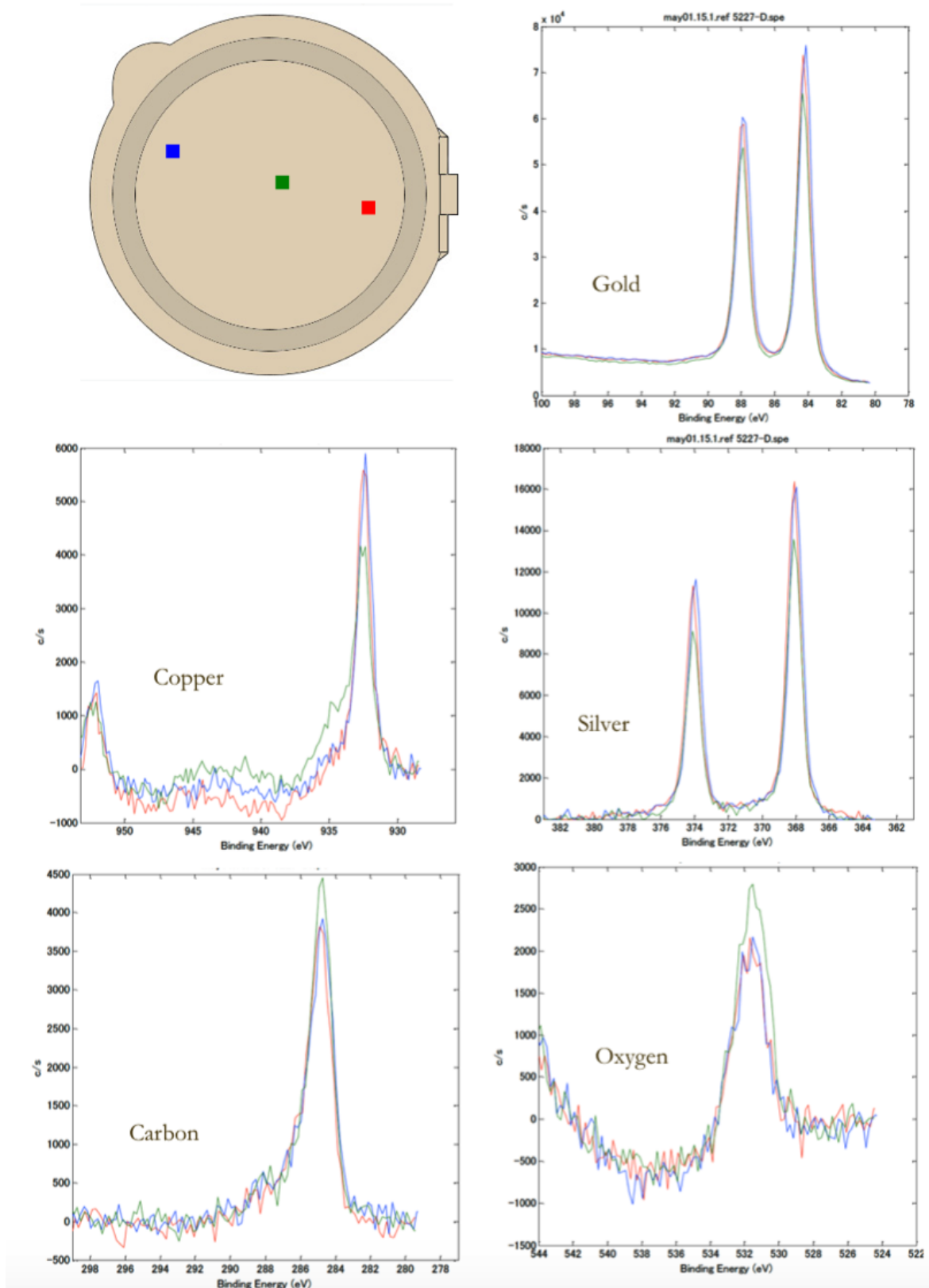


Figure 3.16: Intensity peaks of gold, silver, copper, carbon and oxygen for the defective watch component. The color code of positions marked on the piece correspond to the color of measurement curves. The oxygen peak is not background corrected.

Auger Electron Spectroscopy (AES)

A survey on the surface of the watch component revealed presence of carbon, oxygen, chlorine and sulfur on the surface. With the help of ion gun sputtering, in-depth profiles of the alloying elements together with the surface contaminants have been measured. Figure 3.17 shows the intensities of different signals over a measured depth of 17.5 nm. The acquired data points are directly plotted with no smoothing performed on the curves. One measurement is shown at the center of the good piece and two measurements are performed on the defective piece at the center and inside the defaulted area (bright ring). In all the cases surface contamination is sputtered away already after the first interval of sputtering. This means that the thickness of contamination islands are around 1 nm or less. The intensity of low energy Au1 signal is small at the outer surface. However, once the surface is cleaned it takes a big jump and almost triples in intensity. After a maximum, the gold intensity gradually decreases again in approximately 10 nanometers that follow. Silver with a higher signal at the surface gradually decreases in the first 2 to 5 nanometers. Meanwhile, copper signal shows a slow increase in the first 5 nanometers. The increasing trend is mainly seen for the defaulted piece.

Atomic concentration of the alloying elements are calculated from the intensity profiles. In this calculations, carbon, oxygen and sulfur have not been considered because as seen in the intensity profiles these surface contaminants are no longer detected after cleaning the surface by sputtering only 1 nm. The results are presented in Figure 3.18. The sharp increase that was previously seen in the signal intensity of gold translates in to a jump in gold content between the outer most surface and the first interval of sputtering. A slight enrichment in Au is seen right under the surface with gold content of 65 at% for the good piece and 68 at% for the defective piece. This value decreases by sputtering further and arrives to 54-55 at% at the highest sputtered depth.

Silver has a high concentration at the surface with 26 at% for the flawless piece and even higher amount of 40 at% for the defective piece. This high amount of silver cannot be found under the surface layer as the values descend up to 5 nm below the surface to reach 5-7 at% for the defective piece and the flawless one respectively. Meanwhile, presence of copper has a different behavior in the two samples. On the good piece there is 23 at% of copper at the surface which is remarkably higher than 12 at% and 14 at% for defective piece. This high copper content then takes a small drop followed by a gradual increase. While, in the defective piece no drop is seen in the measurement Figure 3.18 (b) and a much smaller decrease is seen in measurement Figure 3.18 (c).

SEM image obtained on the surface and presented in Figure 3.19 shows islands that appear with a gray contrast to the background alloy color. Mapping the chemical composition of the surface shows that in these islands of surface contamination carbon, oxygen, sulfur, calcium and copper can be found while gold or silver are absent in the surface areas covered by these spots. This contamination islands can be found all over the surface of the samples and they should be residues from the polishing products.

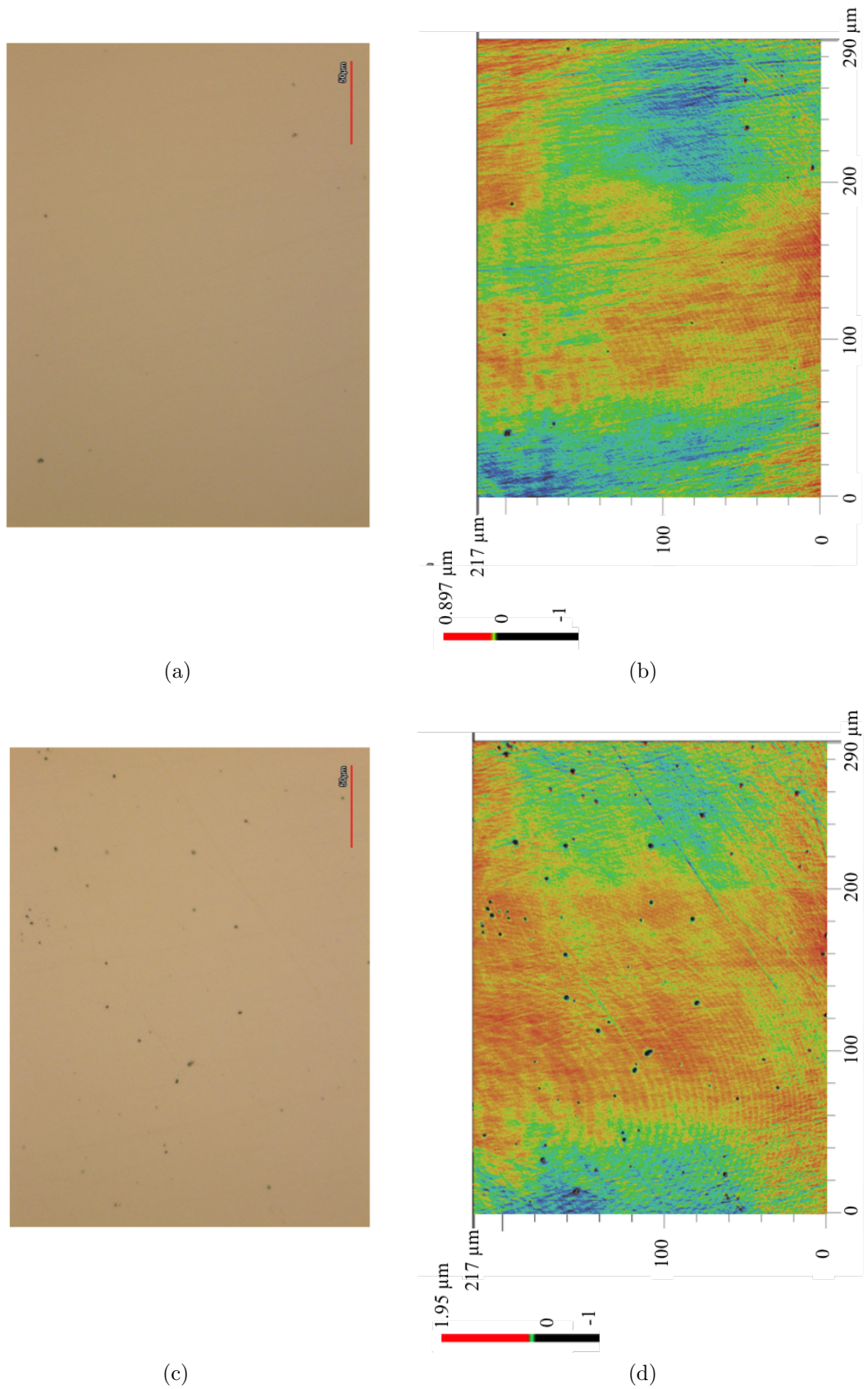


Figure 3.8: Optical images and 3D surface profiles are presented for the flawless and defective watch components measured in location 1 on the samples (near the edge of the flat bottom). a) and b) show optical image and 3D surface topography of flawless sample respectively while c) and d) show similar images of the defective piece.

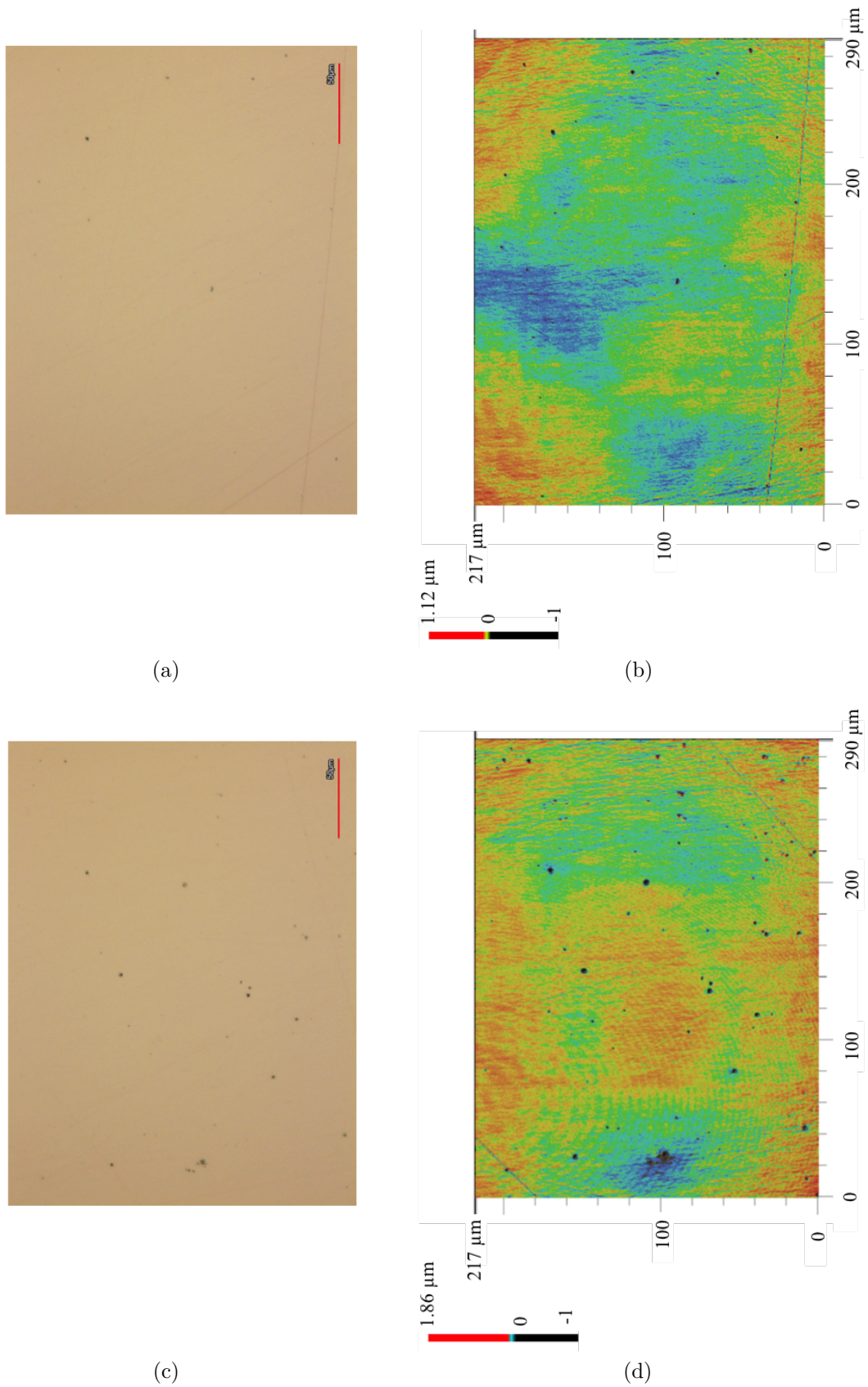


Figure 3.9: Optical images and 3D surface profiles are presented for the flawless and defective watch components measured in location 2 on the samples (in the center of the flat bottom). a) and b) show optical image and 3D surface topography of flawless sample respectively while c) and d) show similar images of the defective piece.

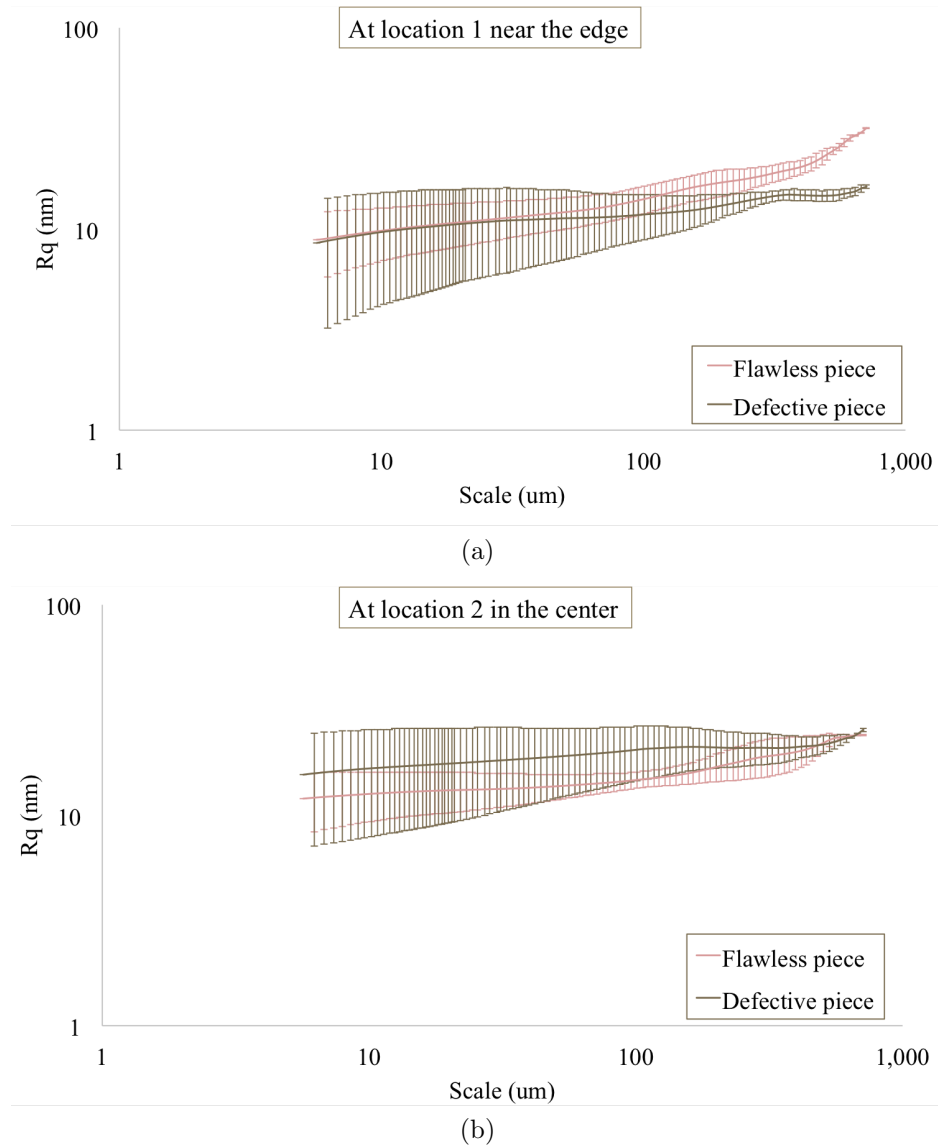


Figure 3.10: Variable length scale analysis are performed for 710 μm long profiles obtained from the defective and the flawless piece: a) at location 1 near the edge of the flat bottom and b) at location 2 in the center.

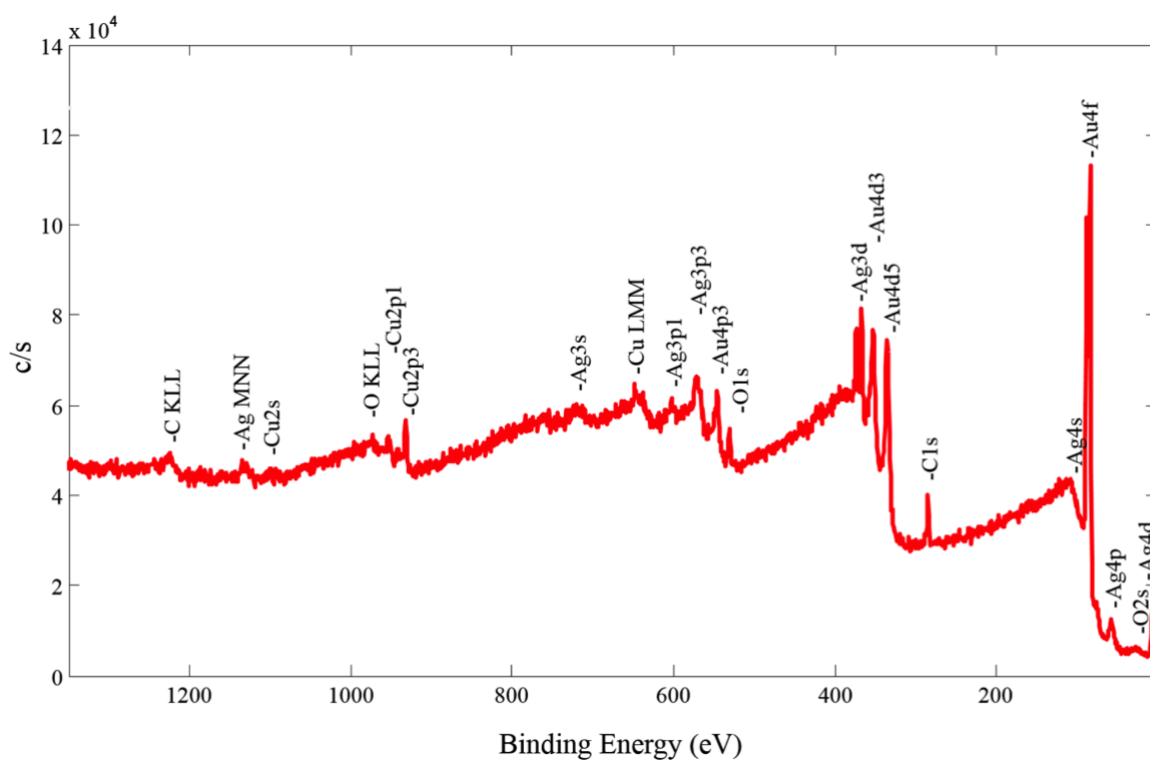


Figure 3.14: Spectra of binding energies and characteristic peaks of elements that could be found on the surface.

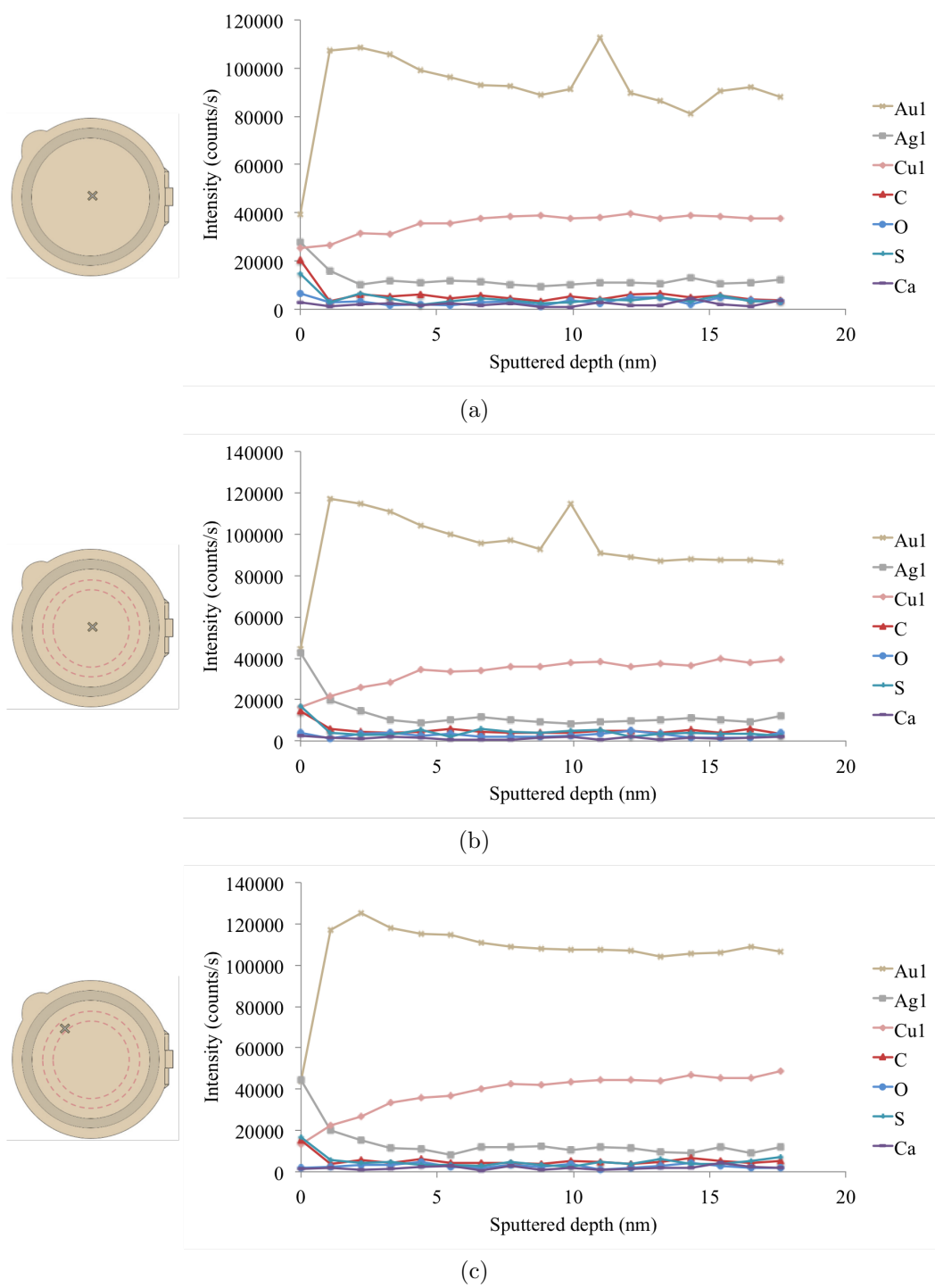


Figure 3.17: Intensity profiles over a sputtered depth of 17.5 nm are plotted for a) flawless piece in the center b) defective watch piece in the center and c) defective watch piece in the defective zone (bright ring). In all cases a sharp increase in gold signal is visible after first sputtering interval. The signals of all the contaminants fall to zero in the same period. All the points in all graphs are measured data points.

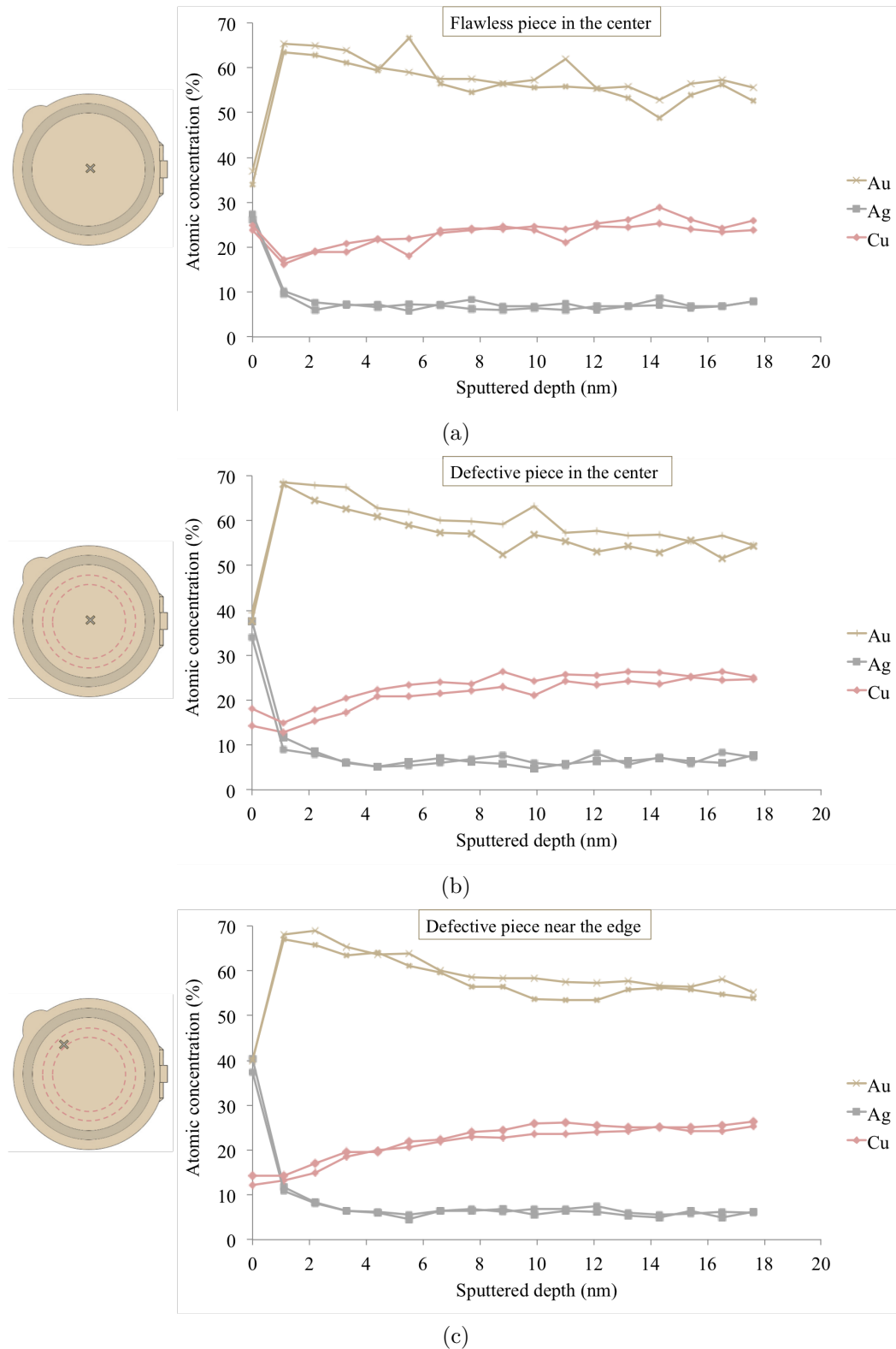


Figure 3.18: Atomic concentration for the three alloying elements are calculated over a depth of 17.5 nm for a) flawless piece in the center, b) defective watch piece in the center and c) defective watch piece in the defective zone. Two measurements are performed and plotted in every location. In all cases, a sharp increase in gold signal is visible after first sputtering interval. The signals of all the contaminants fall to zero in the same period. All the points in all graphs are measured data points.

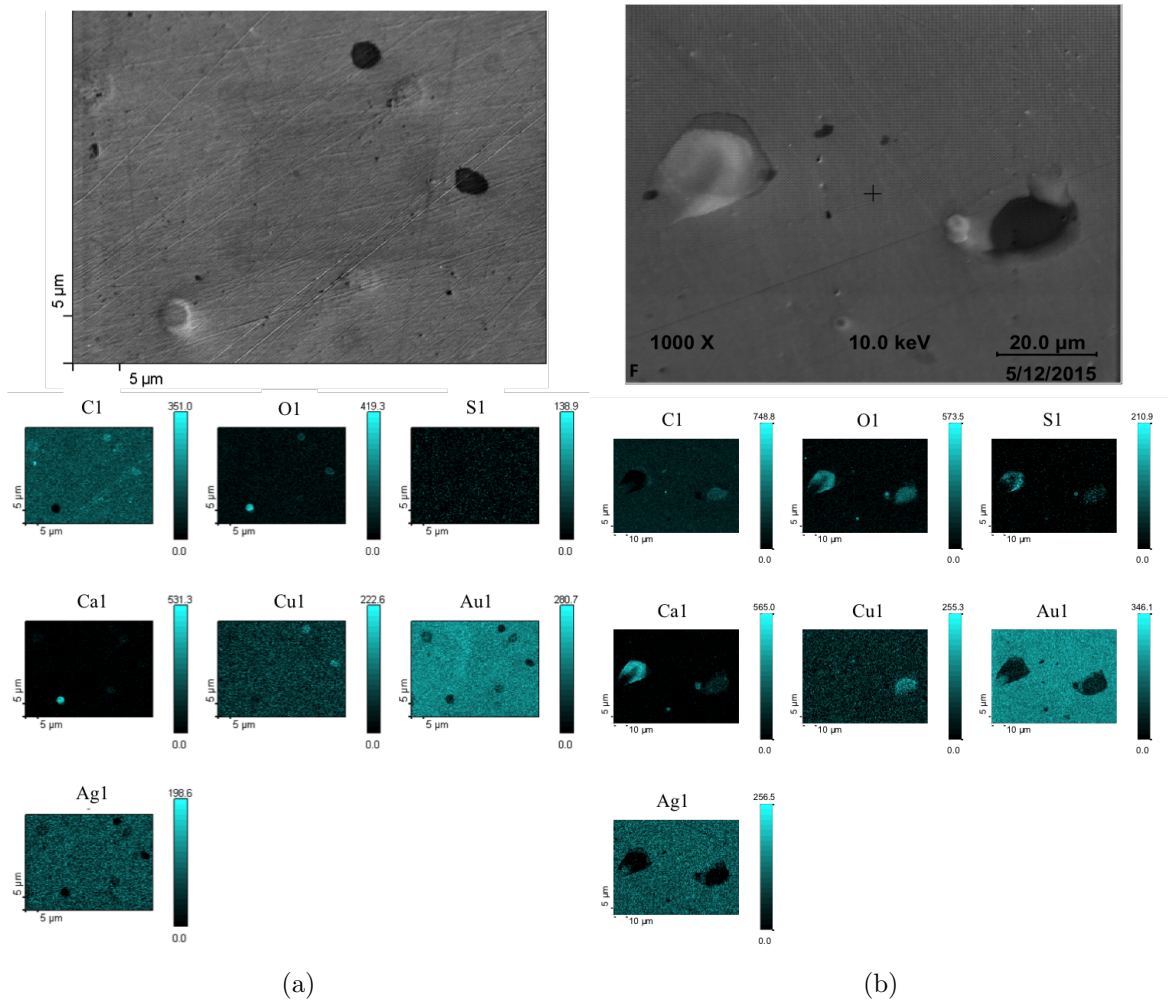


Figure 3.19: SEM images are presented together with chemical map of surface contamination that are obtained using Auger Electron Spectroscopy for a) flawless piece at the center of the watch dust cover and b) the defective piece again at the center.

3.4.3 Hardness measurement

In order to study the degree of homogeneity in the mechanical properties of samples across a single piece, microindentation tests were performed using a Vickers hardness measurement apparatus. Applied load of 100g creates indents with a diameter of approximately 30-45 microns.

In order to compare the defaulted piece and the good piece, a set of microhardness measurement was performed on the surface of two watch covers across the diameter. Indents are placed with 500 micrometer spacing. Figure 3.20 shows an example of an indent. Optical image of the indent shows slip bands around the deformed surface of the indent. A line profile is extracted across the indent as indicated on the 3D topography image. It shows that the indent is approximately 6 micrometers deep. An SEM image of an indent is also shown. The imperfections inside the indent comes from the

defects on the indenter's tip.

In Figure 3.21 every point shows a measurement that is performed with 500 microns distance between every two indents. Measurement is done across the diameter of the pieces on following the dashed line that is schematically marked on the drawing of the piece. A three-point moving average line is also fitted to the data. It can be seen that in central areas the two pieces have similar hardnesses. However, near the two extremes of the good piece there is a peak in hardness values while a slight decrease in hardness for the defective piece can be seen near the external edges.

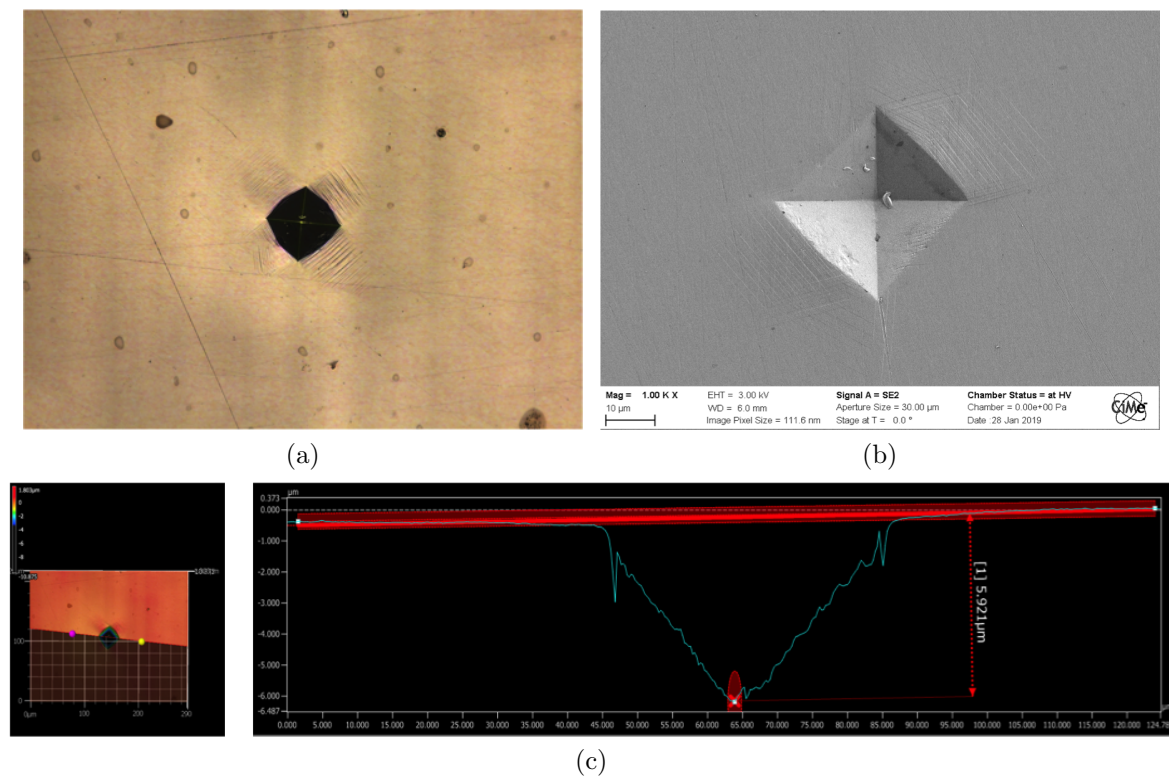


Figure 3.20: Examples of the indent that Vickers microhardness measurements leave on the surfaces of watch pieces are shown in these images by means of a) optical imaging, b) SEM imaging from the top surface and c) line profile extracted from 3D measurement.

3.4.4 Reflectance and color measurements

Results of reflectance measurement are presented in Figure 3.22 for two measurements at 0 degree and 8 degrees on flawless and defective pieces. Mirror-polished surfaces show a very high total reflectance in both cases with the typical reflection edge of colored alloys. The variation between percentage of total reflected light between two samples is small and is more remarkable in the longer wave-length range (yellow to red domain of visible light). Diffuse reflectance curves shown in Figure 3.22(b) show that differences in diffuse reflectance between two samples are even smaller (less than

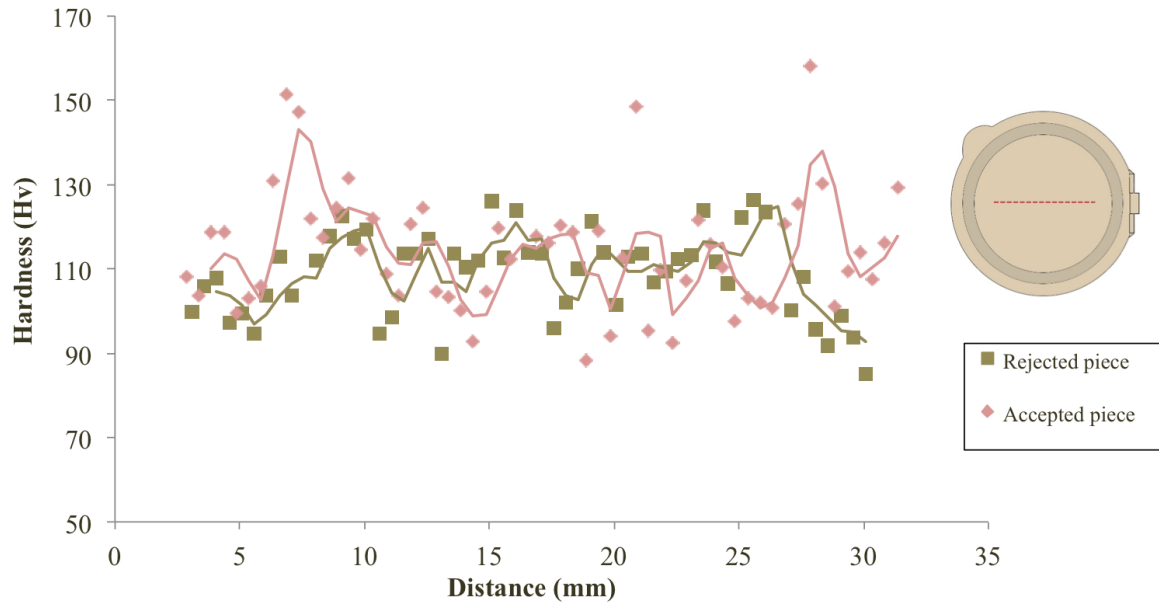


Figure 3.21: Microhardness of watch dust covers measured on a line across the interior diameter of the samples. Two set of data for visually good and defective pieces are presented. Both pieces show remarkable scattering in measured micro hardness but the scatter is larger for the flawless piece.

0.5 % at 700 nm).

From the diffuse reflectance curves it can also be seen that total amount of diffusely reflected light at all angles is only less than 10%. This low contribution of diffuse reflectance to the total reflectance supports the approximation that was made in Chapter 1. In this approximation we chose to focus the study of aesthetically relevant aspects on measurement of total reflectance instead of studying angle dependency of diffuse reflectance. This of course does not ignore the role that spatial distribution of reflection measurement plays on appearance, but rather acts as a simplification. The fact that two pieces with different aesthetics show different total reflectance means that this simplification still allows us to distinguish between two samples that have different aesthetics only by measuring their total reflectance.

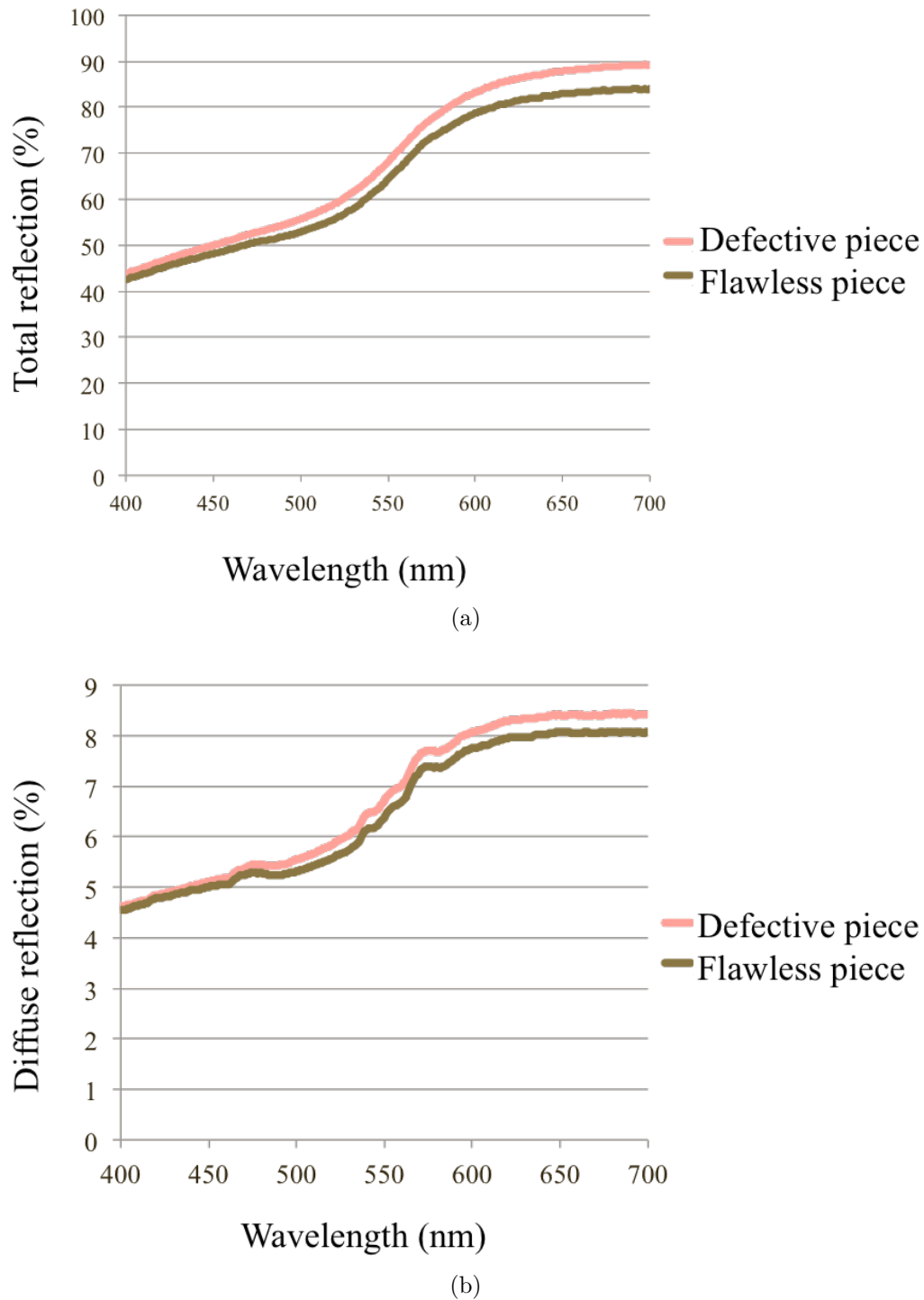


Figure 3.22: Reflection measurement for visible spectrum for flawless and defective samples (a) total reflectance at 8 degree of incidence and (b) diffuse reflectance at 0 degrees of incidence.

Effect of sample geometry

Performing several reflectometry measurements on the same sample showed the sensitivity of the measurement to changes in geometry of the sample. Figure 3.23 shows two measurements on the flawless sample at 8 degrees. A difference both in the intensity of

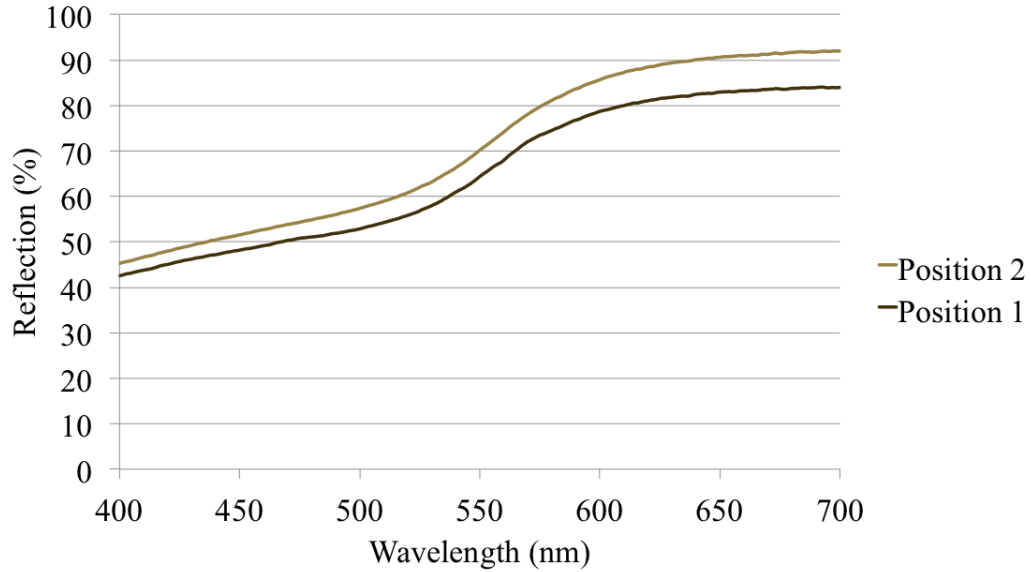


Figure 3.23: Two reflectance measurements in visible spectrum on different positions of flawless sample. A difference in intensity and slope of the curves is observed showing the large uncertainty associated with the measurement of large curved samples.

reflected light and in the slope of the graph is evident between the two measurements. This difference is correlated to the fact that the piece is not perfectly flat and therefore moving from one position on the surface to another can affect the reflection from the surface by changing the angle of incidence and reflection and also by changing the traveling distance of the light. This means that even though this commercial reflectance measurement tool is a powerful and efficient technique for total reflectance and color measurement of flat surfaces, it is not adapted for measurement of complicated shape and geometries. Therefore, it cannot be used to detect small differences in reflectance on mirror polished surface of watch or jewelry components.

3.5 Summary and conclusions

Surface characterization methods and instruments that were chosen for this study provide reliable measurement techniques for assessing surface topography, surface and near surface composition, hardness of the pieces and finally quantitative color and reflectance measurements. These techniques were employed to analyze and compare two industrial pieces one of which had a defective appearance and the other that had an acceptable appearance. The obtained results are summarized below.

Surface topography was studied using several techniques including white light profilometry, confocal laser profilometry, surface roughness measurements and SEM imaging. Measurement results showed that:

- Both pieces have undulations in flat bottom of maximum $90\ \mu\text{m}$ over a 30 mm

diameter.

- Roughness measurements with no cut-off length show higher R_a and R_q values in the defective areas.
- SEM images show similar and homogeneous surfaces that are smooth with some shallow polishing scratches.
- Porosity can be found on both surfaces. However, they are larger and are more frequently found on the defective piece.

Surface chemistry was studied using XPS and AES techniques. Following observations were made:

- XPS analysis shows that on both pieces copper is present in compound form on the surface while gold and silver remain in their metallic form.
- AES chemical maps show presence of islands of surface contamination. These islands have similar compositions in both pieces and the elements that could be found on them include: carbon, oxygen, sulfur and copper. These surface contamination can be removed by sputtering 1-2 nm from the top surface.
- AES depth profiles show a gradient in composition over a depth of 5 nm of the surface. Differences in composition are detected between flawless and defective pieces. For the flawless piece, copper and silver are enriched on the top surface while top surface of the defective piece is enriched in silver and depleted in copper.

Microhardness measurements showed that hardness of pieces varies at different locations on the same piece. A comparison between a set of indentation that were performed across the diameter of two samples shows a decrease in hardness of defective piece as apposed to an increase in hardness of the good piece towards the external edges.

The effect of holes at the surface coverage found on the technical surfaces under study was found to be negligible on aspects of appearance.

Reflectance and color measurements using a commercial spectrophotometer showed high total reflectance and small diffuse reflectance as expected from a mirror polished surface. These measurements also revealed that despite the strength of the method, it is not adapted for measurement of pieces with curved or complicated geometry such as the one of watch or jewelry components.

On the whole, the measurements presented in this chapter revealed the features that can appear on the technical surfaces of industrial pieces. However, they do not yet point out which of these defects are responsible for the aesthetic imperfection. To answer this question, the next chapter is dedicated to studying the correlation of each of these features to aspect of appearance.

Chapter 4

Surface defects and their correlation to appearance

The goal of this chapter is to artificially introduce relevant defects and imperfections that were revealed in previous chapter, on polished surfaces of gold-copper-silver disks and study the correlation between such imperfections and color and reflectance of these surfaces. The particular imperfections studied are roughness variations, differences in surface chemical composition and porosity. The study is done on 4N gold disks as model samples with surfaces that are polished in laboratory. Correlations are drawn between pairs of color/compositions and lightness/roughness.

4.1 Introduction

In this chapter, the link between surface physical and chemical properties to color and reflectance as measures of assessing appearance is studied. This correlations will be explored using model samples. These model samples are disks of a similar 18 karat alloy on the surface of which controlled and reproducible modifications are applied in the laboratory environment. This would provide a clear image of the history of the pieces as apposed to the hand crafted watch components which go through individually adapted processing. Additionally, benefiting from flat surface of model samples as opposed to curved geometry of the watch components allows the use of the commercial reflectometer.

4.2 Model samples: material, surface preparation and characteristics

4.2.1 Material

The model samples used in this study are made of bars of 4N gold alloy with the composition listed in Table 4.1. The three main composing elements are the same as those of the 5N watch pieces studied in Chapter 2. However, here the copper content is slightly lower and this is compensated by higher silver amount. The bars of 4N gold alloy were cut into disks that are 15 millimeters in diameter and 2 millimeters in height.

Table 4.1: Composition of the model samples used in the current study.

	Au	Ag	Cu
Weight percentage	75	10	15
Atomic percentage	53.7	13	33.3

An example of microstructure of these samples is presented in Figure 4.1. In this work a methodology was developed and used to obtain high quality images of 18k gold microstructure. This method is composed of the following steps:

- Cutting a cross section of the samples. In this case a WELL wire cut instrument was used with diamond wire of 0.22 millimeter in diameter.
- Mounting the sample in cold resin. The resin used in this study was Technovit 4071 from KULZER.
- Polishing the cross section down to a smooth mirror polished surface. This was achieved with first grinding with grade 4000 silica paper in water followed by polishing against a nap with a solution of 1 μm diamond suspension (LDP) from PRESI LTD spread in between.

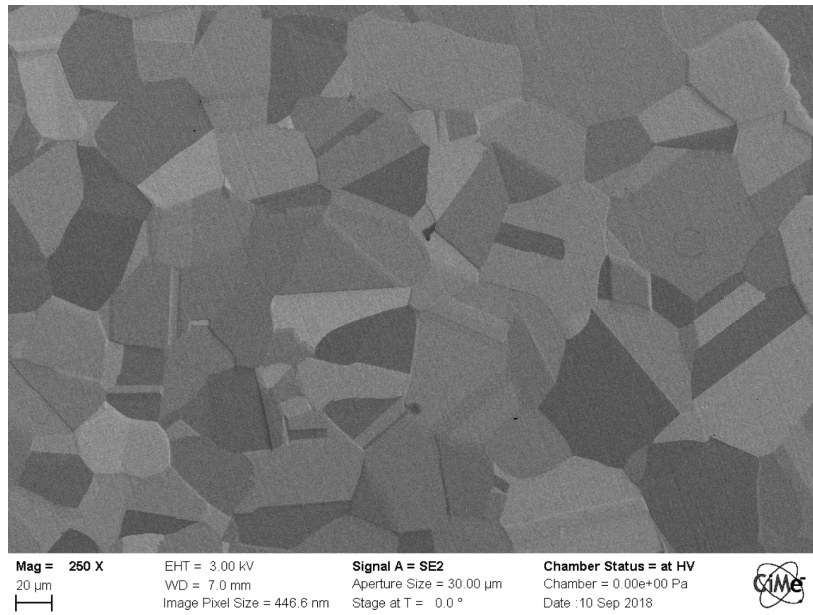
- Ion milling the surface. The ion milling process has been done using a GATAN ILION II System with an argon source and at a voltage of 3kv for 15 minutes.
- SEM imaging.

The gray-scale contrast in the SEM image is an electron emission contrast that is a result of grain orientation dependent sputter rate. The grain size averaged over 130 grains measured in this image is approximately 60 μm . Several twin boundaries can be spotted. They appear as bands with two sharp and precisely parallel edges that have an abrupt color contrast compared to the grain that contains it.

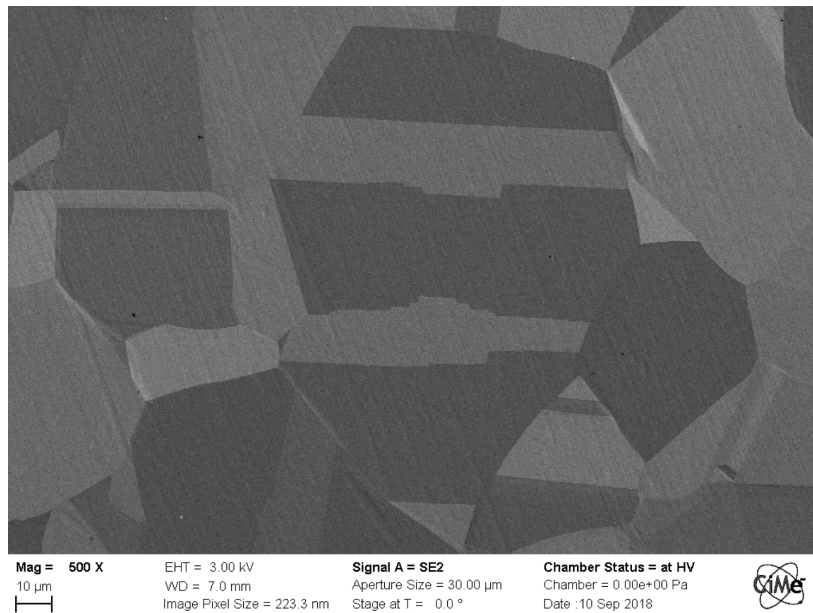
As the goal of this study is to correlate the defects on a mirror polished surface to visual aspects, the first step was to define a standard polishing procedure to be performed in the laboratory. Once a polishing process is defined that produces desired surfaces that are comparable with the industrial ones, surface defects will be introduced and studied.

4.2.2 Surface preparation

After a set of trials with different polishing products, a standard polishing procedure was developed to obtain the mirror-polished surface with roughness comparable to those of watch components. In this method, as received surfaces are first ground using a steering wheel against grinding paper P4000 from Presi in water. The next step of polishing was done against nap with 1 μm poly crystalline diamond suspension (diamond suspension reflex LDP by Presi). Both of these steps were done using a Struers manual polishing machine with a disk rotation at 450 rpm for 5 minutes. The samples were then cleaned with soap, rinsed with distilled water and sonicated for ten minutes in an ultrasonic bath in high purity ethanol for analysis. The surface obtained by this procedure will serve as the reference surface for this study.



(a)



(b)

Figure 4.1: SEM pictures taken at the cross section of as received 4N gold alloy model samples (a) at 250X and (b) 500X.

4.3 Effect of surface roughness on aesthetic aspects of 4N gold alloy

The first surface parameter to investigate was roughness. The goal of this step has been to modify the surface roughness by varying the polishing procedure and to study how the surface evolves accordingly. For this purpose, nine samples were polished with the standard polishing procedure that was described above. From these nine samples, three of them were re-polished with 4000 grinding paper in water to increase

surface roughness. And three other samples followed an extra step of polishing in colloidal silica particles with a size of $0.03\ \mu\text{m}$ (from Presi) to obtain a smoother surface compared to the standard samples. The three set of samples that are obtained and the last step of surface modification that was applied on their surface are summarized and named as the following:

- Sampling 1: Ground with 4000 paper
- Sampling 2: Nap polished with diamond slurry of $1\ \mu\text{m}$
- Sampling 3: Nap polished with silica slurry of $0.03\ \mu\text{m}$

In the measurements that have been performed on these samples and will be explained in next sections, the intervals between surface preparation and measurements were fixed in order to avoid variations in aging between samples in contact with air and/or humidity.

Evolution of surface topography has been followed by SEM imaging as well as surface profilometry after every step of polishing. Figure 4.2 shows SEM micrographs of the three samples. At the first step of sampling, after grinding against 4000 paper, the surface is relatively smooth but yet several scratches are visible. Material appears to have also been smeared around on the surface. After the second step of polishing, the surface is already a lot smoother and the scratches are a lot shallower. Surprisingly at the last step, despite the surface being very smooth, a grain contrast appears. As this last step is performed in an aqueous solution, the appearance of the grains possibly is the result of grain orientation dependent etching of grains. Figure 4.2(d) shows the same surface at lower magnification where several grains are visible. The size and the shape of the grains correspond to the microstructure of the sample that was previously presented in Figure 4.1. No porosity was detected on the surface of any of the model samples.

3D image of surfaces measured with laser scanning confocal microscope are shown in Figure 4.3 and optical images are shown in Figure 4.4. The topography of the three surfaces are different. In the first sampling the main surface features are the scratches while in second sampling, islands at different heights appear on the surface. At the third sampling these islands take the shape of flat plateaus of grains.

From the 3D surface profiles, line roughness was calculated after each step. Three roughness parameters namely R_a , R_z and R_q are presented in Table 4.2. The measurement was done over a length of $285\ \mu\text{m}$ with a distance of $0.14\ \mu\text{m}$ between every two measured point and no cut-off length is applied. Each value is the average of nine measurements (three lines on each individual sample). For sampling one where the surface texture is directional, line roughness has been measured at 45 degrees of scratch direction. For the other samples that have no directional pattern, profiles were extracted in a random orientation.

Surprisingly Table 4.2 shows that the last step of fine polishing yields higher roughnesses. To explore this matter, variable length scale analysis were performed on these profiles and the results are shown in Figure 4.5. It is evident that sampling 1 has

Table 4.2: Several roughness parameters measured for three surfaces. In each case 9 measurements are averaged.

Sample	$R_a(nm)$	$R_z(nm)$	$R_q(nm)$
1st Sampling	41 ± 7	739 ± 220	60 ± 12
2nd Sampling	9 ± 2	62 ± 9	11 ± 2
3rd Sampling	19 ± 9	119 ± 48	23 ± 11

higher roughnesses at all scales with high dispersion. Sampling 2 and 3 have similar roughnesses at length scales below $20 \mu m$ while at larger scales sampling 3 has higher value. These results explain previous topography measurements. At sampling 3 each grain is smoothly polished so roughness is small at length scales that correspond approximately to the size of the grains. Since these plateaus of the grains are at different step heights longer scale measurement, beyond the grain size, shows higher roughness values compared to previous step of polishing.

Probability density function of surface heights (PDF) is used to assess the texture of surfaces. Figure 4.6 shows the PDF obtained from the 3D topography measurements of the surfaces after each step of polishing. It can be seen that the distribution of probability density function of surface heights has a continuous, nearly Gaussian form for the first and second sampling while the third sampling exhibits a step-like distribution corresponding to the plateaus observed in Figure 4.3.

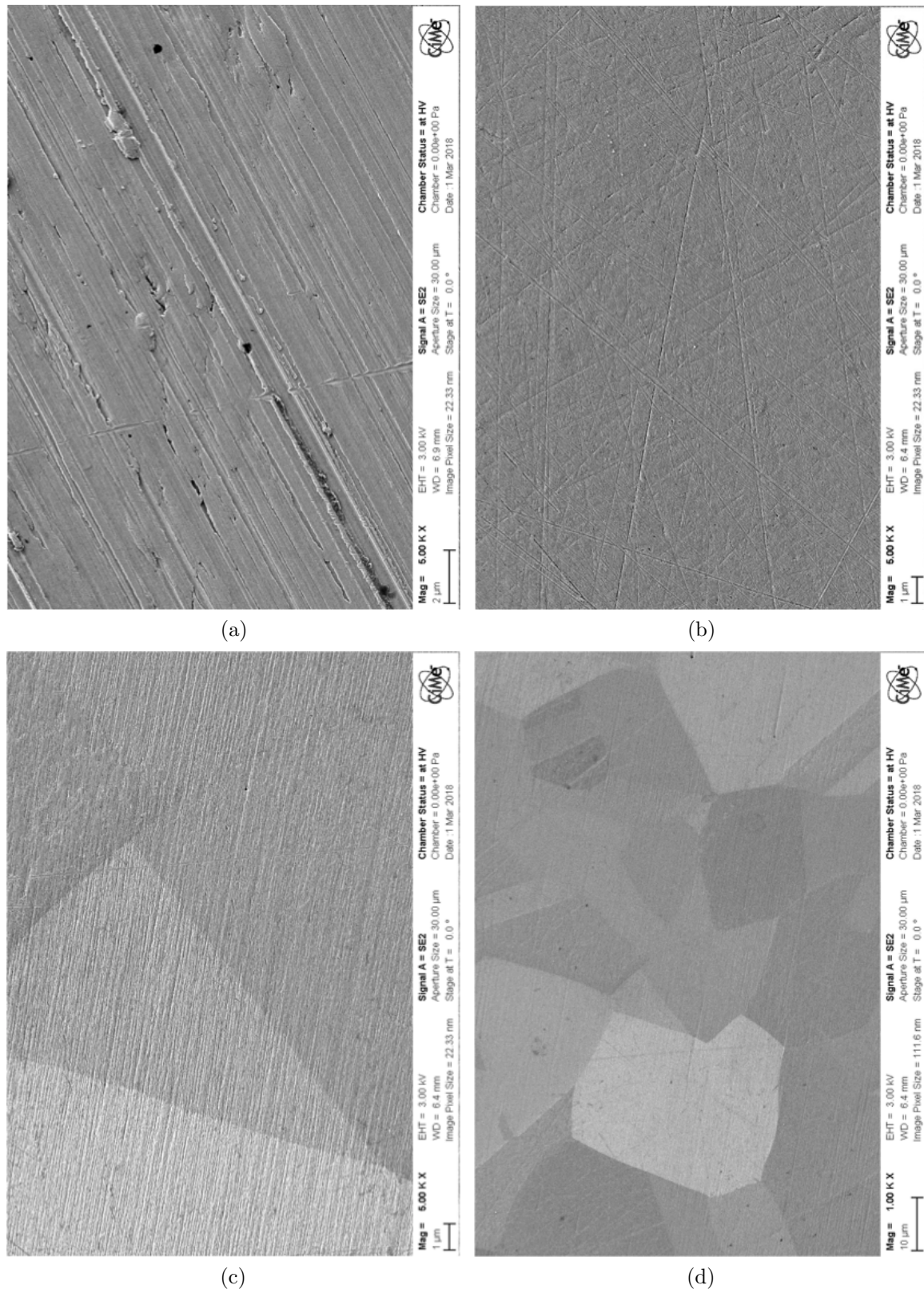


Figure 4.2: SEM images of surface of 4N gold disks at a) 1st sampling, b) 2nd sampling and c) 3rd sampling. The scratches from polishing are evident at the first step of polishing. The surface appears drastically smoother on the second step. Surprisingly, on the 3rd step grain contrast appears on the very smooth polished surface. d) shows the surface at sampling 3 at lower magnification where several grains are clearly visible.

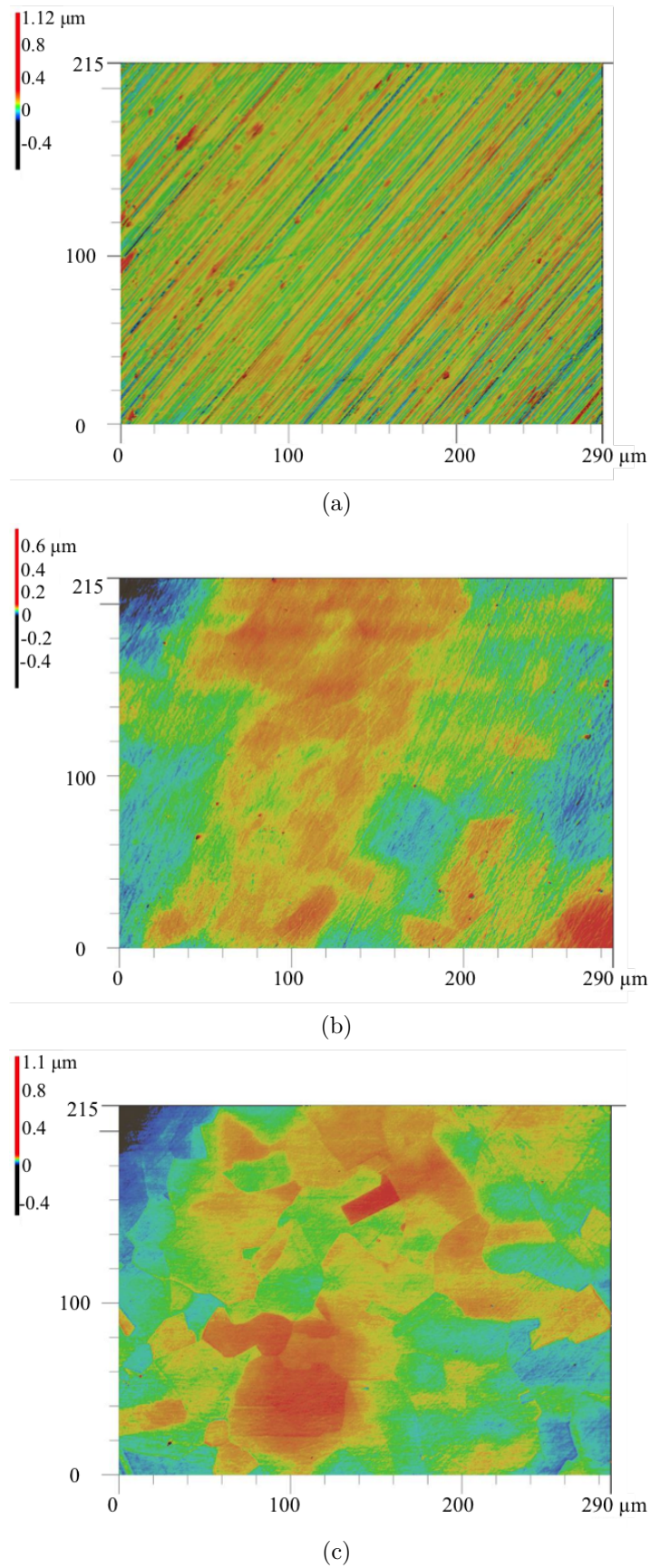
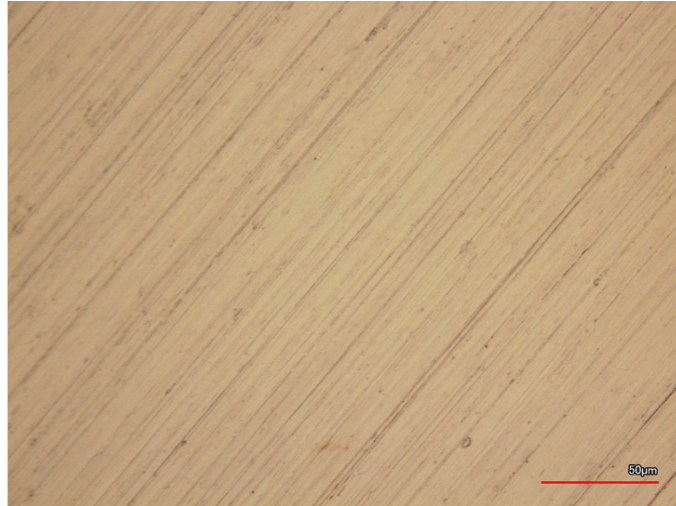
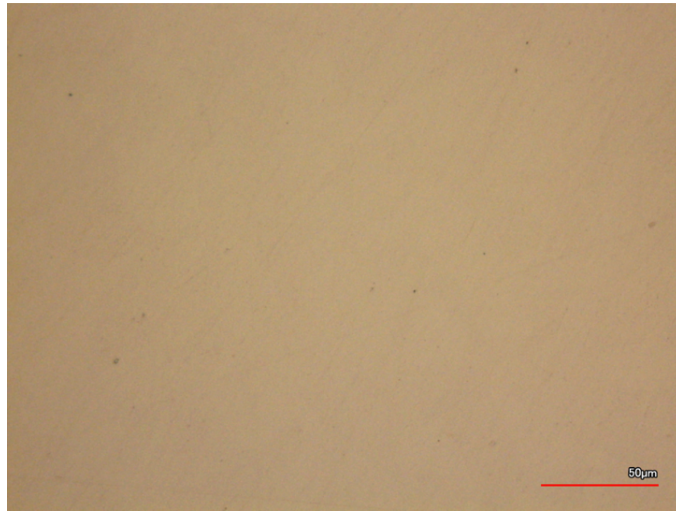


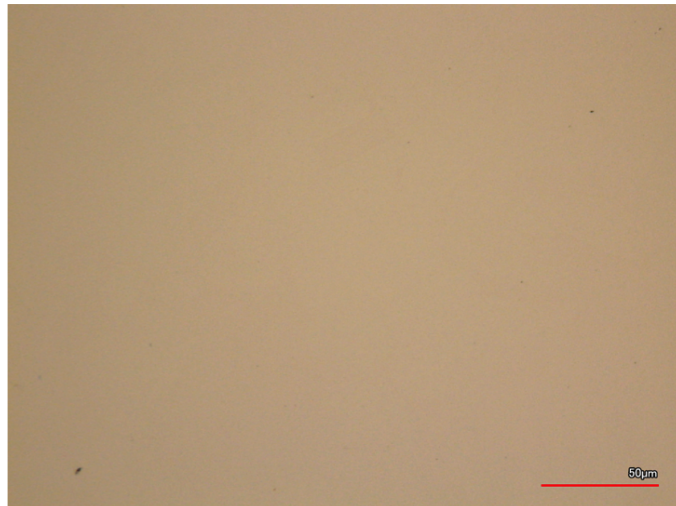
Figure 4.3: 3D surface profiles of 4N gold disks obtained with laser scanning confocal microscope at magnification of 50X for a) 1st sampling, b) 2nd sampling and c) 3rd sampling.



(a)



(b)



(c)

Figure 4.4: Optical images of 4N gold disks obtained with laser scanning confocal microscope at magnification of 50X for a) 1st sampling, b) 2nd sampling and c) 3rd sampling.

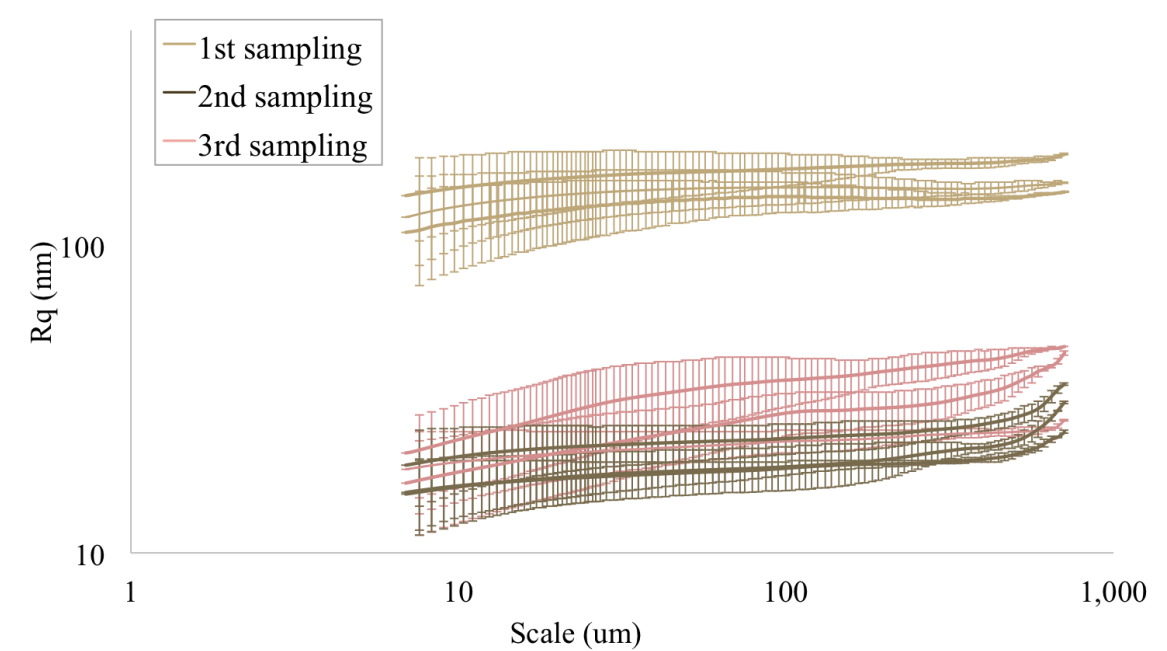


Figure 4.5: Variable length scale analysis on a profile extracted from each one of the total 9 samples and results are plotted in double logarithmic scale.

4.4 Effect of polishing on chemical composition of the surface

X-ray Photoelectron Spectroscopy (XPS)

Details of XPS instrument and the methodology for performing the analysis are the same as those already discussed in Chapter 3. Figure 4.7 shows the intensity peaks for gold, silver, copper, carbon and oxygen. Gold and silver peaks are of the same energies for all the samples. For copper peaks, a shoulder and a satellite appear by going further in the steps of polishing. These are typical indications of oxidized metal. Oxygen and carbon peaks do not show meaningful variations between three cases.

Auger Electron Spectroscopy (AES)

As a first step in AES analysis, a survey was run for kinetic energies between 0 and 2500 electron volts. This survey is used to identify elements that are present on the surface as well as defining energy windows that will then be used to perform multiplex analysis. Multiplex analysis is essentially a more detailed and accurate measurement that is done in specific energy windows corresponding to the elements that have been detected in the survey in order to gain more precise and sharper intensity peaks. In the surveys that have been done on the gold disk model samples, peaks in intensity of gold, silver and copper can be seen as well as those of carbon and oxygen.

After distinguishing all the elements that are present on the surface, a depth profile was run. The detailed explanation of this method and the condition used in this experiment can be found in Section 3.3.2 of Chapter 3. The intensity of signals of each element is plotted over the sputtered depth for each of the three set of sampling in Figure 4.8. Every point that is marked on the graph, is a measurement data. The data acquisition has been performed for very small intervals of 30 second of sputtering near the surface. The intervals have gradually been enlarged to 60, 120 and finally 300 seconds of sputtering between every two AES analysis steps while going further in the depth of the samples.

In all the cases the gold signal that has a very low intensity at the outer most surface, increases sharply to values almost ten times larger, after sputtering only a few nanometers. Some oscillations in the gold signal can be seen specially for the first and third sampling. An overnight pause in measurement at 9 nm for sampling one has clearly caused a discontinuity in gold, copper and carbon signals. This discontinuity, that corresponds to real variations in gold signal amplitude, could be the result of surface diffusion/adsorption phenomena that occurs while sputtering is paused. A similar overnight pause at 11 nm did not induce a similar response. Fluctuations that occur in gold signal in third sampling are probably due to the signal background as they do not appear in higher energy gold peaks.

Carbon and oxygen peaks that are present at the outer most surface, flatten after only a few cycles of sputtering. The depth at which surface is cleaned of this contaminants, corresponds to the depth at which gold recovers its intensity. This means that the contaminants on the surface mask the metal signals in the first few nanometers. This effect is particularly present for the very low kinetic energy and therefore highly surface sensitive Au1 signal.

From the intensity profiles and using sensitivity factors, atomic concentration of the samples can be calculated. To verify reproducibility and homogeneity, three profiles are measured for each sample the resulting atomic concentration depth profiles are shown in Figures 4.9 to 4.11. These very interesting results show, as before, depletion in gold on the top surface in all cases that is compensated by enrichment in copper and silver. This gold concentration quickly recovers in the next 1.5 nm in the depth where even some enrichment of gold can be seen especially for sampling 3. After this peak of enrichment, gold content slowly stabilizes and remains mostly constant between 15 nm and 45 nm below the surface. Obviously the same oscillation that have been measured in the intensity signals of gold in sampling three is translated into the atomic concentration profiles.

Silver in contrast has a remarkable presence on top surface. Atomic concentrations before sputtering range from 26% to 32% and again 32% for sampling one to three respectively. This amount decreases in the first 5-7 nm before stabilizing at around 13%. From this point on, the silver content remains steady at around 11% .

The enrichment in copper is highest in sampling one with 63 at% which drops to 45 at% and 35 at% for sampling 2 and 3 respectively. Again in all cases, the copper content drops sharply after sputtering away only 1.5 nm of the surface. However, from here on, the three surfaces show three different trends in copper content. For the first sampling, the descent continues smoothly with a small slope between 1 and 6 nm of sputtering. Afterwards the curve takes an increasing turn with a very small slope. This trend is only disturbed by a peak at around 10 nm. From 25 nm onward, the copper content remains almost constant. For sampling 2, the sharp initial drop, already starts to recover after 1 nm of sputtering. A gradual increase continues up to a depth of 20-25 nm after which the values remain almost unchanged. In the case of sampling three, a remarkable valley of copper deficiency is present at around 2 nanometers. The copper content remains below 25 % up to 4 nanometers. The slope of the increasing curve that follows this valley is sharper than the one of last two cases. Up to 40 nm some undulation can be seen in copper curve however as always, the values remain largely unchanged after 25 nm.

To better elaborate the comparison of chemical composition between the three alloys, depth profiles of the first 10 nm where most of the variations occur, have been overlapped in Figure 4.12. Three important observations can be made here:

1. The three samples have different chemical compositions at top most surface.
2. Composition of the three samples are different both on the top surface and the 6 nm below it. From 6 nm downwards the three compositions merge.
3. All these variations amounts samples are remarkable in gold and copper content while silver shows almost identical behavior in all cases.

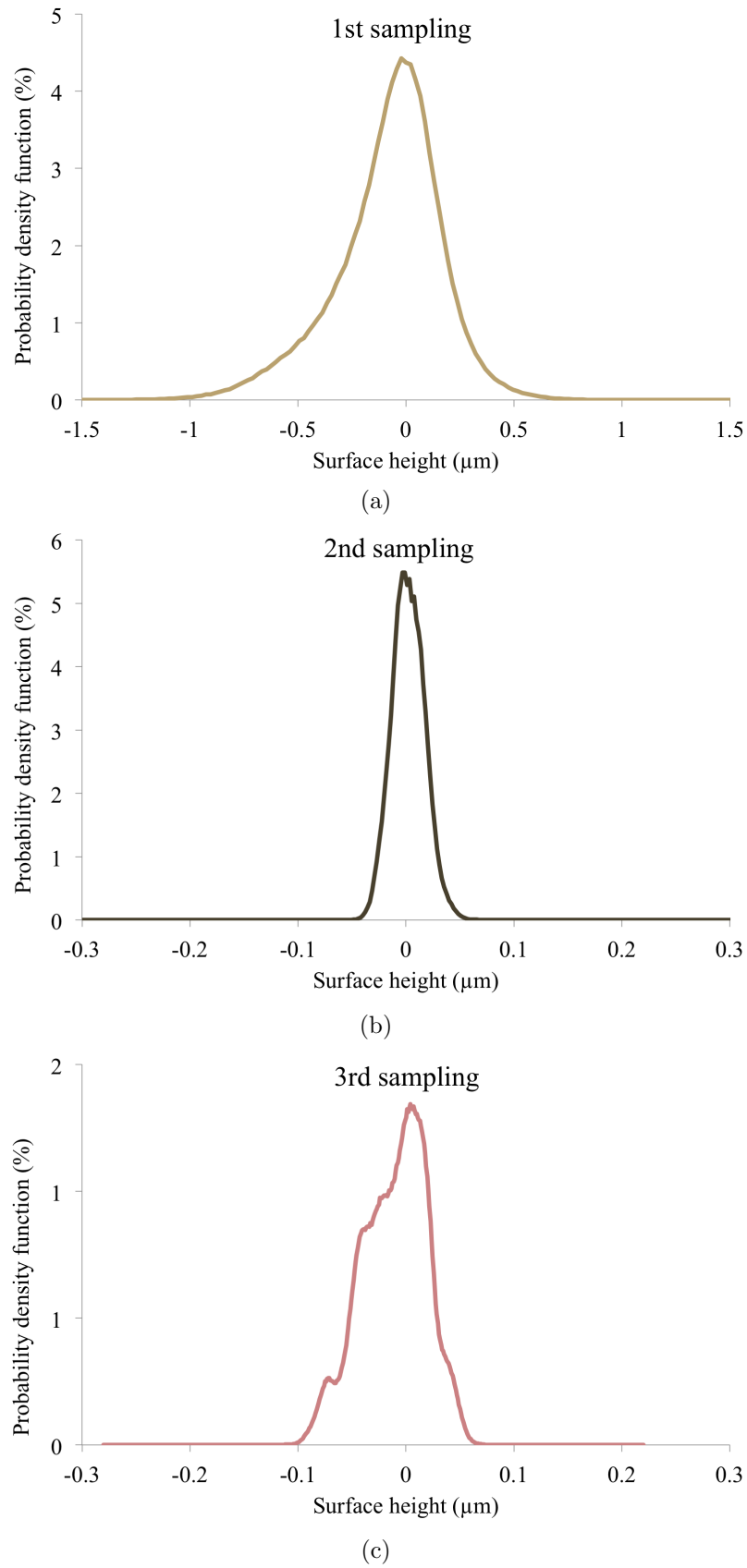


Figure 4.6: Probability density function of surface height are plotted for surfaces at a) 1st 1, b) 2nd and c) 3rd step of sampling. For the first and second sampling the distribution is continuous and nearly Gaussian while for the third sampling with the surface texture of plateaus, a step-like distribution of surface heights is observed.

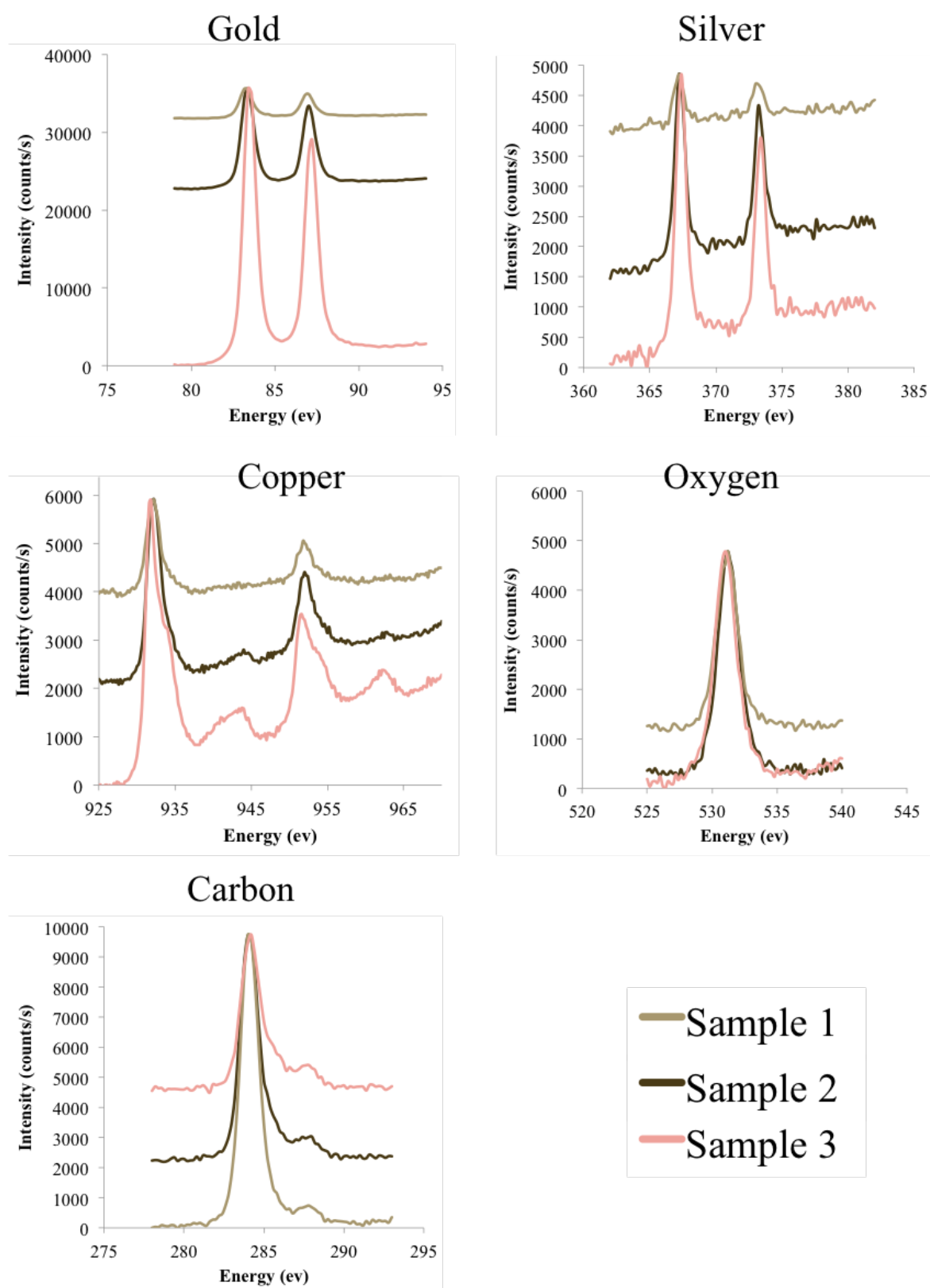


Figure 4.7: XPS peaks for the three alloying elements and the contaminants at the three stages of sampling.

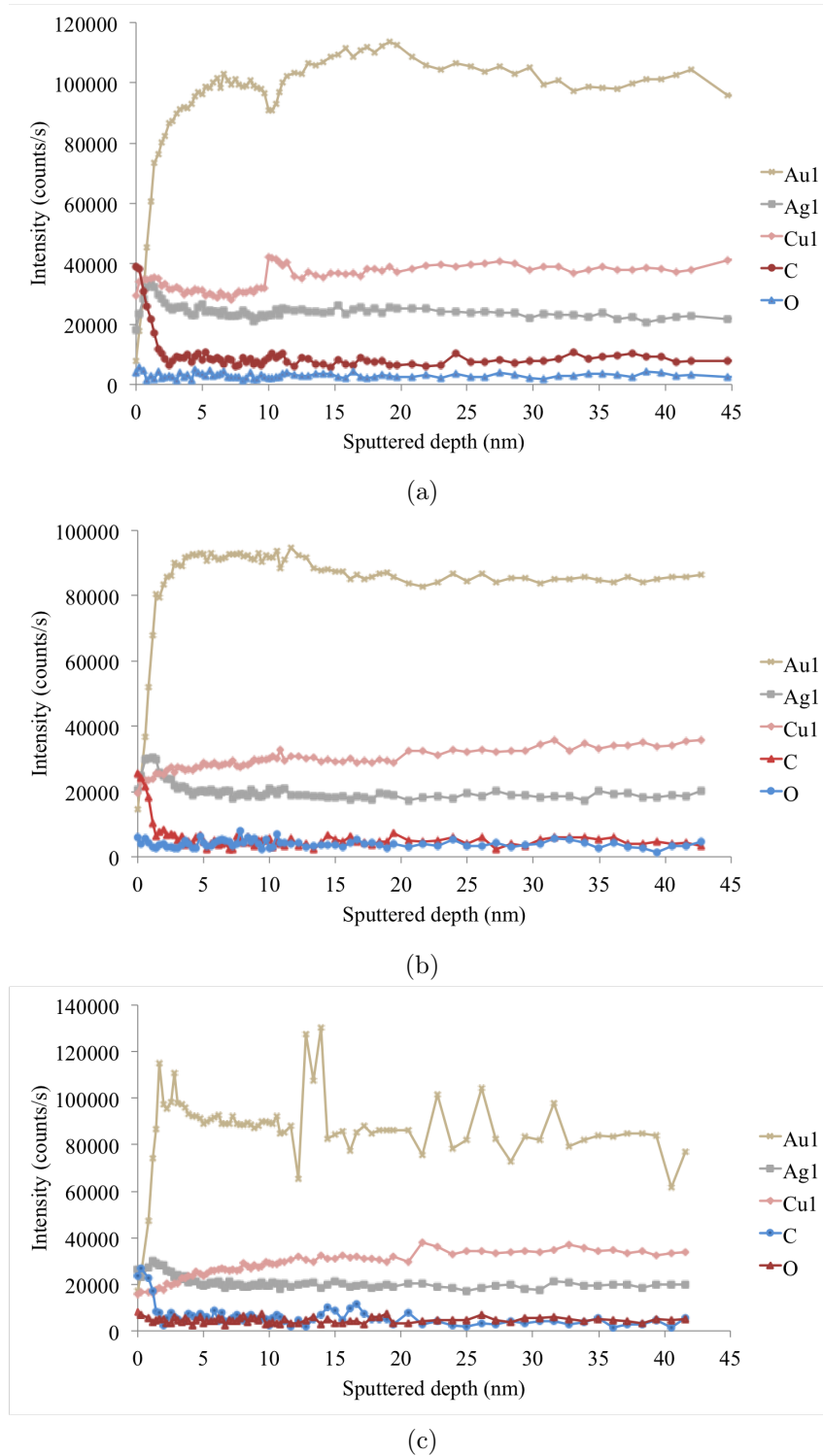


Figure 4.8: Intensity of signals for the alloying elements are plotted as well as carbon and oxygen for a) first sampling, b) second sampling and c) third sampling. C and O are found on the top surface of the samples due to contamination created by polishing process. At the outer surface where these contaminants are present, all three signals metals have lower intensities. An overnight pause in the measurement for sampling one at 9 nm of sputtering and for sampling three at 11 nm of sputtering has caused a drop in gold signal as well as a jump in copper signal. The rest of elements remain unaffected.

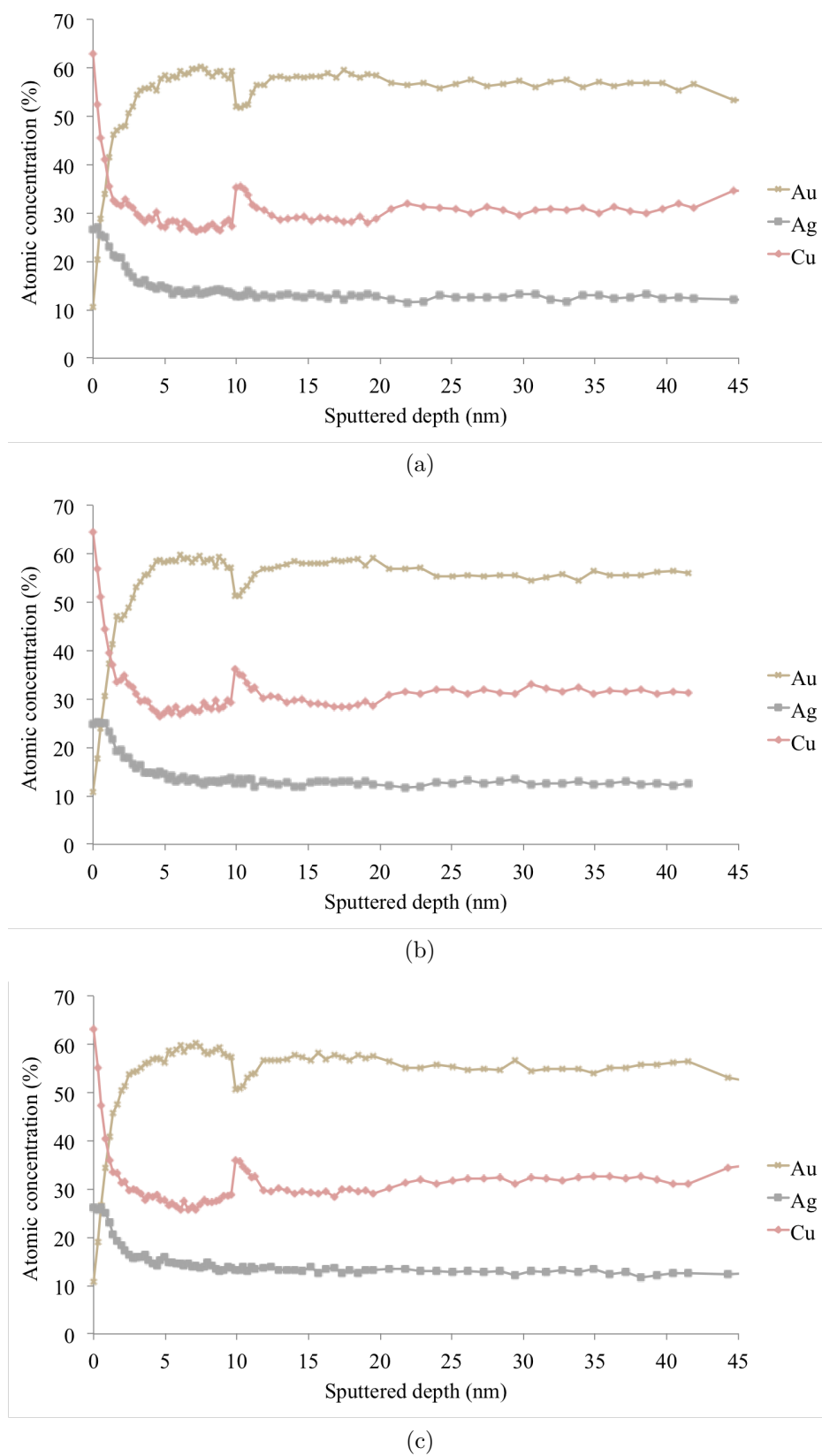


Figure 4.9: Atomic concentration of three alloying elements as a function of sputtered depth for sampling one. Three repetitions of the measurement and three points are presented to show reproducibility and homogeneity of results. An overnight pause in measurement has caused the sudden drop for gold and jump for copper at 9 nm while silver remains unaffected. This might be caused by surface diffusion of copper.

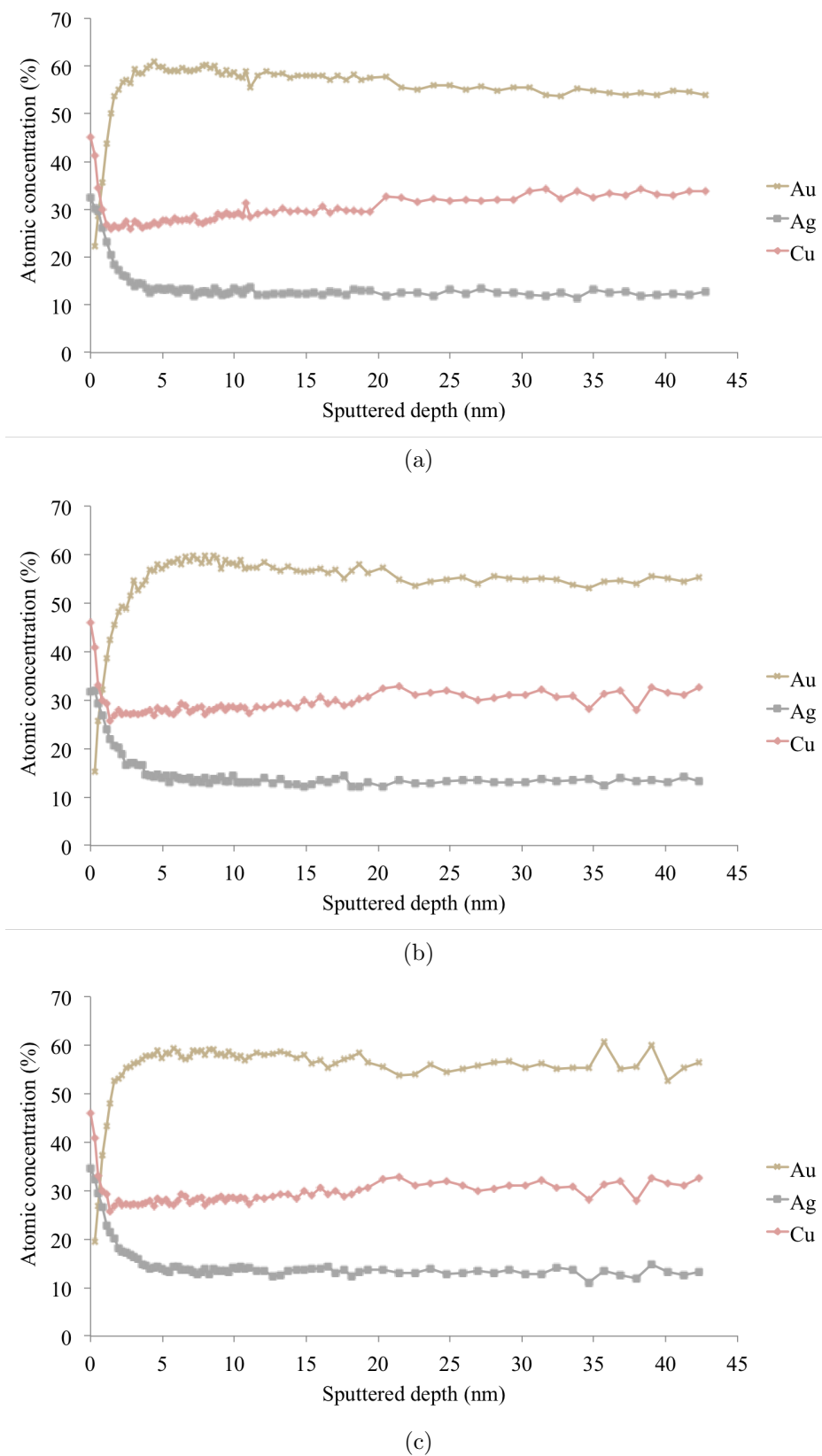


Figure 4.10: Atomic concentration of three alloying elements as a function of sputtered depth for sampling two. Three repetitions of the measurement at three different points are presented to show reproducibility and homogeneity of results.

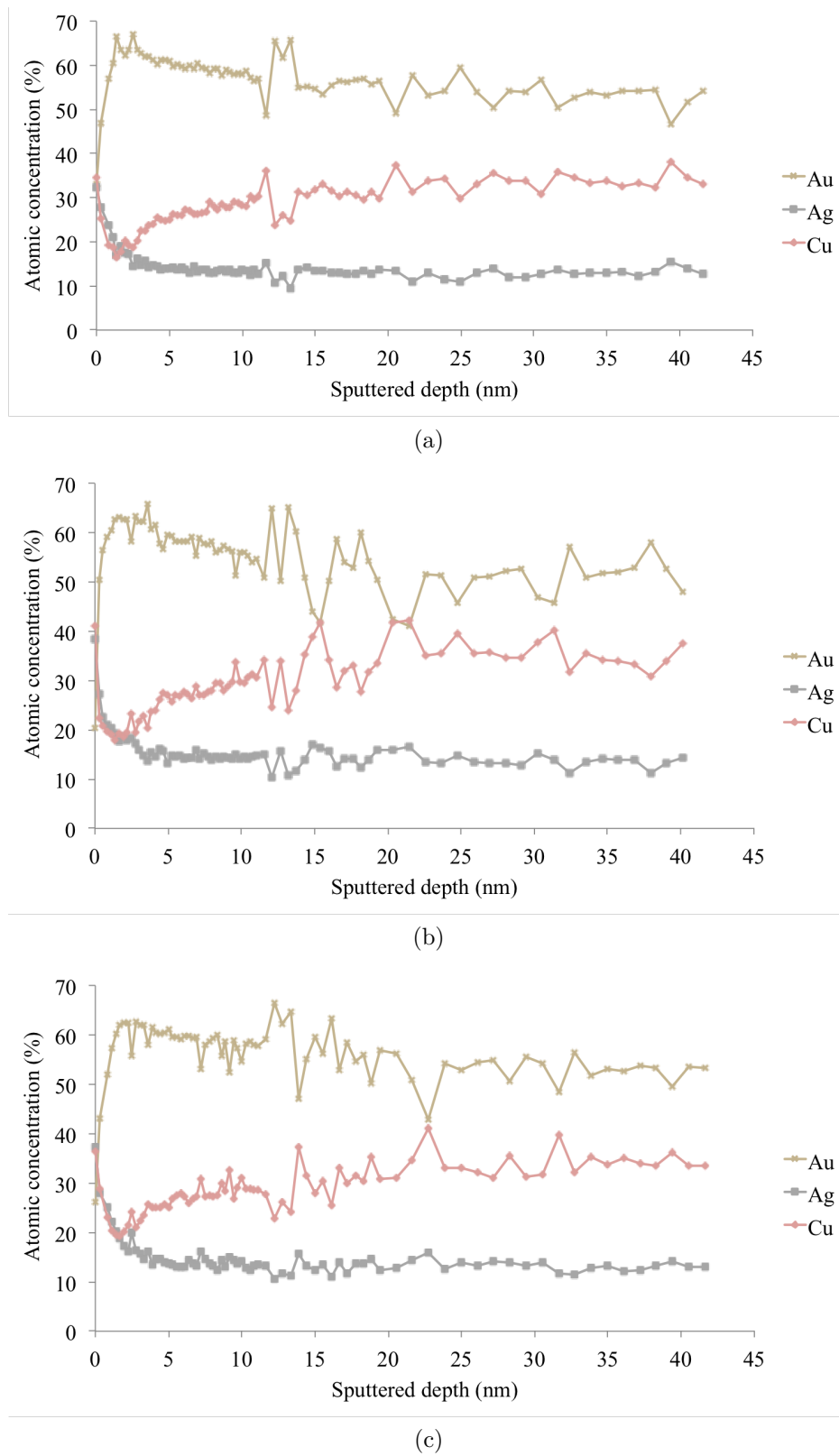


Figure 4.11: Atomic concentration of three alloying elements as a function of sputtered depth for sampling 3. Repetition of the measurement at three points on the same sample are presented to show reproducibility and homogeneity of results.

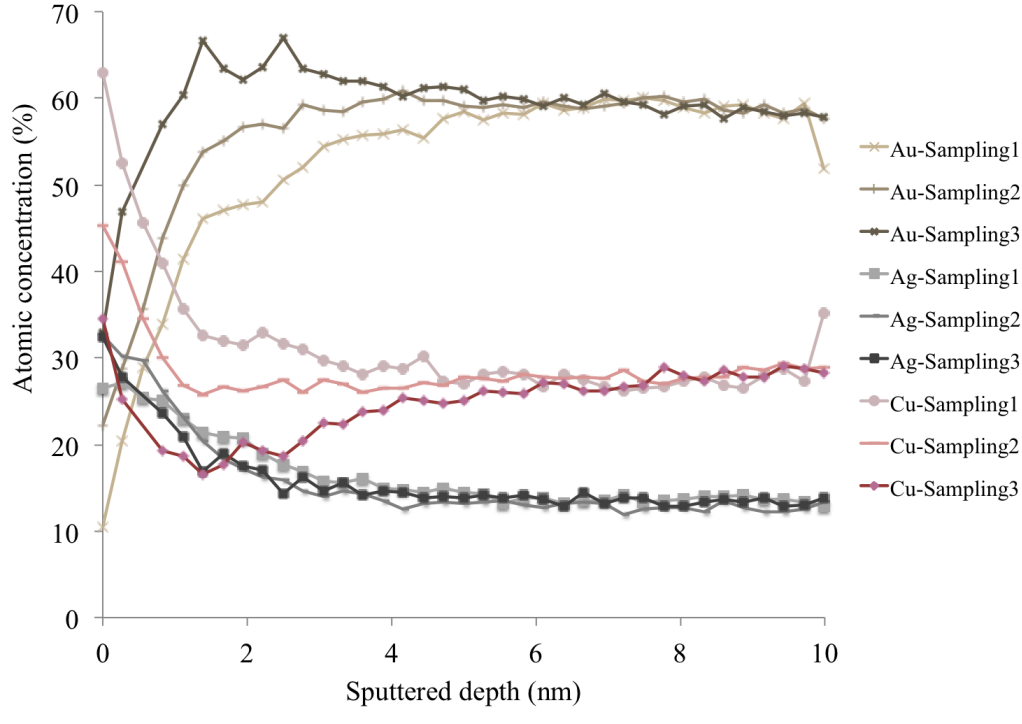


Figure 4.12: Atomic concentration of the three samples over the first 10 nm in depth are overlapped. The color code from lighter to darker colors correspond to sampling 1 to 3 respectively. It can be seen that remarkable difference exists between gold and copper profiles while silver has a similar atomic concentration in all three cases.

4.5 Reflectance and color measurements

The reflectance percentage versus wavelength of incident light is plotted in Figure 4.13. In each case, three curves are presented obtained from three identically prepared samples. It is evident that the samples polished only with grinding paper having the highest roughness values, have the lowest reflectance as well as the highest dispersion in reflection properties. The scatter in reflectance data from the ground surface can be due to the anisotropic surface texture. The residual marks from hand polishing of the surface were directional while they have been random positioned compared to light incident angle.

Going towards lower roughness and smoother surfaces with arbitrary and isotropic distribution of polishing residue marks, the reflectance increases while the deviation among three measured values decreases to the point that all the three reflectance curves obtained for the sample polished with very fine colloidal silica abrasive overlap.

Color values have been calculated based on the reflectance curves and a^* values are plotted versus b^* values in Figure 4.14. Standard color values of 3N, 4N and 5N gold alloys are marked as reference on the graph. All three alloys are 18 karat gold alloys

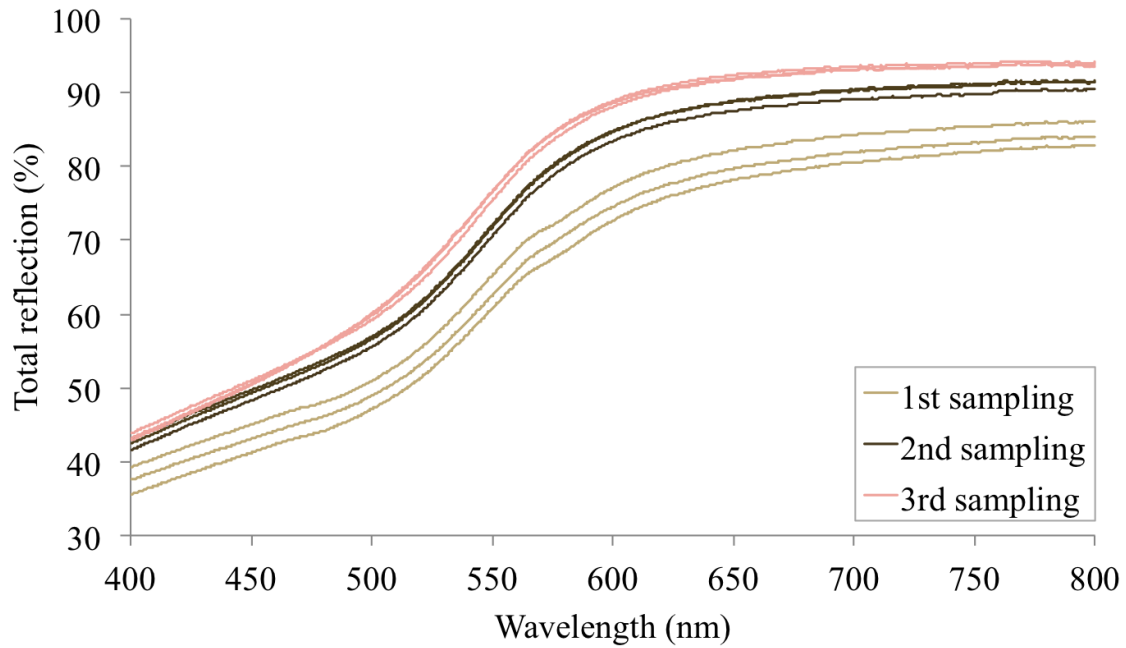


Figure 4.13: Reflectance is measured using a commercial spectrophotometer over the wavelength of 400 to 800 nm. The results are presented as a percentage compared to a reference sample. This reference sample is calibrated at 100% of reflectance before each set of measurements. One measurements is plotted on three samples after each step of polishing.

(therefore containing 75 wt% of gold). However, differences in copper to silver content creates their distinct colors and so they are typically known as yellow gold, rose gold and red gold respectively. The copper content of these three alloys are 12.5 wt% for yellow gold, 15 wt% for rose gold and 20.5 wt% for red gold. The rest of the alloy is composed of silver. Very interesting results of color measurements show a remarkable dependence of color values on the surface preparation method. Following steps of polishing, the color value shifts in a linear trend between 5N and 3N alloy.

The three surfaces of first sampling that is taken after the first step of polishing in water have the highest a^* values that means higher saturation in red and lowest b^* values corresponding to lower saturation in yellow. These values shift from standard colors of our original rose gold alloy towards the one of 5N alloy with higher copper content (red gold). At the second step of polishing, surfaces have color values corresponding to those of standard 4N alloy. While after the last step of polishing (at the third sampling) the colors continue to shift towards lower a^* and higher b^* values (less saturation in red and more in yellow), corresponding to the direction of the 3N alloy with lower copper content.

The extent of this implication of surface preparation in color provides a significant insight. Taking this actuality into account is particularly crucial in luxury goods with high aesthetic values where a lot of importance is given to gold colors. This phenomenon

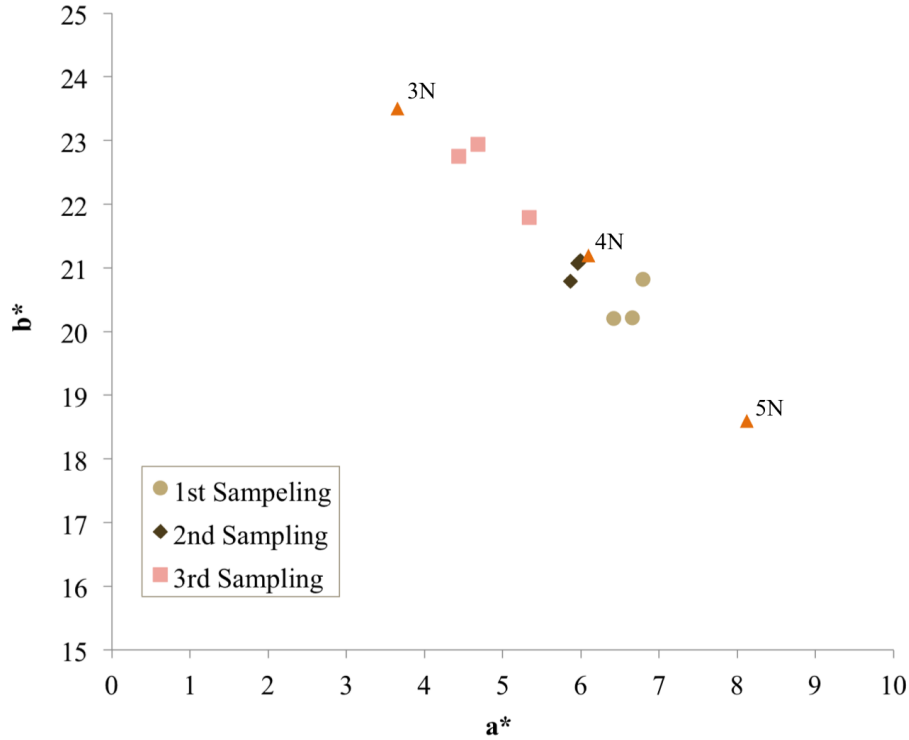


Figure 4.14: a^* and b^* color coordinates for nine samples in three surface roughness states. Color references for 3N, 4N and 5N alloys are plotted for comparison. Going further in polishing process shifts the color towards the alloy with lower copper to silver ratio.

also has important implications in the study of aesthetic and colors of jewelry gold alloys. The effect that surface preparation has on color indicates that correlations that are made between nominal composition of the alloy to the color without considering surface composition might be compromised. It also shows that reproducing and comparing the results is only possible if all the steps of surface preparation are detailed.

The evolution of color during surface finish by mechanical polishing can be explained through tribocorrosion mechanism. Our theory on how tribocorrosion acts as a major role player in determining the color of these alloys is detailed in Chapter on the origin of defects.

4.6 Quantitative correlation of reflectance and color to surface features

As seen in Chapter 2 Section 2.5.1, light scattering from the surface depends on the roughness and the roughness value itself is dependent on measurement method and the length scale of the measurement above others. Accordingly, in order to study

the correlation between lightness and surface roughness, L^* values have been plotted against R_a and R_q roughness parameter that are measured at two different length scales calculated with variable length scale method. Roughnesses are measured and plotted at $20\text{ }\mu\text{m}$ as the length scale below which all the surfaces are very smooth and $710\text{ }\mu\text{m}$ as the total length of the profile. Line roughness profiles have been measured at magnification of 20X using the Keyence laser scanning confocal microscope with lateral resolution of $0.693\text{ }\mu\text{m}$.

In Figure 4.15, for all four combinations of roughness parameters and length scale of measurement a similar linear correlation exists for the samples that are extracted after the first and the second step of polishing. However, surfaces at the third step of polishing, which exhibit grain plateaus (as seen in 3D profilometry and SEM images) and therefore steps in the PFD distribution, do not follow this correlation.

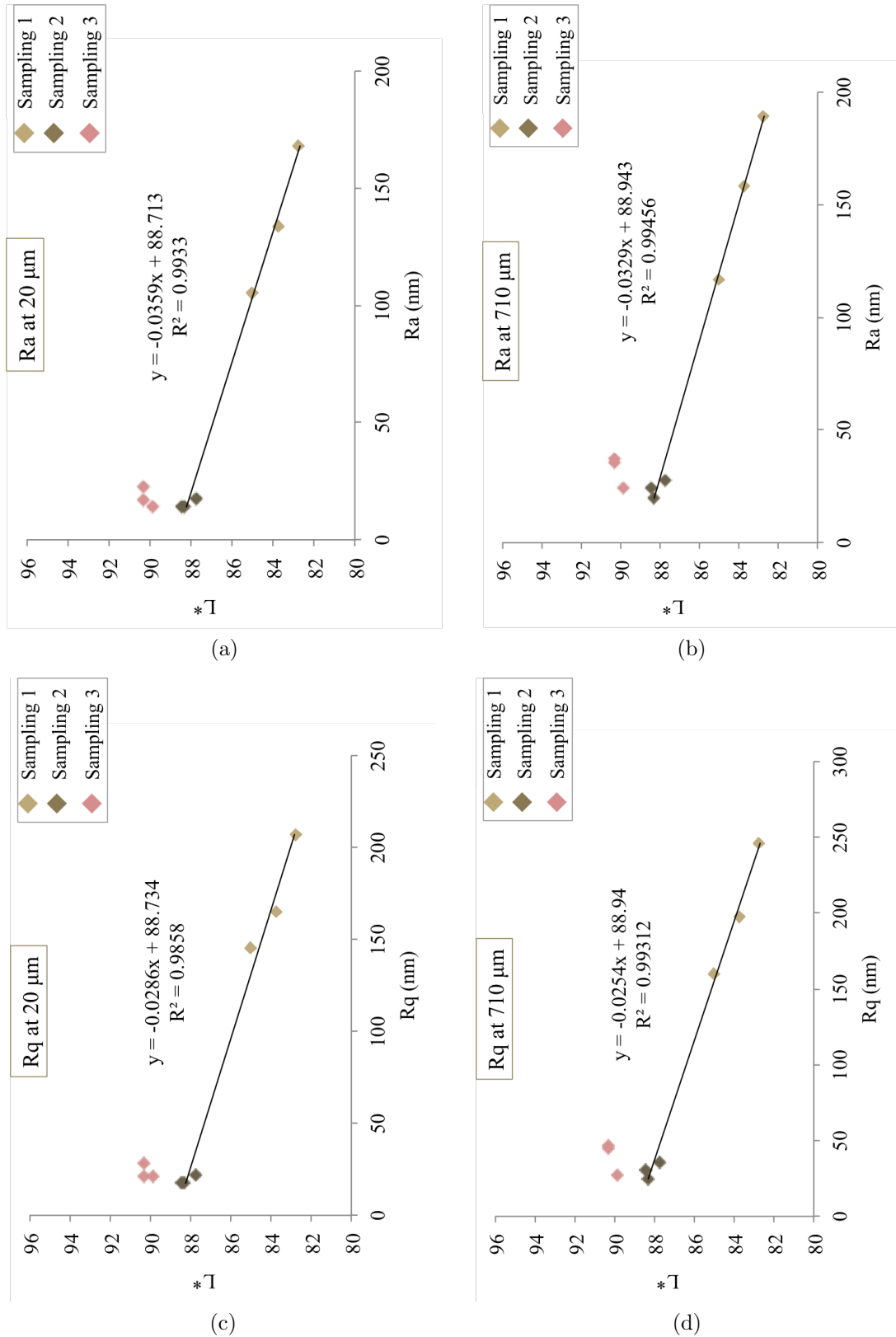


Figure 4.15: Correlations between L^* and roughness parameters R_a and R_q at two length scales of analysis. 20 μm corresponds to the length scale below which all the surfaces are smooth and 710 μm corresponds to the length of the roughness profile. In all four cases a linear correlation exists between roughness and L^* for sampling 1 and 2 with Gaussian distribution of PDF. However, sampling 3 with a step-like PDF does not follow this relationship.

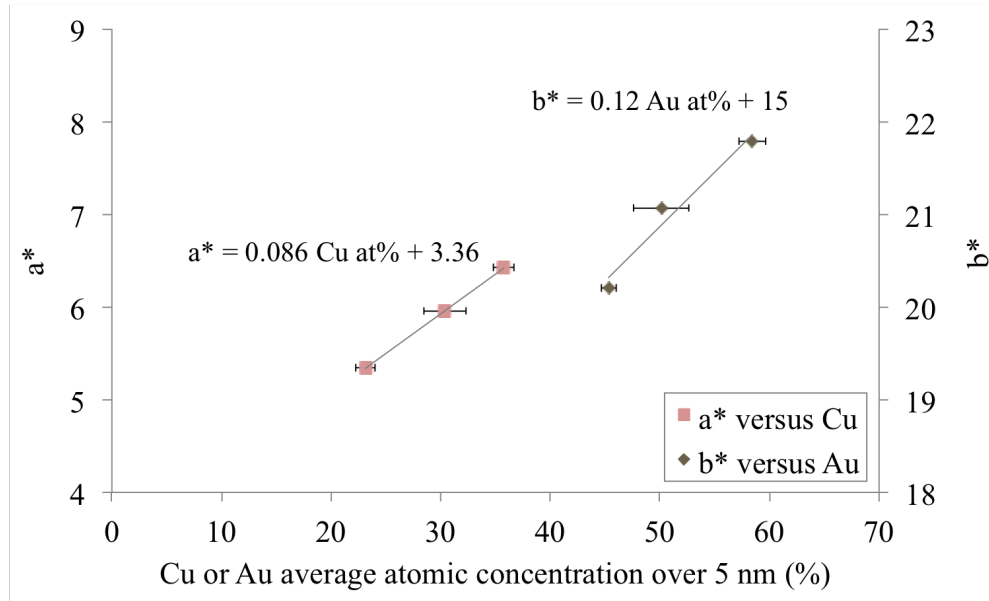


Figure 4.16: a^* is plotted against atomic concentration of copper averaged over 5 nm of the depth profile and b^* is plotted versus similar values of gold for three samples that have been studied by AES. A linear relationship was found in both cases

Total Integrated Scattering (TIS) at incident wavelength of 700 nm was calculated from the spectrophotometry data by dividing diffuse reflectance measured at 0 degree of incident by total reflectance at 8 degrees of incident. The link between measured TIS and roughness and also roughness at power 2 is plotted in Figure 4.17. R_q is measured at length scale of 710 μm and measured as previously explained. There is a scattering in the data that can have its source in resolution and other limitations of both reflectance and roughness measurements. Considering the scattering, there is a better fit between measured TIS and R_q than R_q^2 .

In order to compare measured TIS to theoretical one, the two values are plotted in Figure 4.18. Theoretical values are calculated using Equation 2.8 for $\lambda = 700$ nm and R_q at length scale of 710 nm. Even though the absolute values do not correspond, the trend is in line with the theoretical expectation.

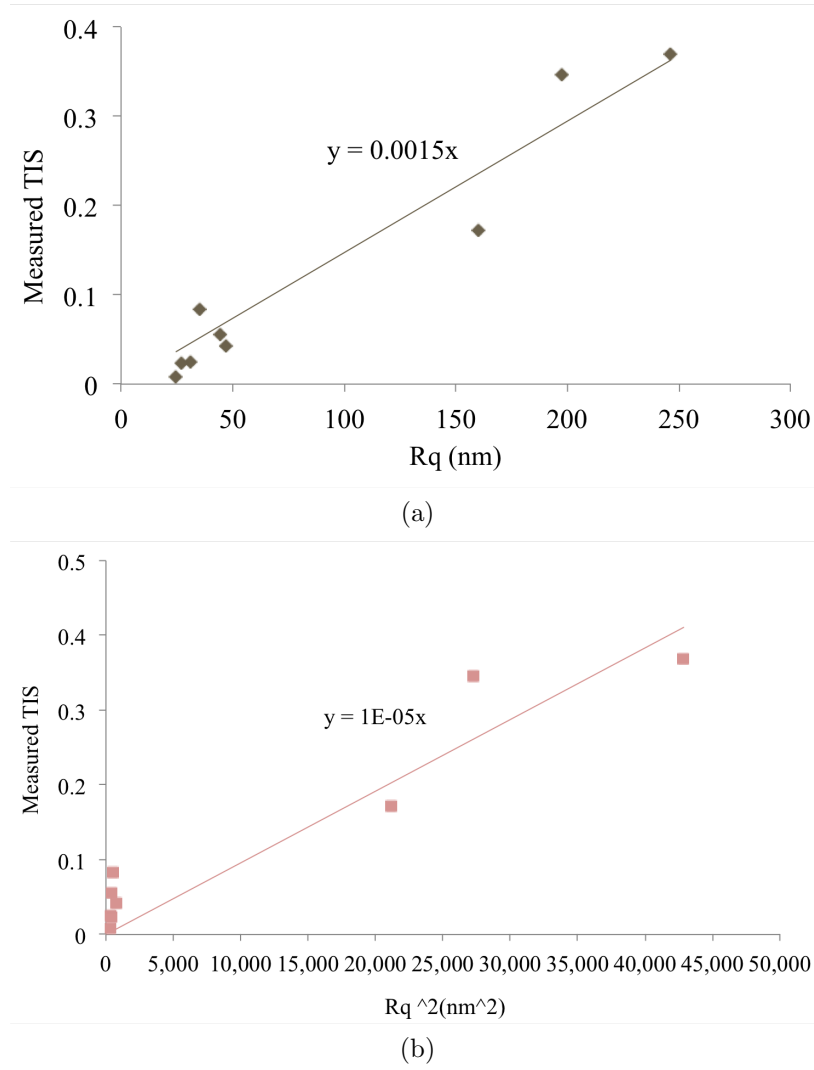


Figure 4.17: Measured TIS values at wavelength of 700 μm are plotted against both R_q and R_q^2 .

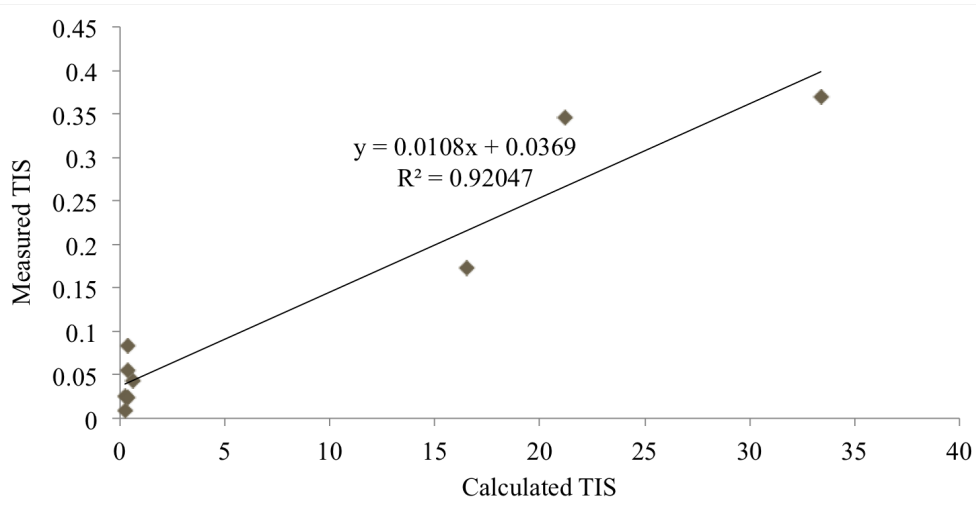


Figure 4.18: Measured TIS at incident wavelength of 700 nm is plotted versus TIS calculated through Equation 2.8.

4.7 Summary and conclusions

Using model samples enables us to introduce surface defects in a controlled manner and study their correlations to aspects of appearance. To produce samples with different roughnesses, a three-step fine mechanical polishing process was defined and a set of samples were extracted after every step of polishing. Surface chemistry of these samples was also expected to have been altered.

Topography assessment showed that after the first and second step of polishing, surfaces are smooth with scratches that become shallower by going toward smaller abrasive particles. From sampling 1 to 2, R_q values that go from 60 nm down to 11 nm. In the final sampling after the third step of fine polishing, the polishing scratches become extremely narrow and shallow. However, due to preferential attack of the alloy by the slurry environment, the grain structure is revealed in form of mirror like plateaus at different step heights. These samples have R_q values of approximately 23 nm that are twice larger and also have larger scatter compared to the previous step. No holes was found on any of the samples.

XPS analysis show copper oxidation on all samples but more severely on the second and the third samplings. AES depth profiles show enrichment in copper on the top surface in all cases. This enrichment is as high as 63 at% for sampling one but it decreases to 46 at% and 35 at% for the next two sampling respectively. A 5 nm near surface layer that follows is enriched in copper for sampling one and depleted in copper for sampling 3. Second sampling falls right in between. Silver is enriched on the surface in all cases with higher amounts for the first sampling. Gold is as at very low concentration on all the surfaces but its concentration also recovers to nominal content after sputtering 5 nm.

Total reflectance increases with further polishing of the samples and its highest value is found for third sampling. It is particularly interesting because these samples have roughnesses that are twice larger than the one of the third sampling but still lower than the first sampling. CIELAB color measurements show that by going further in the process of polishing, a^* and b^* values shift toward lower saturation in red and higher saturation in yellow. Knowing that copper is the cause of red color and gold is responsible for the yellow tint, these interesting results are in line with previous surface chemistry assessments.

Taking into account translucency of gold thin films would mean that color of these alloys is not only a result of top most surface composition but rather a consequence of near surface composition. The thickness of surface layer that plays a role in color is however unknown. Yet, as surfaces with various colors have identical composition at 5 nm below the surface it became evident that a thickness of 5 nm or less is responsible for the difference in colors.

A linear relationship was found between L^* and both R_q and R_a at different length scales of roughness measurement for sampling 1 and 2 with Gaussian distribution of probability density function of surface height. This correlation does not apply to the surface with non-Gaussian distribution of PDF. a^* and b^* color values were also linearly correlated to copper and gold content averaged over a depth of 5 nm of the surface respectively. The equations that present these quantitative links are the following equations:

$$\begin{aligned}L^* &= -0.025R_q + 88.94 \\a^* &= 0.086 \text{ Cu at}\% + 3.36 \\b^* &= 0.12 \text{ Au at}\% + 15\end{aligned}$$

Effect of surface roughness on TIS was also studied. Despite the scatter in the data, the correlation between total integrated scattering with R_q is in line with what is predicted from theory as described in Chapter 2 Section 2.5.1. For roughnesses measured at higher length scale (waviness), following linear relationship could be drawn from measurement data:

$$TIS = 0.0015R_q$$

Effect of surface holes on appearance was considered to be a decrease in lightness proportional to surface coverage of holes. As this value cause a negligible ΔE^* it was concluded that holes appearing on the surface are not the cause of the defect in appearance on the industrial polished surfaces under study.

Chapter 5

Origin of defects

Surface defects that appear on the final product and cause a defect in appearance have the origins either in the raw material or the process of fabrication. Recognizing the processes of production that can lead to a defect in appearance helps the industry to avoid their occurrence. In this chapter, origins of inhomogeneous hardness, variation in surface composition and surface porosity are studied. These defects are attributed to local mechanical deformation experienced by heat treatment, tribocorrosion acting during polishing and severe thermomechanical deformation respectively.

5.1 Introduction

Previously, surface features and defects that can be found on polished surface of industrial watch and jewelry components have been recognized and their correlation to aspects of appearance have been studied. Ideally, products with flawless appearance could be fabricated if the manufacturer is able to avoid these defects from occurring in the first place. To do so, it is essential to recognize origin of the defects in the process of fabrication. Accordingly, in this chapter we will study the origin of inhomogeneities in hardness, modifications in surface composition and the surface porosity.

5.2 Inhomogeneity in hardness and microstructure

In Chapter 2 we measured hardness of two watch components across the diameter and made the following observations: local hardness varies across a single piece and the good piece is harder near the external edges compared to the bad piece.

Local variation in hardness can originate from inhomogeneous microstructure created during steps of production. The process followed by a dust cover from the initial punched disk to the final product induces different grade of mechanical deformation in different locations on the sample. Local high degree of deformation induced in processes such as stamping can cause uneven accumulation of stress and strain in the pieces and consequently uneven grain growth during the cycles of heat treatment.

In order to explore the effect of processing steps involving deformation and heat treatment on microstructure and hardness of 18 karat gold alloy, we have studied the cross sections of three pieces in 5N alloy at three stages of production. First one is a disk punched in an alloy sheet at the entrance of production process. The second one is a piece that has been through most of the steps of fabrication including deformation, machining and heat treatment. And finally a fully fabricated flawless dust cover. Considering symmetry around the center of the piece, we have cut the sample in a quarter and analyzed the cross section over the radius. Cross sections were prepared according to the method explained in Chapter 3 Section 3.3.3.

Figure 5.1 shows SEM images at different locations on the initial material. It is observed that the raw initial alloy has large dispersion in grain size but similar homogeneous distribution of this microstructure across the cross section. Figure 5.2 also shows a similar cross section from a dust cover later in the process of fabrication. A set of nine indentations are made at three locations on the sample and results are marked at the corresponding locations. It is evident that the hardness values are higher in center compared to proximity of edges.

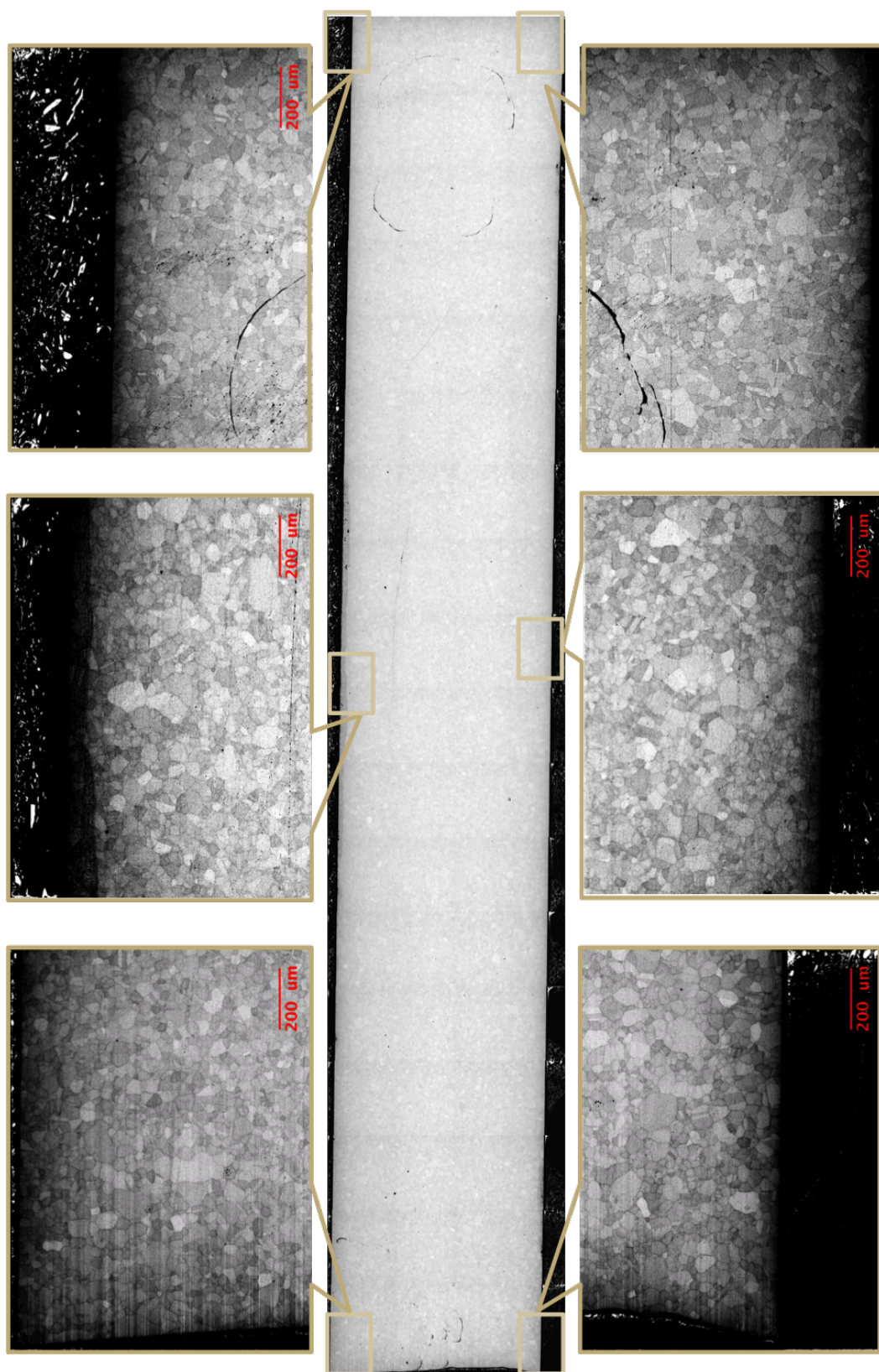


Figure 5.1: SEM images of microstructure of a punched disk as row material before entering the process of fabrication. Grain structure had a similar dispersion in size at different locations on the cross section

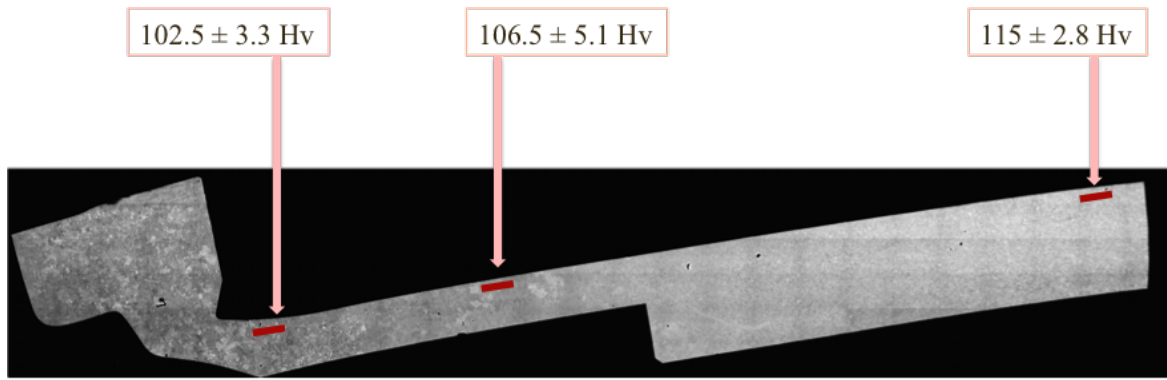


Figure 5.2: Average of three hardness measurements are marked at different positions on the surface. A slight gradient towards higher hardness is seen by moving from the edges towards the center of the piece.

It is interesting to compare these results to laser intensity images obtained from different locations on the flawless dust cover as the final product shown in Figure 5.3 (principal of measurement is explained in Chapter 3 Section 3.3.1). Here, the flat end of the image corresponds to the center of the dust cover and the other end of the image corresponds to the edge of the piece. It is evident that central flat bottom that has been less deformed during the process of fabrication has smaller grains while near the edges and in highly deformed areas, grains are remarkably enlarged. This means that the non-homogeneous microstructure and hardness that are induced in the pieces in the initial steps of fabrication persists until the final step. This uneven hardness can make uniform mechanical polishing of the whole surface very challenging and consequently negatively affect the outcome of polishing process. Therefore, non-homogeneous microstructure can indirectly induce an aesthetic defect.

To examine the possible direct effect of non-uniformity in microstructure on reflection of light from this Au-Ag-Cu alloy, a local high resolution reflectance measurement was performed on a polished cross section of a watch component. The watch component under study is a 5N 18 karat watch component extracted from the production line after most steps of mechanical deformation. Cross section of the piece is mirror polished using the standard polishing procedure down to $1 \mu\text{m}$ size of abrasiveness particles with the procedure previously explained. Once the reflectance measurement is performed, the microstructure was revealed by a further step of polishing with colloidal silica particles of $0.03 \mu\text{m}$ in size which through preferential chemical attack create a grain topographical contrast. The reflectance was measured using a multi-angle reflectance setup that is home made at the Swiss Federal Institute of Metrology (METAS). This instrument takes advantage of Basler acA1920-40um with Computar M7528-MP lens cameras for detection and a Hamamatsu opto-spectrum generator as spectrally tunable illumination source. Spatial resolution of the measurement is $42 \mu\text{m}$ per pixel. This apparatus provides the opportunity of measuring with several combination of illumination and detection angles. Figure 5.4 shows the microstructure imaged by the confocal laser microscope and the reflectance .

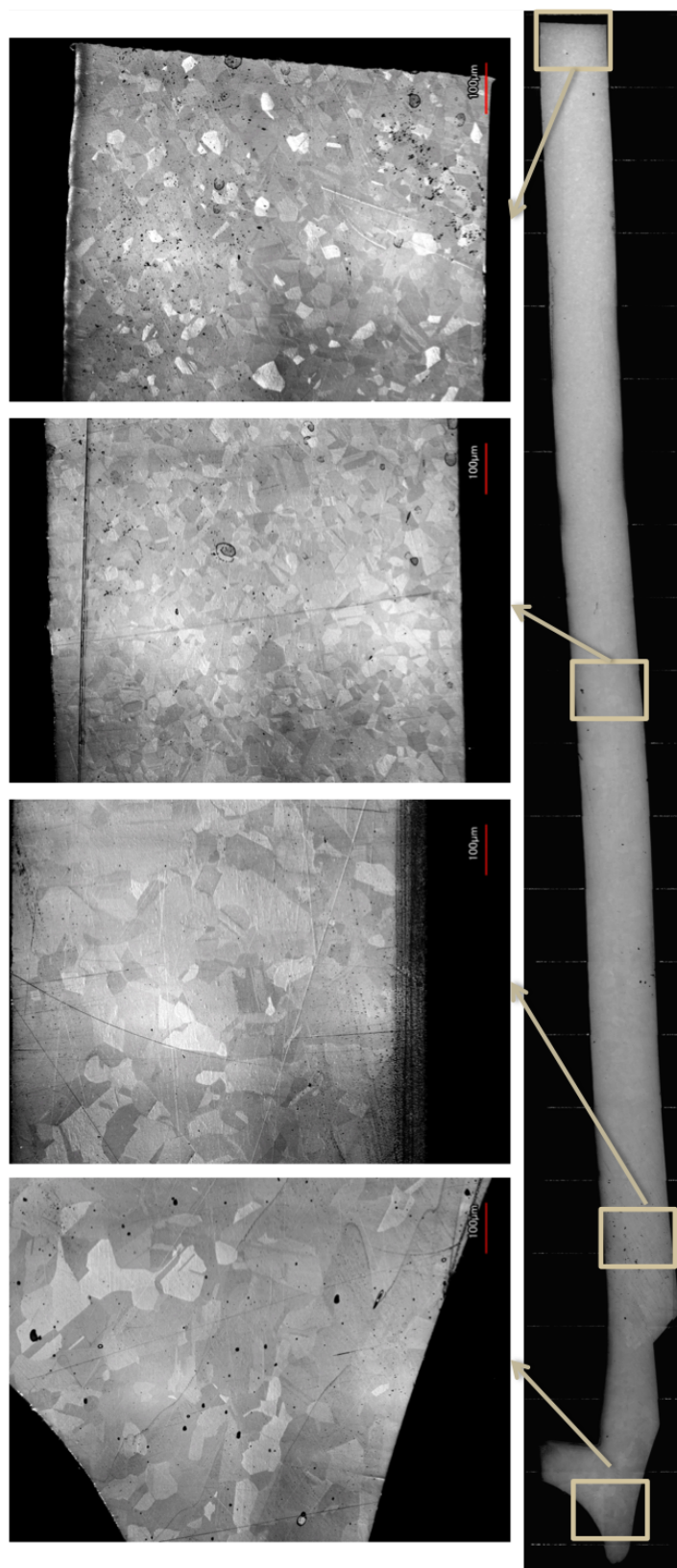
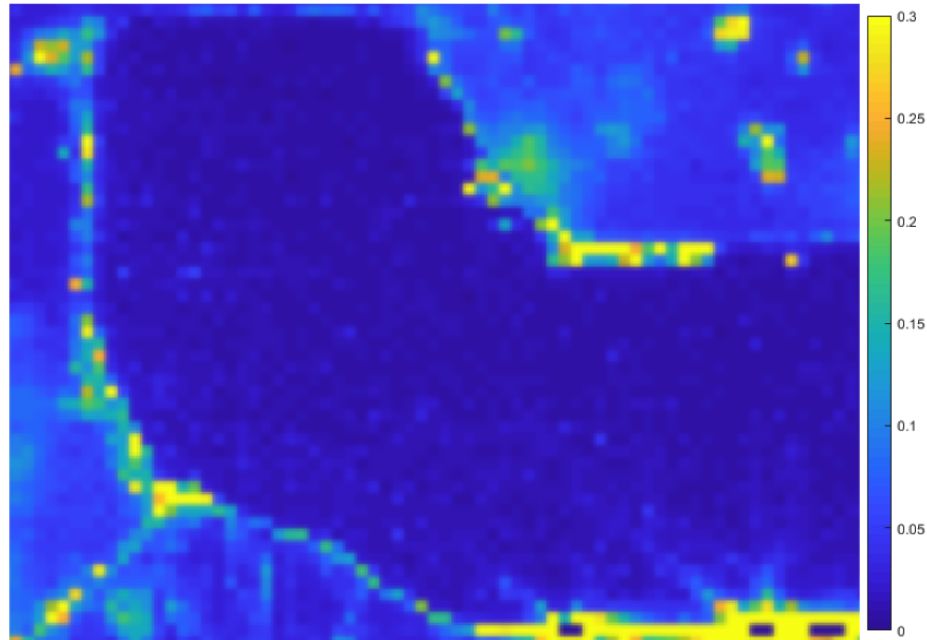
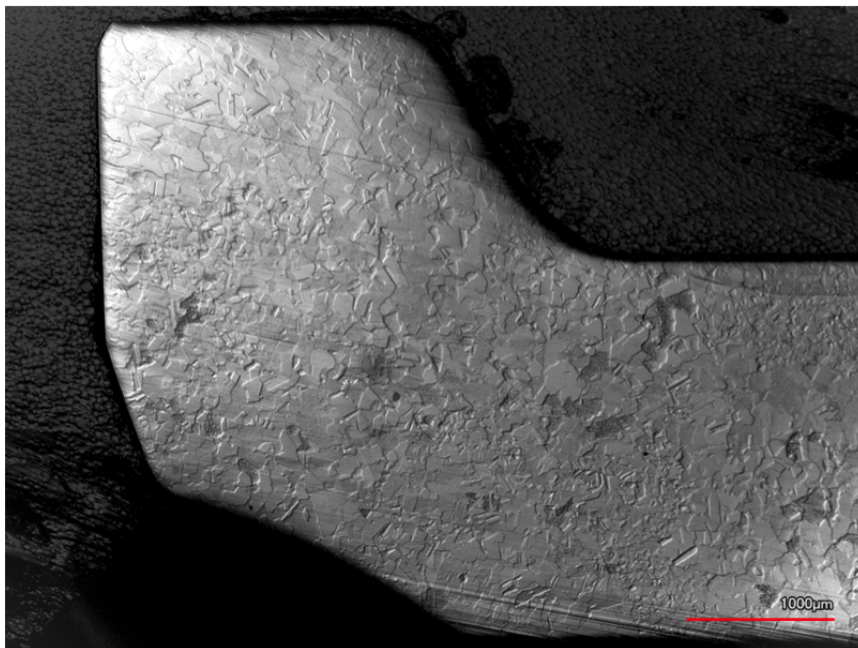


Figure 5.3: Microstructure of a final product is shown at different locations on the cross section. The flat end of the image corresponds to the center of the dust cover and the other end of the image corresponds to the edge of the piece.

The results show no contrast in diffuse reflectance for regions that have different grain size. Therefore, it is concluded that the distribution that exists in the grain size of the watch components does not directly contribute to variations in diffuse component of reflection.



(a)



(b)

Figure 5.4: A 5N 18 karat watch component extracted from the production line after most steps of mechanical deformation: a) diffuse reflectance measurement shows similar contrast all over the cross section. High diffuse reflectance on the outline of the sample happens at the interface between the resin that the piece is mounted in. b) microstructure of the piece is imaged using the laser confocal microscope.

5.3 Modified surface composition

As shown in Chapter 3, surface composition of industrial pieces differs from their bulk composition. The surface defective piece was shown to be depleted in copper and gold while enriched in silver. This depletion in copper continues down to around 5 nm below the surface. In comparison, flawless piece had higher copper concentration and lower silver presence on the surface and yet, copper depletion was found in the first 5 nanometers.

We suggest that these modifications in near surface composition results from tribo-corrosion during the polishing process that induces selective copper oxidation. The proposed mechanism is explained below and it will be followed by a study on the effect of selective copper oxidation on color and reflectance of the 18 karat 4N gold alloy.

5.3.1 Tribocorrosion: a side effect of polishing

During a typical polishing process, the working surface is under mechanical loading and in relative motion against a counter part. The material removal happens either as the result of this relative motion against an abrasive counter part (usually in presence of a lubricant) or against a soft counter part with a slurry of abrasive particles spread in between. Metallic working piece can potentially react with the active environment of the slurry or lubricant (even water) leading to oxidation. This oxidation is then followed by material removal. Such combination of acting elements forms a tribocorrosion system. This system is schematically presented in Figure 5.5.

Based on the study of surface chemical composition together with color measurements, we propose that the mechanism under which the surface composition of the jewelry gold alloy and consequently its color are altered, is the following:

1. Once the bulk material is in contact with an active environment, the least noble metal that is copper in our case, oxidizes. This active environment can be either simply air that contains humidity, water that is typically used as lubricant in grinding or more chemically complex commercial solutions containing abrasives particles or lubricants.
2. Due to presence of abrasives and under mechanical loading and relative motion, the surface oxide layer is removed. Difference in copper concentration of the surface and the bulk then acts as a driving force for diffusion of copper atoms from the few nanometers below the surface. These atoms will also oxidize in contact with the active environment.
3. This diffusion controlled process continues until it forms a surface layer that is depleted in copper. Once the polishing process (and thus material removal) stops, the top surface of our working piece is composed of a copper depleted region that is sandwiched between a thin oxide layer and the bulk composition.

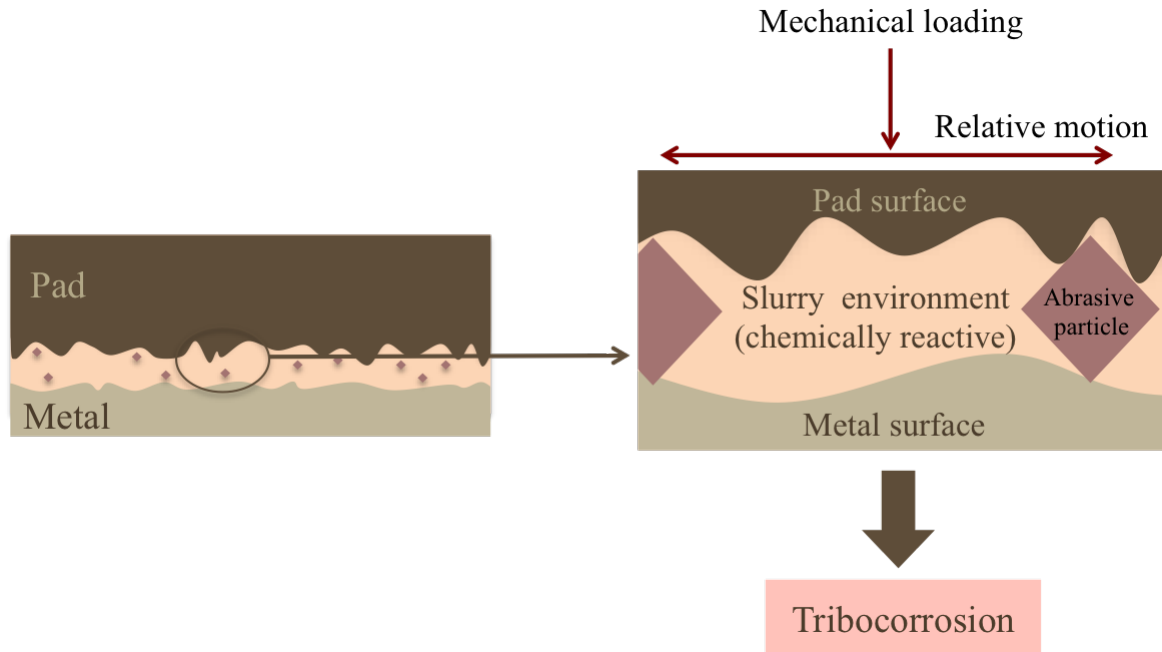


Figure 5.5: The combination of mechanical loading and relative movement of two surfaces in presence of a slurry means that polishing is potentially a tribocorrosion system.

The first two layers play a remarkable role in color of the surface and create an offset in color of bulk material that would depend on their composition.

This mechanism is schematically presented in Figure 5.6.

In order to assess the effects of selective copper dissolution on near surface composition of 18 karat gold alloy and its consequences on color and reflectance, a set of electrochemical experiments were performed and are detailed below.

5.3.2 Electrochemical copper dissolution

An electrochemical cell was used for this purpose that is schematically shown in Figure 5.7. In this cell, the gold alloy under study is the Working Electrode (WE) with a circular exposed area of 1 cm in diameter. Two platinum Counter Electrodes (CE) are placed on the two sides of the WE. The Reference Electrode (RE) is a mercury/mercury sulfate and the electrolyte is $1M Na_2SO_4 + 0.02M H_2SO_4$. The solution was chosen based on a study by Laurent on selective copper dissolution [72]. The pH of the electrolyte was measured to be 2.16. The cell was sealed and in all cases, the solution was aerated with argon gas to remove oxygen. The sample was then inserted into the solution. Data acquisition was performed using a Metrum Autolab PGSTAT30 potentiostat with Nova software. Open circuit potential (OCP) was recorded for 20 seconds before starting the potentiostatic or potentiodynamic tests.

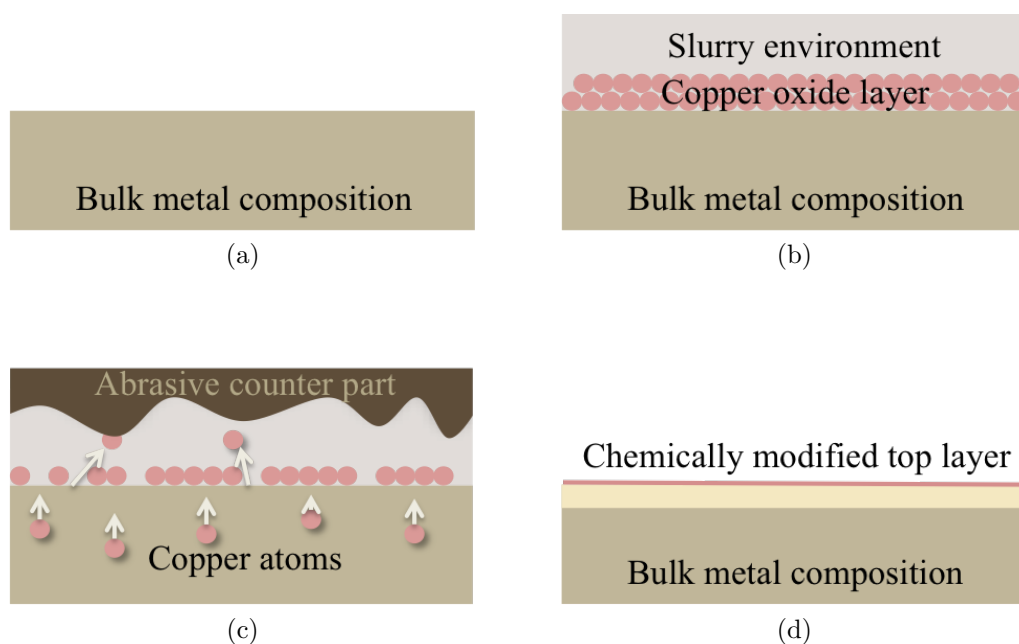


Figure 5.6: Schematic representation of how polishing as a tribocorrosion process induces a chemically modified layer on the surface of Au-Ag-Cu alloy. a) The homogeneous bulk composition before polishing, b) exposure to potentially reactive environment causes oxidation of Cu on the surface, c) the oxide layer is removed by abrasion and due to gradient in composition, Cu atoms migrate from few nanometers below the surface to the top surface and d) at the end of polishing the surface is composed of a sandwich of thin oxide layer, chemically modified thin film on top of the bulk material.

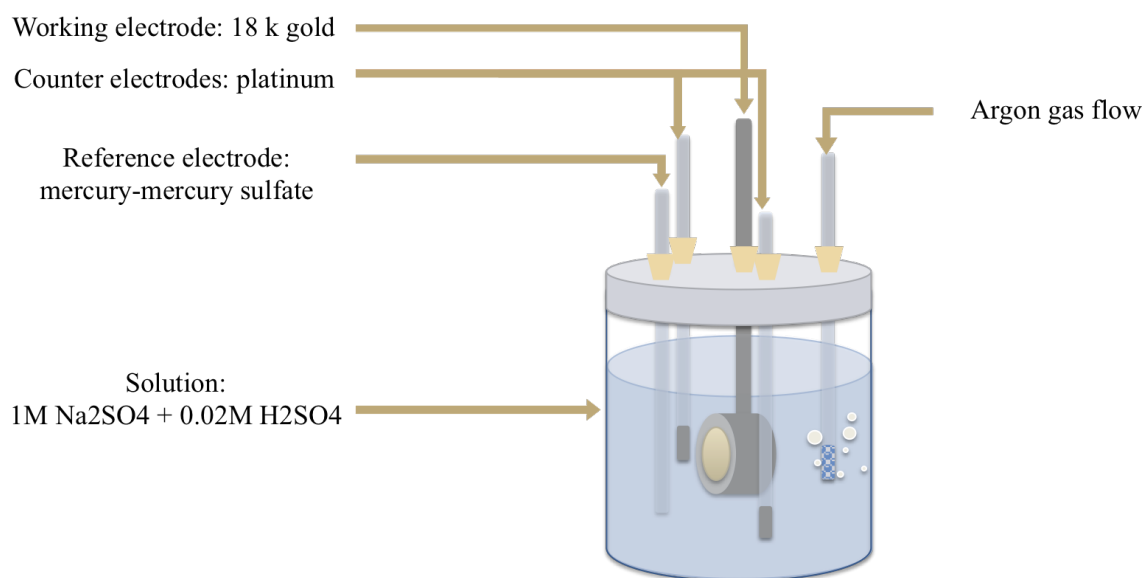


Figure 5.7: Schematic presentation of the electrochemical cell used in this study. Details of electrodes and the solution are marked in the image.

For selective copper dissolution potential of 0.55 V was chosen. Three samples were prepared and studied here. They are labeled and prepared as following:

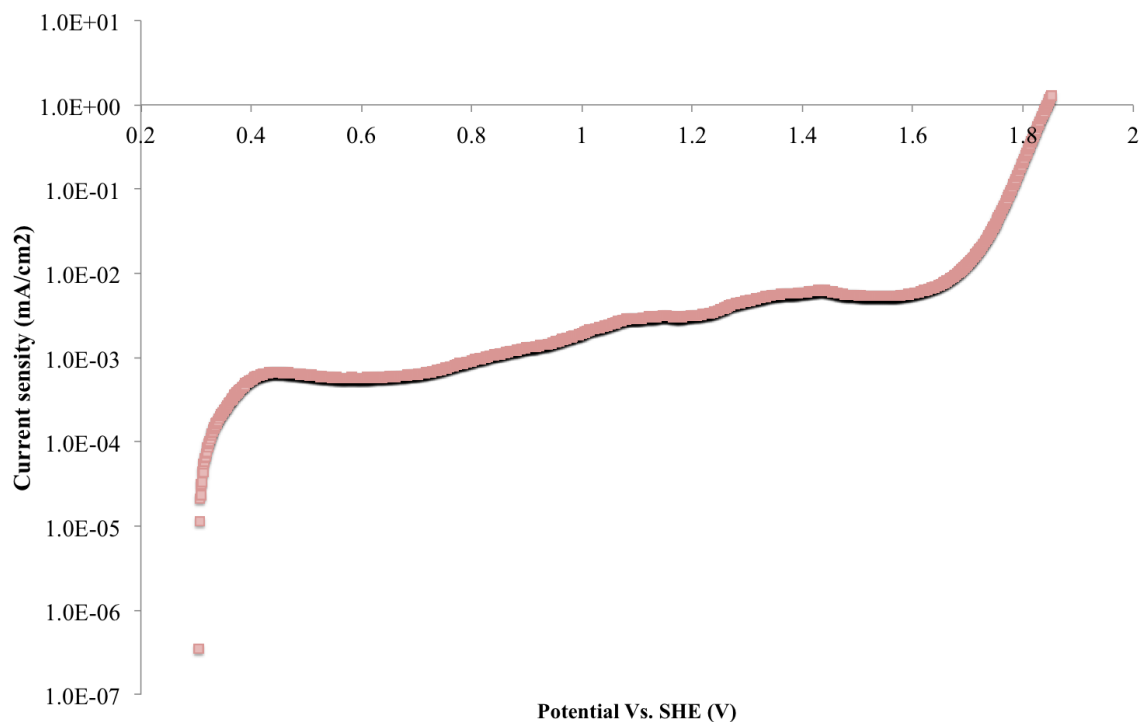


Figure 5.8: Polarization curve for the 18 K gold alloy in $1MNa_2SO_4 + 0.02MH_2SO_4$ solution.

- E01: Applied potential of 0.55 V versus SHE during 0.5 hour, total charge of 0.27 mC was measured.
- E02: Applied potential of 0.55 V versus SHE during 4.5 hour, total charge of 1.83 mC was measured.
- E03: Cathodic cleaning by applying a current of $-1 mA/cm^2$ during 300 seconds.

Roughness of surfaces are measured before and after electrochemical tests and the results are presented in Table 5.1. Roughnesses are measured over a length of 285 micrometers with a distance of $0.280 \mu m$ between every two points and values are averaged over three measurements. No remarkable change has been induced on surface roughness as a result of the electrochemical tests.

Table 5.1: Roughness values averaged over three measurement lines are presented for three samples before and after the electrochemical tests.

Sample	R_a before the test (nm)	R_a after the test (nm)
E01	8 ± 1	7 ± 2
E02	8 ± 0.5	8 ± 0.6
E03	8 ± 1.5	6 ± 1.5

Chemical analysis

Surface and near surface compositions are analyzed for samples E01 and E03 using AES. Results are shown in Figure 5.9 for peak intensities. Sulfur that is present in the electrolyte was found on the surface of E01 but not on E03. For sample E03, two drops

occur in gold signal at 3.5 nm and 8 nm that coincide with step jumps for copper signal.

Atomic concentrations of alloying elements are calculated and plotted as a function of sputtered depth in Figure 5.10. For E01, gold content at the surface is very low. However, it quickly recovers to slight saturation at 2.5 nm below the surface. In contrast, silver is highly saturated on the surface at 47 at%. The silver content drops down to 3 nm below the surface and is stable from there on. Copper is also slightly enriched on the surface at 37 at%. However, it drops down to 20 at% after sputtering only 1 nm. After forming a depletion valley in the depth profile right below the surface, copper content slowly recovers in the next 30 nm to finally reach the bulk composition.

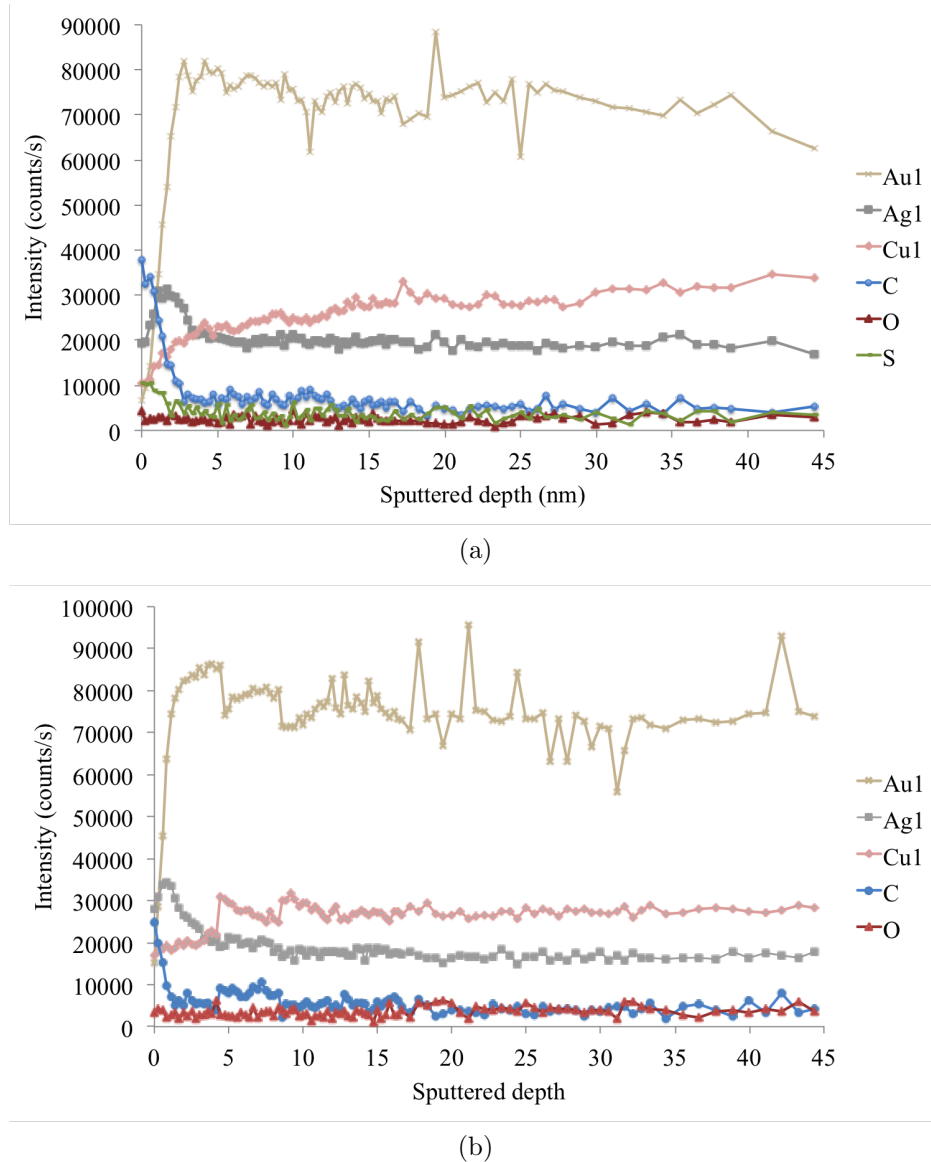


Figure 5.9: Intensity signals for in-depth profiles of a) E01 and b) E03.

For E03 compared to E01, there is higher amount of gold and lower amount of silver present on the surface while copper content is similar. Here again, copper profile forms

a valley beneath the surface, but as seen in overlapped profiles of Figure 5.11, there is more copper in E03 than in E01 from 4 nm and below. On the whole, both samples have modified surface composition and this modification continues below the surface.

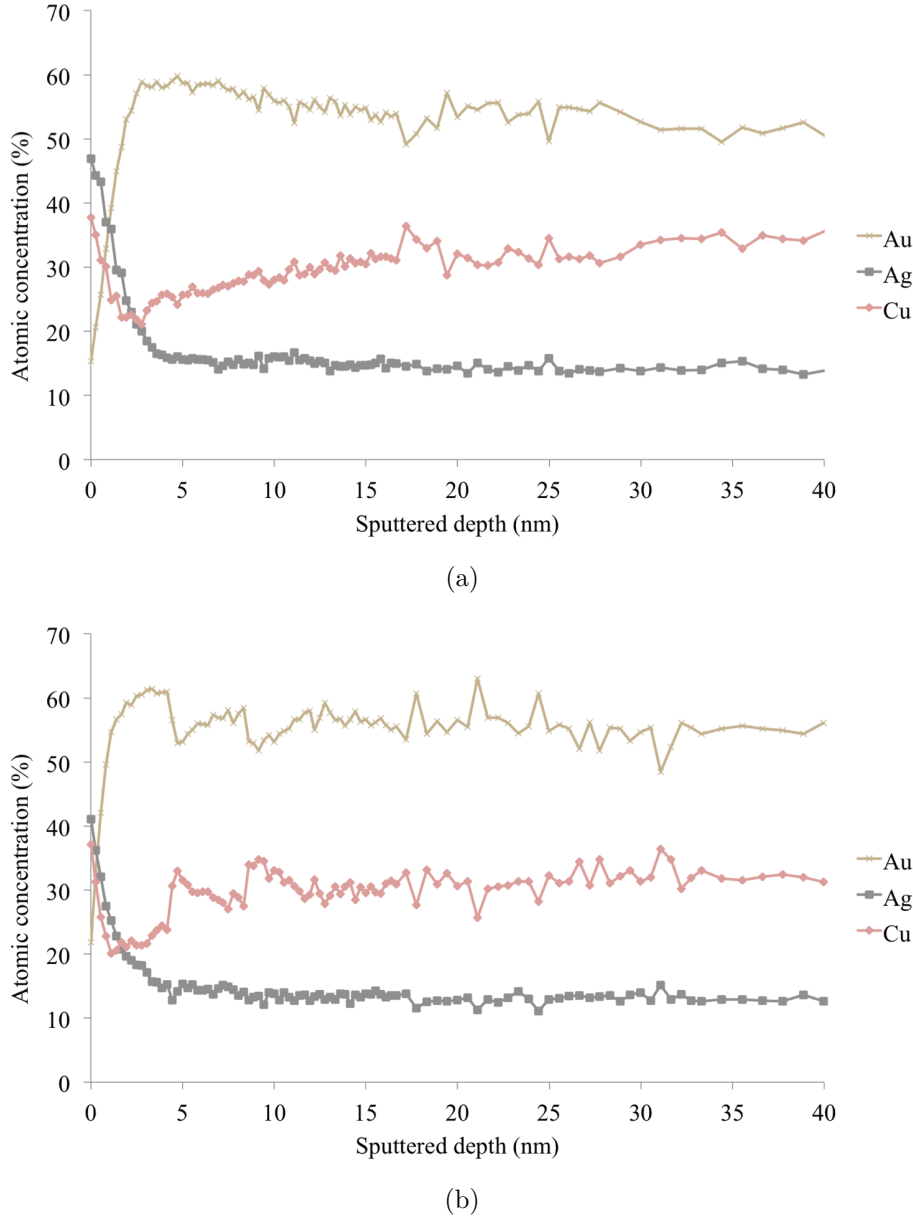


Figure 5.10: Intensity signals for in-depth profiles of a) E01 and b) E03.

Reflectance and color measurements

Reflectance measurement results are illustrated in Figure 5.12. Total reflectance curves of samples E01 and E02 overlap and E03 shows a slightly lower reflectance values at higher wavelengths. CIELAB color values are calculated from total reflectance curves. a^* and b^* values are plotted in Figure 5.13 along with standard values for 3N, 4N and 5N 18 karat gold alloys. All three samples have a color closer to the one of the initial alloy than 3N and 5N variations. From E01 and E03 that have the higher difference in color between three samples, there is a shift of 0.26 towards lower a^* values and a

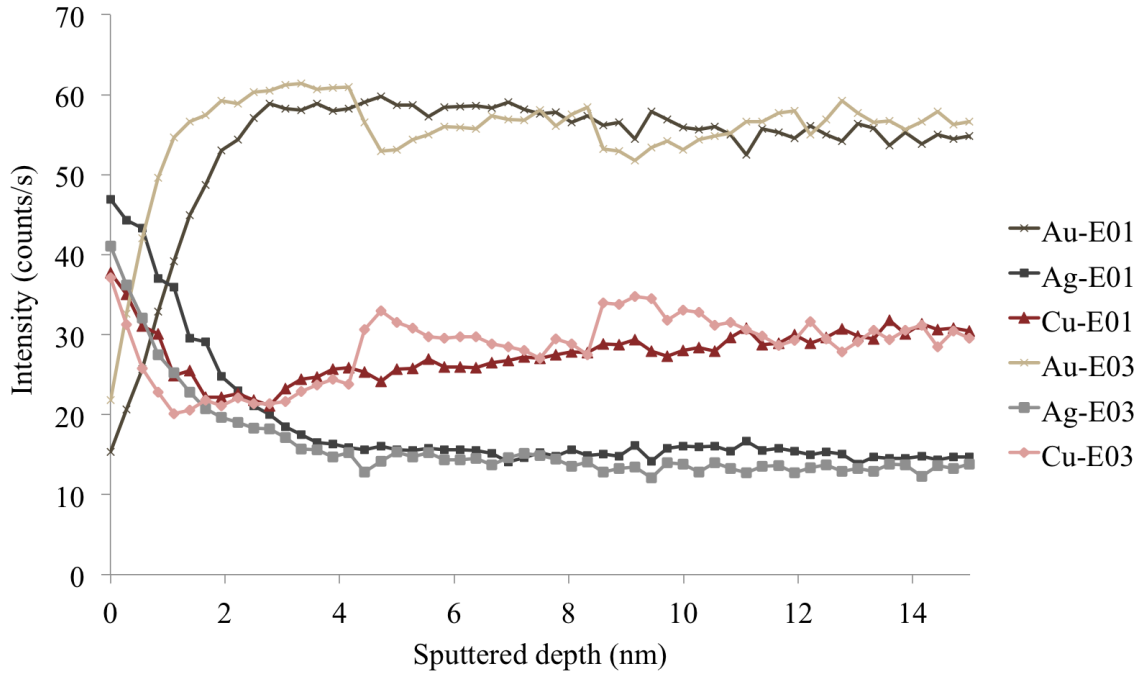


Figure 5.11: Depth profiles of the two samples are overlapped in the first 15 nanometers.

shift of 0.85 towards lower b^* values. This would essentially mean that E03 is slightly less saturated in red and yellow compared to E01.

Comparing color measurement results with chemical analysis, as presented in Figure 5.11, shows that this shift towards less saturation in yellow corresponds to less gold concentration on the top surface. However, the shift towards less red saturation cannot be justified by copper content of the top surface as two samples have similar atomic concentrations. Instead, it is interesting to note that the sample that has a less strong red tint has lower copper content in a 2 nm layer below the surface. This shows that near surface chemical modification affects the color and thus the appearance.

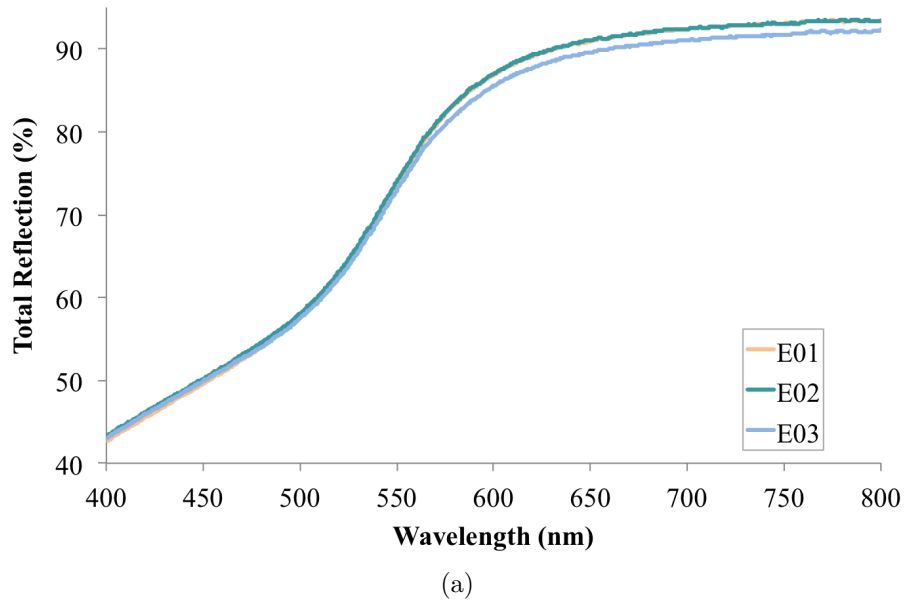


Figure 5.12: Total reflectance measurements for 2 samples with forced copper dissolution and 1 sample with cathodic surface cleaning. At lower wavelengths, all three samples have similar reflectance. However, E03 has slightly lower reflectance intensity at higher wavelengths.

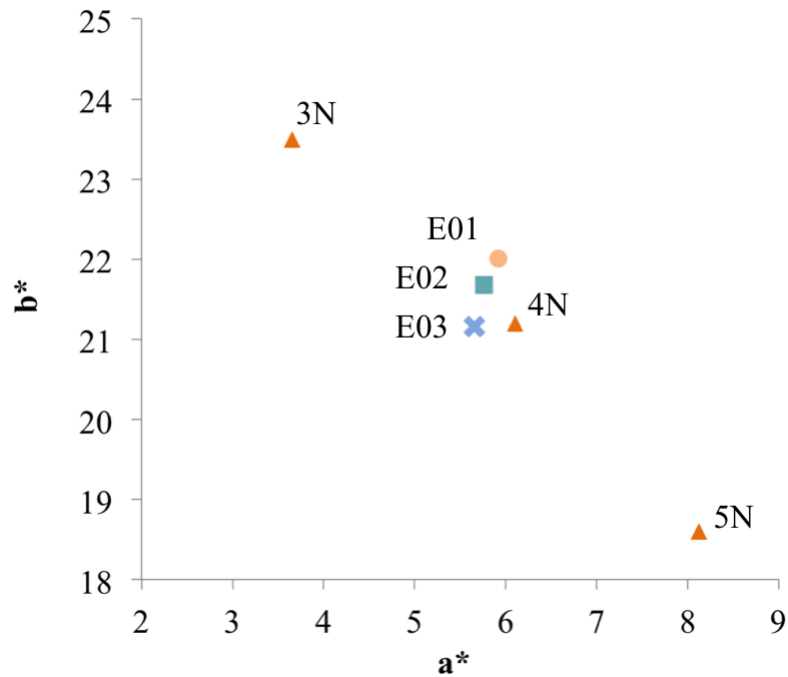


Figure 5.13: Color values for disks E01, E02 and E03. For purpose of comparison, standard colors of 3N-5N 18 karat gold alloy with different proportions of copper to silver are plotted as well.

5.4 Surface porosity

During some of the steps of production such as stamping, 18 karat gold pieces go through severe local deformation that is followed by steps of heat treatment. The combination of the two processes can potentially be the source of porosity that was found on the industrial pieces and accordingly we are interested in examining this combined effect. To induce local mechanical deformation, a tribological test setup is used. This enables us to create severe local deformation as a result of a counter part rubbing against the working surface under applied load. This deformation will then be followed by the standard industrial heat treatment.

These tribological tests were performed using a home-made tribometer that is described in details in reference [73]. This tribometer with ball on flat configuration and reciprocating linear movement was employed using an alumina ball as counter part. Speed of 10 mm/s was set over a stroke length of 10 mm giving rise to a frequency of 1Hz. The tests were performed in dry conditions at ambient temperature and humidity. A load of 10 N was applied over 200 stroke cycles. The same 4N model samples are used here as well. Prior to the test, surfaces of these 4N disks were polished with the standard polishing procedure explained earlier in this chapter.

Once the test was completed, the samples were cut in the middle of the wear track perpendicular to the direction of movement using a diamond wire-cut. One half of the deformed surface went for the heat treatment and the other half was kept as reference of changes that were induced solely by the tribology test. The heat treatment was performed in an oven with controlled atmosphere at 650 degree Celsius for 30 minutes. Samples were subsequently quenched in water.

SEM images taken of the wear track before and after the heat treatment are presented in Figures 5.14 and 5.15 respectively. It is seen that the flat smooth surface of the wear track is transformed after the heat treatment and many pores appear on the deformed surface. No porosity was created on the external flat surface of the sample.

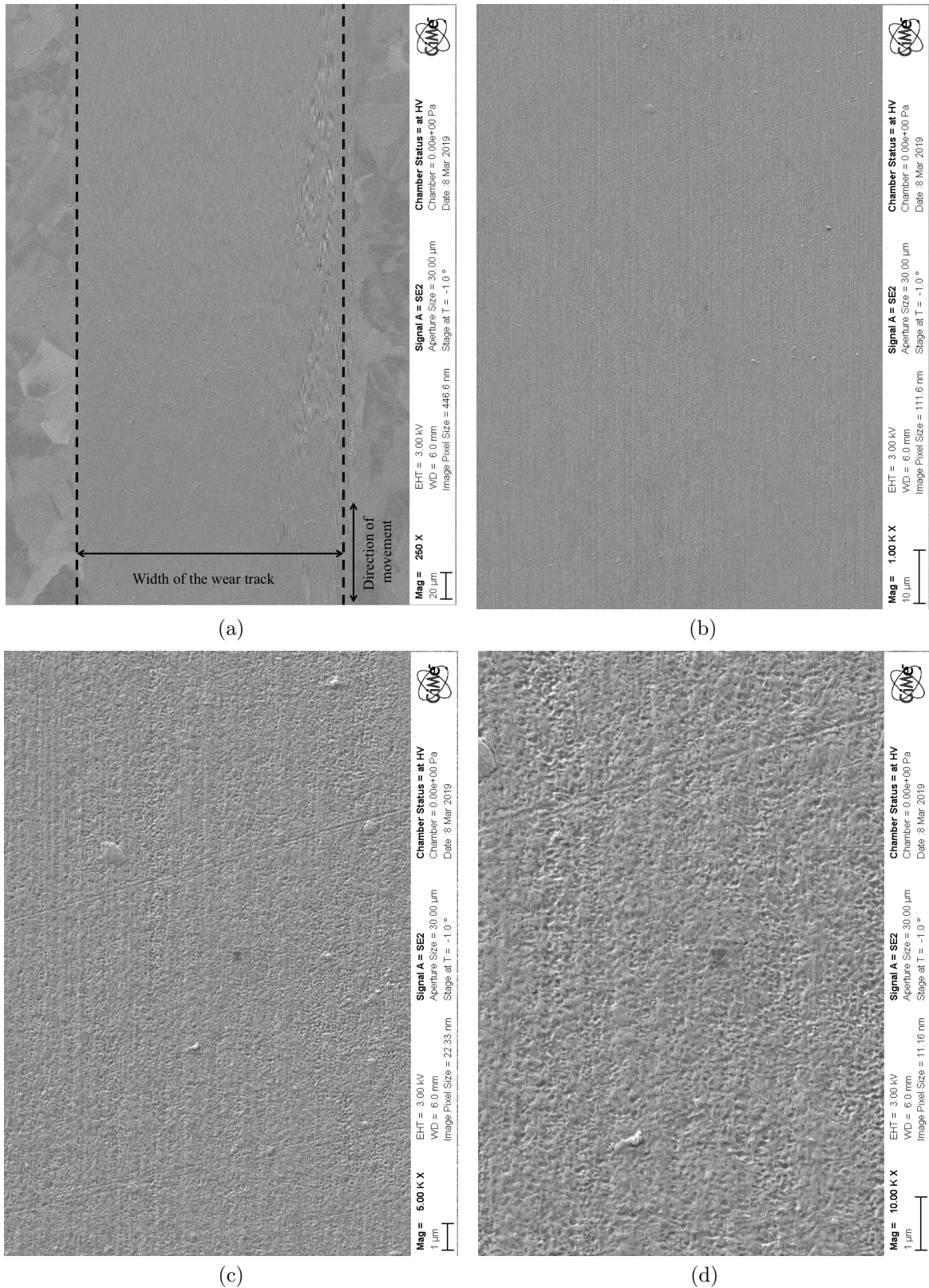


Figure 5.14: SEM image of the wear track after before heat treatment at various magnifications of (a) 250, b) 1000, c) 5000 and d) 10,000. The surface of the wear track is very smooth.

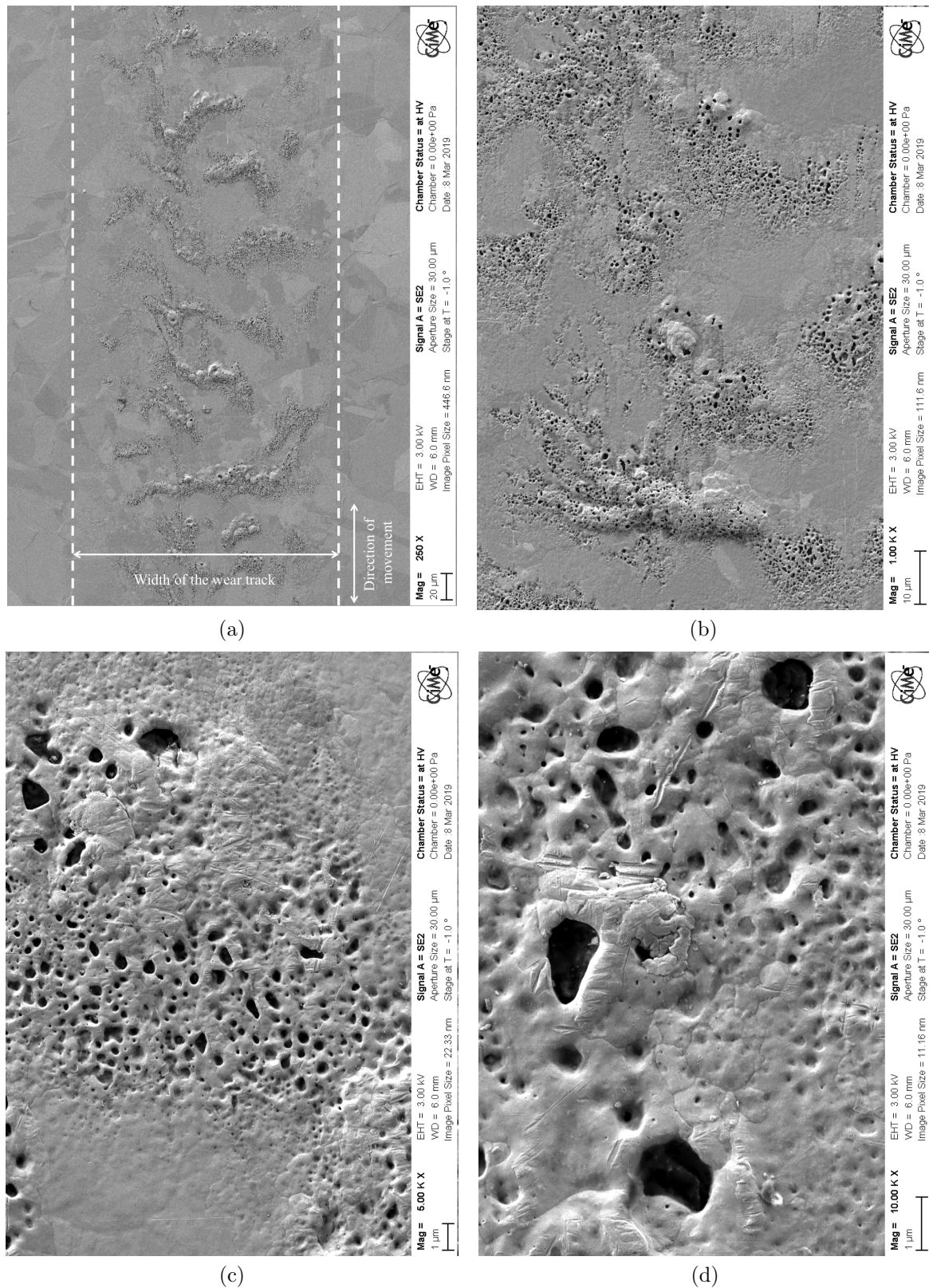


Figure 5.15: SEM image of the wear track after heat treatment at various magnifications of: (a) 250 times, b) 1000, c) 5000 and d) 10,000. Remarkable amount of porosity appears only inside the wear track and only after the heat treatment.

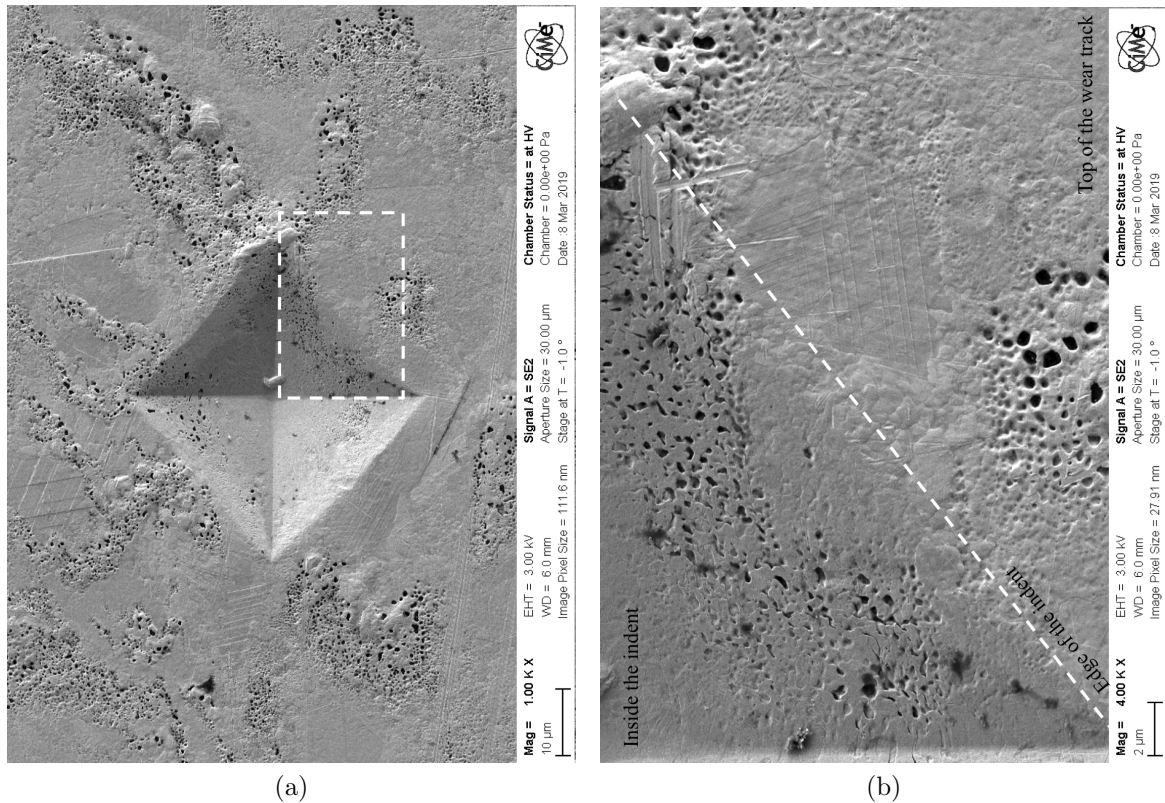


Figure 5.16: a) SEM image of an indentation performed with a Vickers testing instrument inside the wear track after heat treatment and b) a zoom in on the area that is marked on the indent. The image illustrates that the pores created after the heat treatment could be partially closed by further mechanical deformation.

5.5 Summary and conclusions

Tracking the cause of inhomogeneities and defects that appear on the final product back to the process of fabrication provides the relevant industry with the opportunity of eliminating defects at their source. This work showed that variation in hardness of pieces comes from inhomogeneities that are induced in the microstructure during steps of fabrication. No direct link between the microstructure of the pieces and their reflectance was found here.

The variance between surface and bulk composition was recognized as the result of tribocorrosion phenomenon during polishing. Finally, surface holes were shown to be induced by severe mechanical deformation combined with heat treatment.

Chapter 6

Revisiting the watch components

The last step of this work is coming back to industrial problem of aesthetic defects on mirror polished watch components and determining the surface properties responsible for it. For this purpose, a brand new dust cover will be studied that had been prescribed by a visual quality controller to have a visible defect. We performed a complete set of measurements and recognized a contrast in diffuse reflection caused by non-uniform surface roughness to be the principal origin of the concerned aesthetic defect.

6.1 Introduction

In previous chapters, we revealed surface features present on industrial watch components and correlated these surface features and aspects of appearance through optical properties of the surface. In this chapter, the goal is to bring all the know-how that was previously developed and apply it to a case study. We come back to the industrial problem with a piece that has local aesthetic defects on the surface. We will apply the measurement techniques chosen and developed in this work to detect the surface feature(s) responsible for this defect.

6.2 Appearance of the polished surface

The watch component that has been provided for this study is a dust cover made of 3N gold alloy (commonly known as yellow gold). It is composed of 75 wt% Au, 12.5 wt% Ag and 12.5 wt% Cu. Atomic concentrations for the three elements are therefore equal to 54.9%, 16.7% and 28.4% for gold, silver and copper respectively. This alloy has lower copper content and higher silver content compared to the 4N alloy used as model samples and the 5N alloy of the first two watch covers under study.

Watch dust covers used in this study were analyzed by a trained visual expert in production line of the industrial partner. Four pieces were analyzed by the expert two of which were found to be flawless (They will be called F1 and F2) and the other two were found to have local aesthetic defects (D1 and D2). Figure 6.1 shows the defective areas as marked by the visual expert in light gold color. This so called stain by the expert, spreads around the flat bottom of the dust cover in shape of a ring in both defective pieces. This visual judgment has been made in a dark room with a spot light at a distance of approximately 20 cm and with naked eyes.

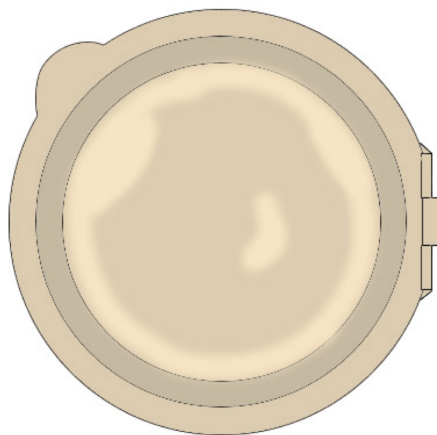


Figure 6.1: Schematics of a watch cover that has been analyzed by a visual expert. Areas marked in light gold color are judged to be stained by the expert.

6.3 Reflectance measurement

In order to compare reflection from a flawless and a defected piece, diffuse radiance was measured on the four watch dust covers mentioned above (F1, F2, D1 and D2) using the multi-angle reflectance setup introduced in Chapter 5 Section 5.2. The location where the measurement is performed is schematically presented in Figure 6.2 and falls in the defective zone of samples D1 and D2.

The measurement is performed at 15 degrees of illumination and 0 degrees of detection compared to normal to the flat surface for the visible wavelength of light. 31 points on the indicated line are measured and the averaged radiance together with the standard deviation is plotted in Figure 6.3. Here, 0 means no reflection and 1 means that the surface diffuses light as much as the white diffuse reference sample that is used for calibration (a perfect Lambertian diffuser). The results show remarkably higher radiance at wavelengths for the defective pieces in the zone of aesthetic flaw. This indicates that the source of the aesthetic defect under study can potentially be a contrast in the intensity of diffusely reflected light.

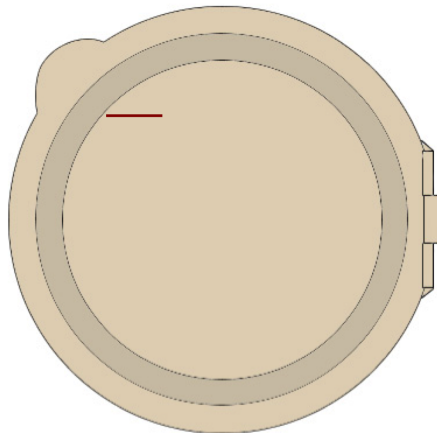


Figure 6.2: The line marked on the schematics show the location where diffuse radiance is locally measured using the multi-angle setup.

6.4 Physical and chemical surface features

After recognizing the aspect of appearance that is causing the aesthetic defect, the next step is to discover the surface property that creates it. For this purpose, quantitative measurements of surface properties are performed using the methodology that has been developed throughout this work.

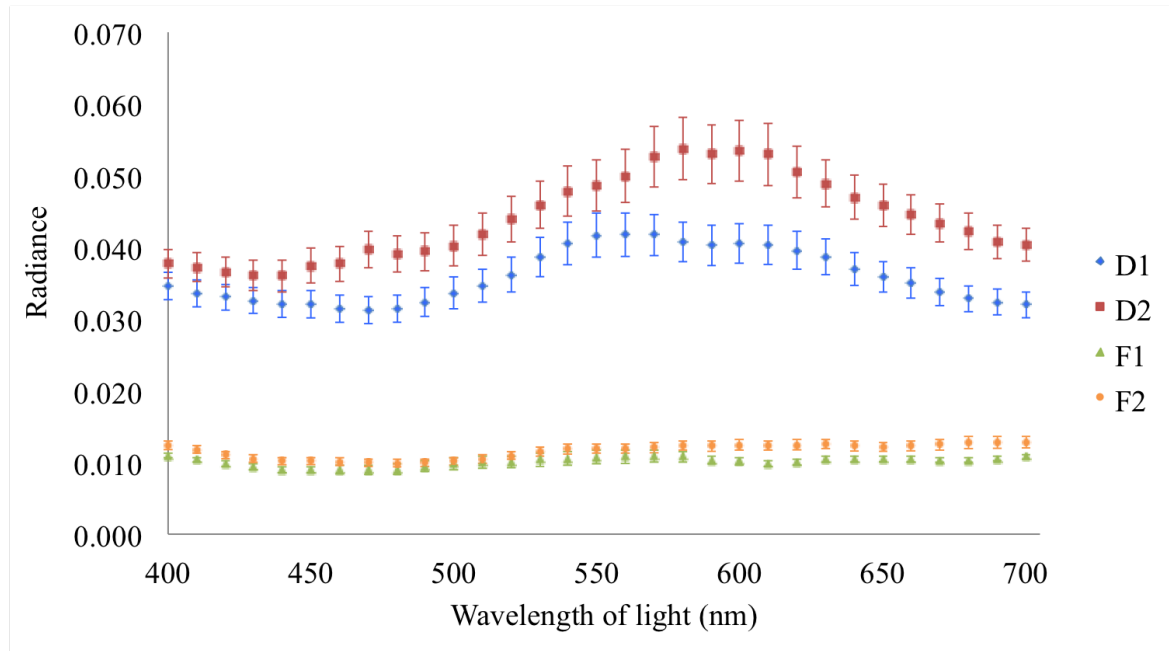


Figure 6.3: Radiance measured at illumination angle of 15 degrees and measurement angle of 0 compared to the normal of the surface. 0 radiance represents no reflection at the given angle and 1 means that the surface diffuses light as much as the white diffuse reference sample that is used for calibration. The defective watch components (D1 and D2) have remarkably higher diffuse reflectance compared to flawless pieces (F1 and F2).

6.4.1 Surface topography

Surface topography was analyzed using the 3D laser profilometry and SEM imaging. Figure 6.4 shows optical and laser images captured across the defective area as well as in the flawless center of the piece. It is seen that the surface is smooth with occasional scratches. Several dark spots are visible on the laser intensity images specially in the central area among three measurement patches. These dark spots are contamination islands and holes.

Figure 6.6 shows the result of the variable length scale analysis that were performed on two profiles obtained inside and outside the defective zone in locations marked as 1 and 2 in Figure 6.5. The profiles have been extracted over a length of $710 \mu\text{m}$ with the lateral resolution of $0.693 \mu\text{m}$. The surface has been corrected for the tilt before extracting the profile but no filters or cut off have been applied to the line profile itself. It can be seen that at length scales below approximately $20 \mu\text{m}$ both profiles have similar roughnesses while at larger scales, defective piece has a higher roughness.

Lightness values were also calculated based on the correlation that was found between L^* and R_q in Chapter 4 Section 4.6 for roughnesses (measured at two length scales of 20μ and 710μ by variable length scale analysis method). The result of these calculations are shown in Table 6.1. Similar low scale roughnesses at two locations yield

identical L^* values while higher length scale roughnesses contribute to a decrease of 0.18 % in lightness of the defective area. This difference is insignificant and therefore no remarkable contrast is anticipated in apparent lightness between the defective and flawless areas.

Table 6.1: L^* values for R_q roughnesses measured at two different length scales using correlations found in Chapter 4 Section 4.6.

	R_q at $20\mu\text{m}$	L^* calculated for R_q at $20\mu\text{m}$	R_q at $710\mu\text{m}$	L^* calculated for R_q at $710\mu\text{m}$
Location 1 (inside the defect)	12.61 nm	88.62	19.62 nm	88.45
Location 2 (outside the defect)	12.70 nm	88.62	14.9 nm	88.57

An estimation of total integrated scattering prediction was also made based on the linear relationship to R_q that was drawn in Chapter 4 Figure 4.18(a). The resulting values being 0.029 and 0.022 for defective and flawless areas respectively, show approximately 30 % higher values in defective area.

Figure 6.7 shows stitching of several images that were captured in magnification of 5000 times at different locations on the sample. As seen in Figure 6.7(d), near the edge and inside the defective zone, some deeper scratches can be observed compared to other two locations. Holes were found on the surface in various locations and some examples of them are shown in Figure 6.8.

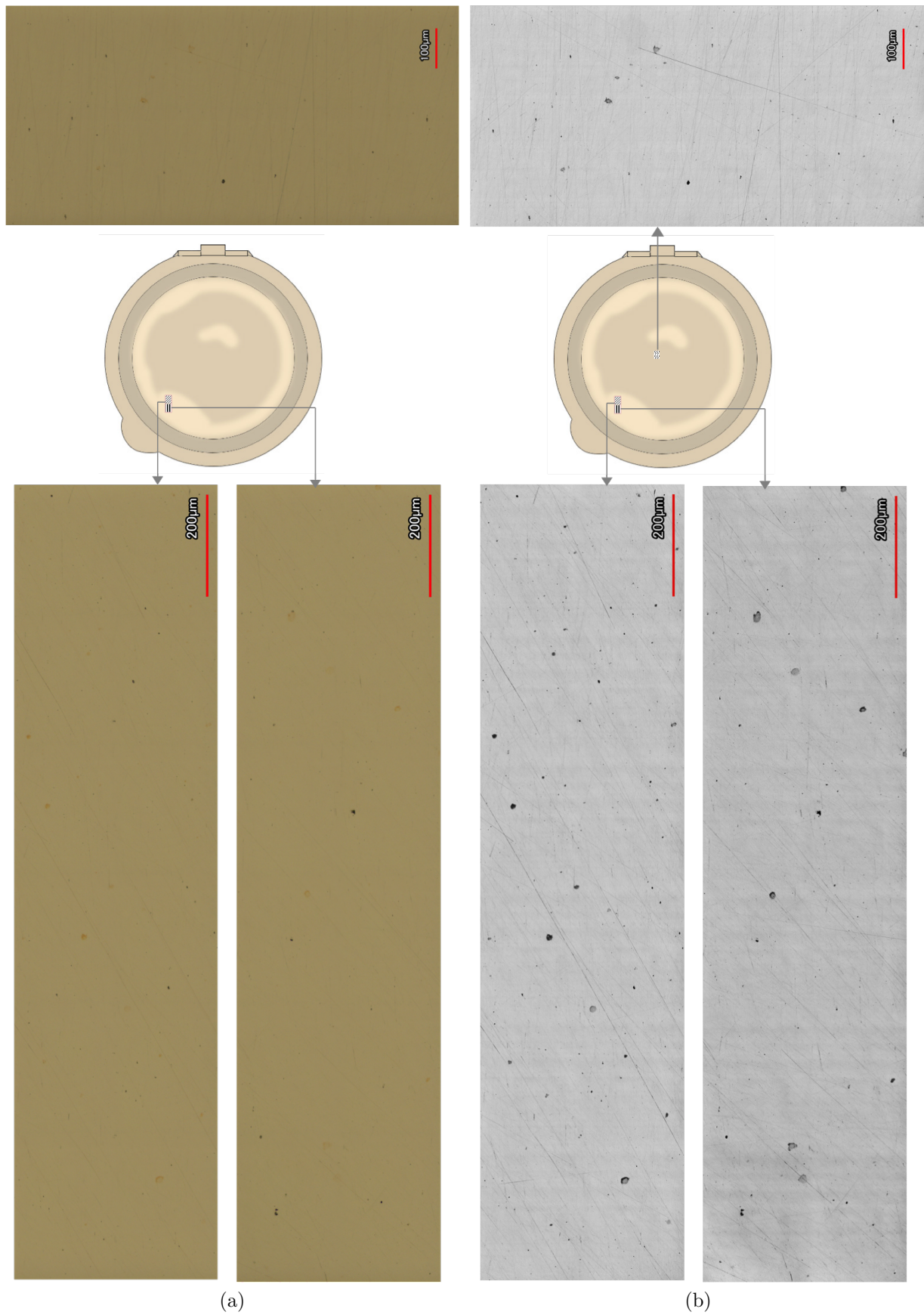


Figure 6.4: a) Optical and b) laser intensity images obtained by laser confocal microscope. The three strips from top to bottom correspond to the three areas marked on the schematics of the dust-cover from right to left.

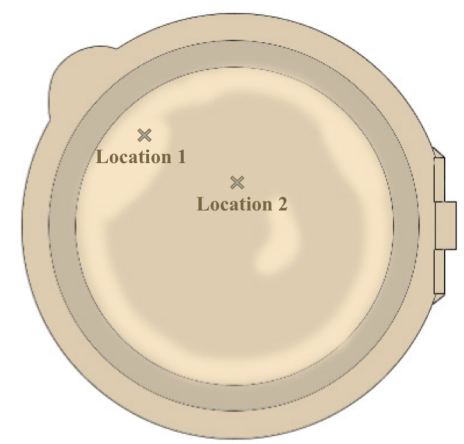


Figure 6.5: Locations 1 and 2 where measurements were performed are marked on the schematics of the sample. Location 1 is inside defective area while location 2 is on the flawless area.

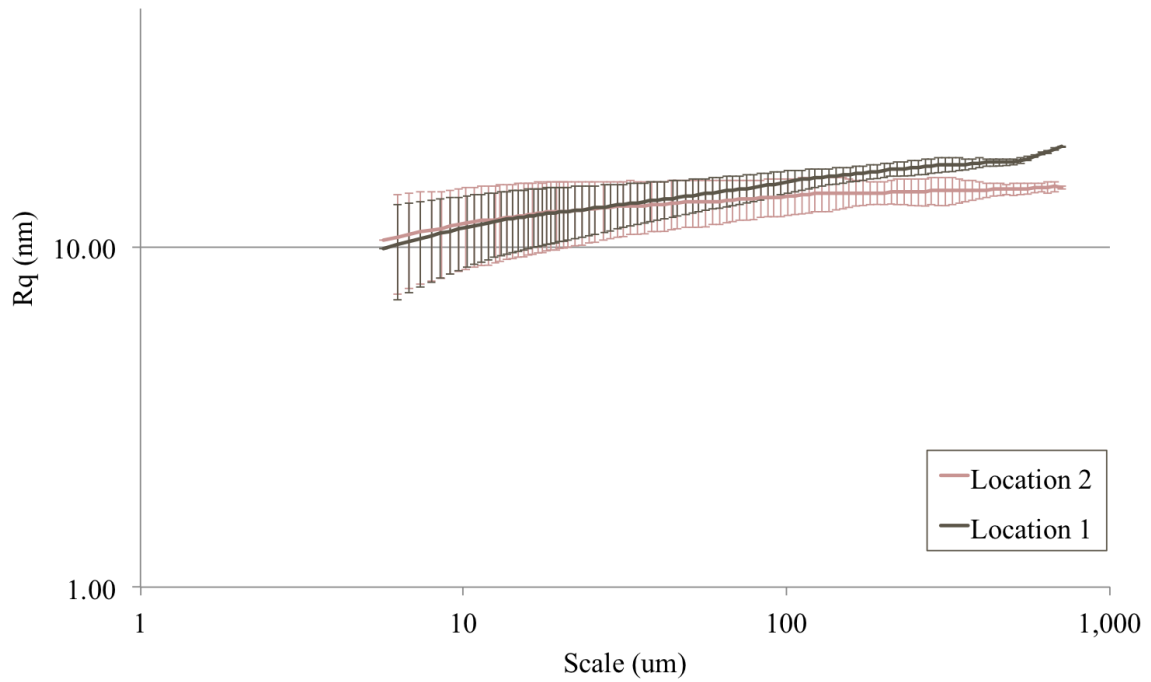


Figure 6.6: Variable length scale analysis were performed on two profiles that have been obtained in location 1 inside the defective zone and in location 2 in the center of the piece. The results plotted in double logarithmic scale show similar R_q in lower scales but roughness in defective exceeds the one of the good area.

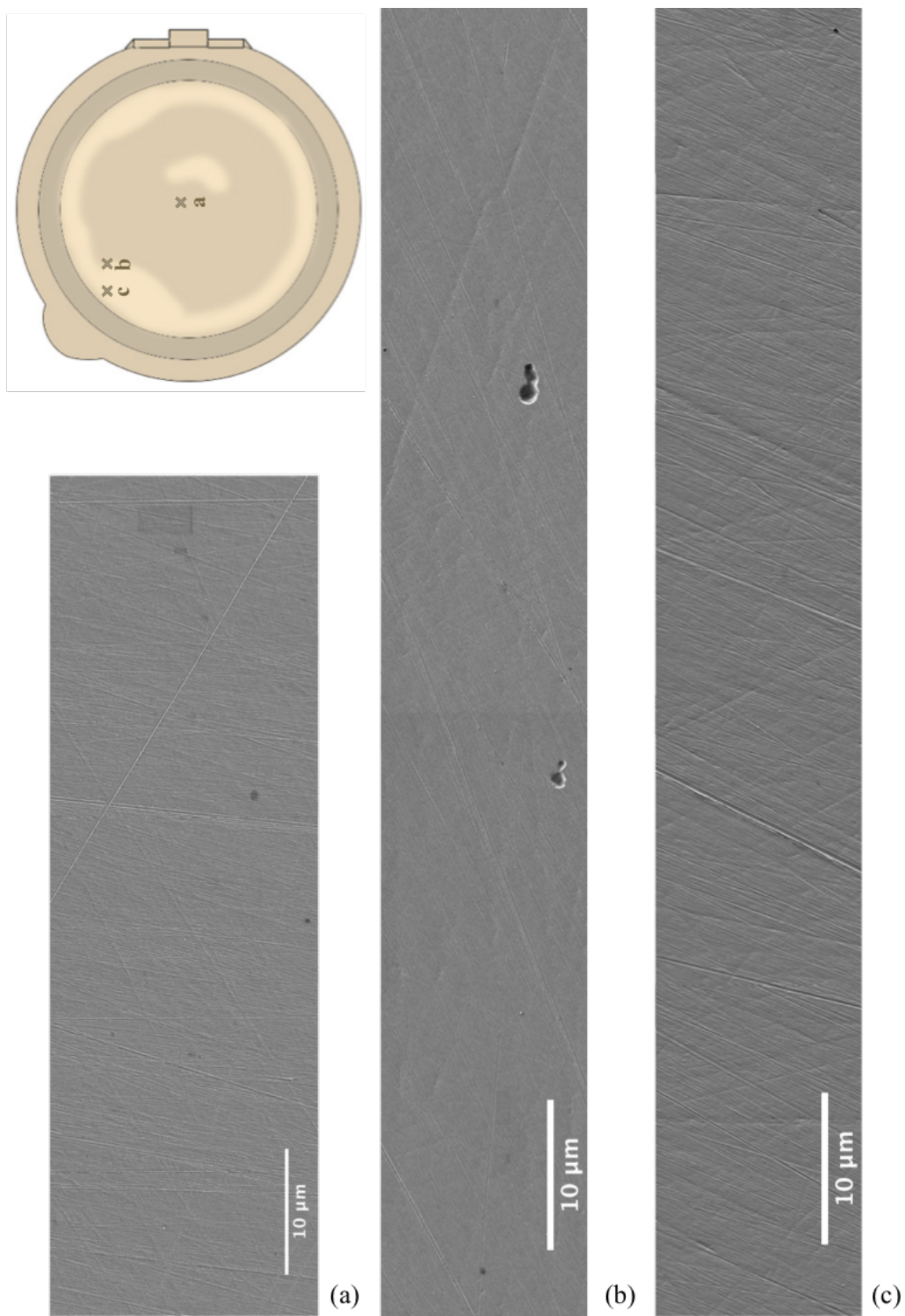


Figure 6.7: Images are obtained by stitching several SEM images at magnification of 5000 times. The locations where the images are taken are marked with corresponding letters on the schematics of the piece.

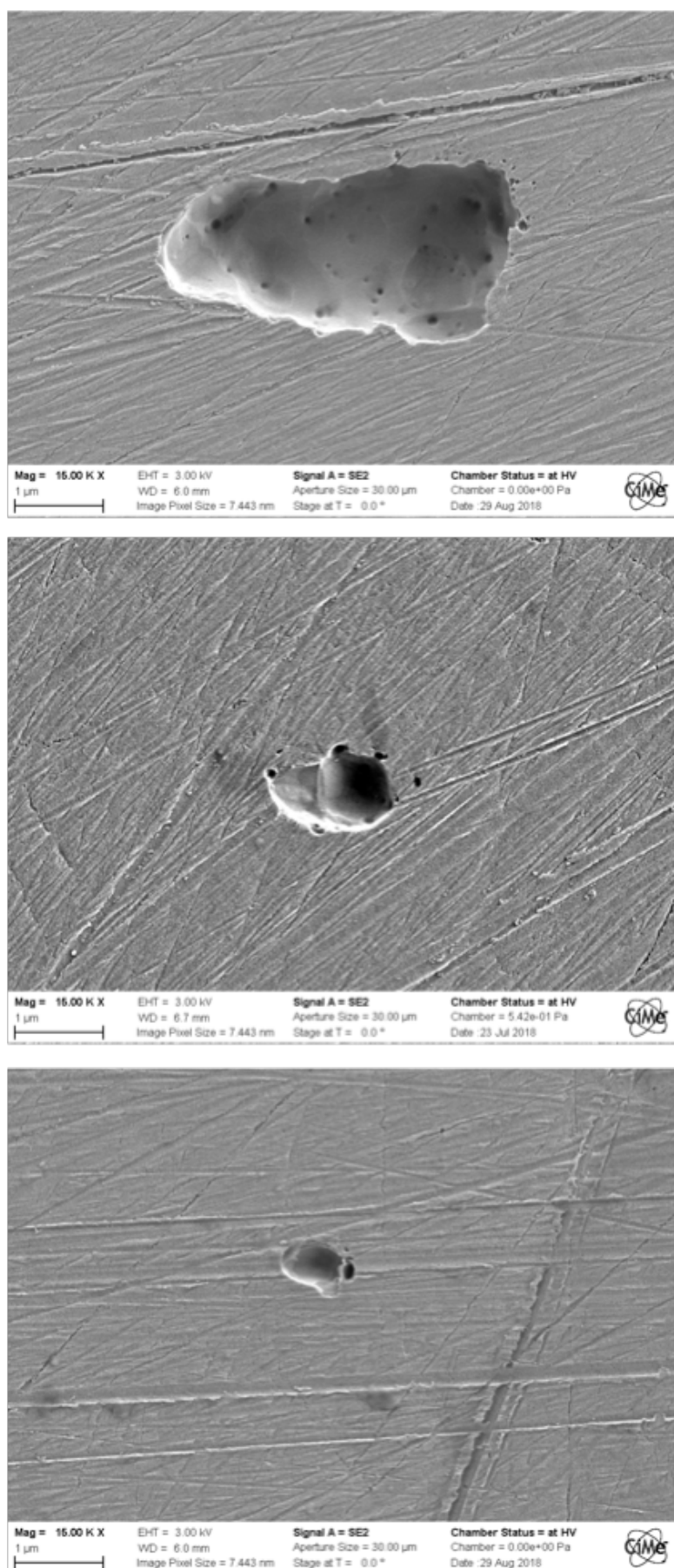


Figure 6.8: Examples of holes that can be found at different locations on the surface.

6.5 Chemical analysis

Surface and near surface chemical compositions were studied using AES analysis. Measurements are done on two locations, one in the defective area marked as location 1 in Figure 6.5 and the second in a non-defective area marked as location 2. In each location three depth profiles were measured and a representative intensity profile is presented in Figure 6.9. Atomic concentrations were calculated based on this profile over the depth of the sample and are shown in Figure 6.10.

Obviously copper and silver content in this 3N alloy are different from those of previously studied 4N and 5N alloys. In contrast with previous cases where copper had a very high concentration on the outer most surface, here silver is dominantly present at the top surface. Silver concentration on the surface, 67 at%, is four times higher than the nominal bulk composition of 16.7 at%.

On the other hand, copper is depleted from the outer surface down to 8.5 at%. Copper content gradually increases in the next 45-50 nm that are sputtered down to the bulk. Meanwhile, depth profile of gold in this 3N alloy has a similar shape to the ones of 4N rose gold alloy and 5N red gold alloy. This means that gold is severely depleted on the top surface but quickly recovers after sputtering only 2-3 nm to an enriched composition. From this point on, gold content slowly descends to bulk composition.

For better comparison of the near surface compositions in the two measured locations (inside and outside defective areas) and also to visualize the reproducibility, first 10 nanometers of AES depth profiles are overlapped in Figure 6.11. Interesting results reveal identical chemical composition on the top surface (depth 0) for the two locations. Nevertheless, the trends in which the profiles evolve below the surface slightly differ. At location two, copper to silver ratio is higher for the first 5 nanometers compared to location 1. Gold content is also slightly higher in the first two nanometers. The same small differences are seen in all 6 profiles.

Average composition of gold and copper are calculated over the first 5 nm for three profiles in each location and the results are presented in Table 6.2. Equations found in Chapter 4 Section 4.6 were applied to these average values in order to predict corresponding a^* and b^* values in these two locations and the results can be seen in Table 6.3.

Table 6.2: Gold and copper atomic percentage averaged over the first 5 nm of the depth profiles for three measurements in each location.

	Au (%)	Cu (%)
Location 1 inside the defect	56.5 ± 0.6	13.1 ± 0.5
Location 2 outside the defect	56.9 ± 1.3	15.4 ± 1.2

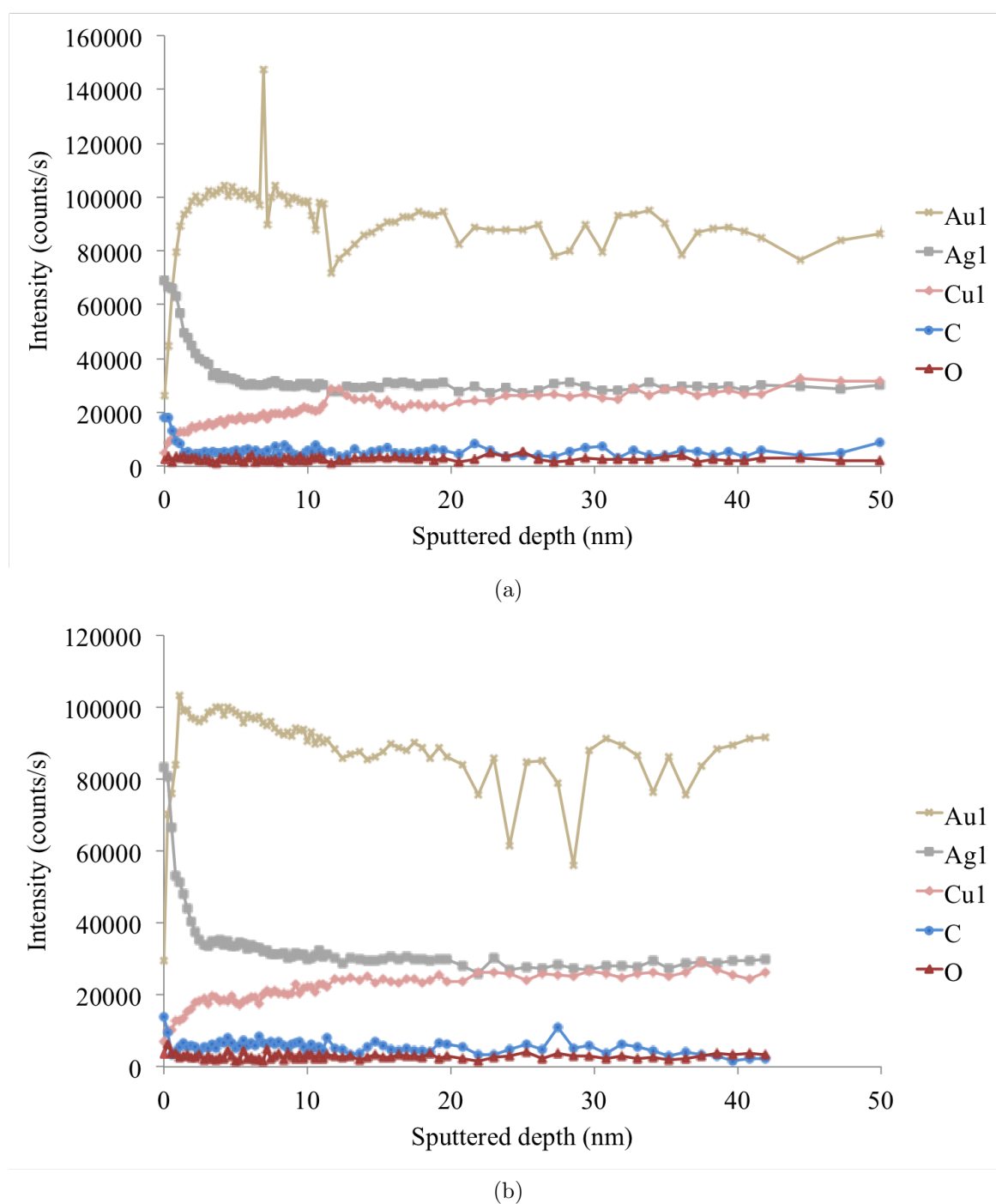
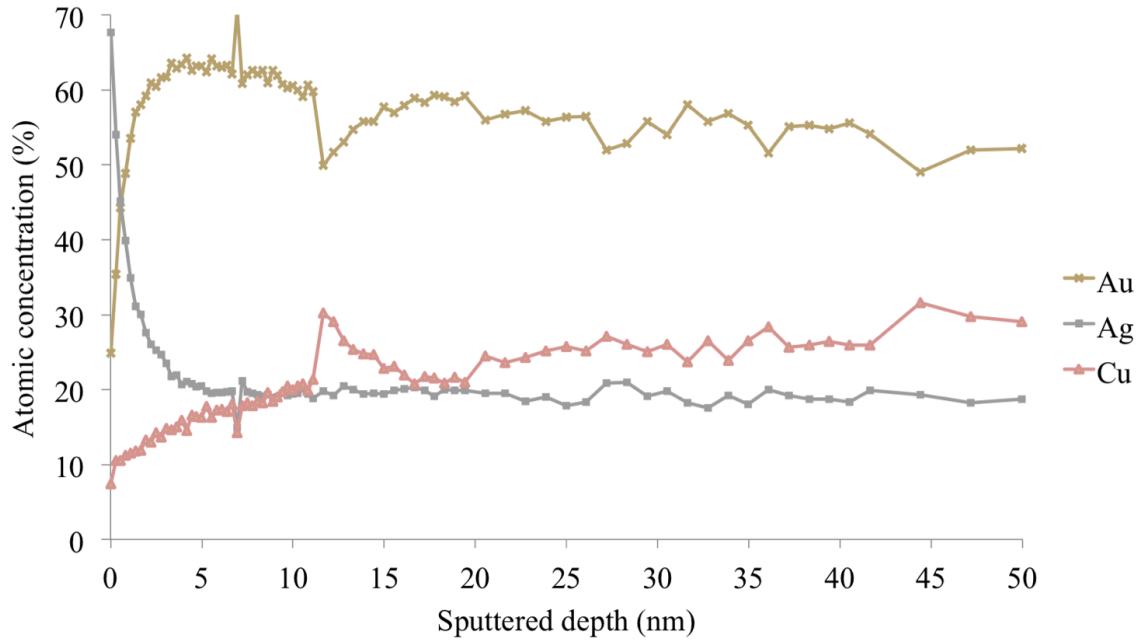


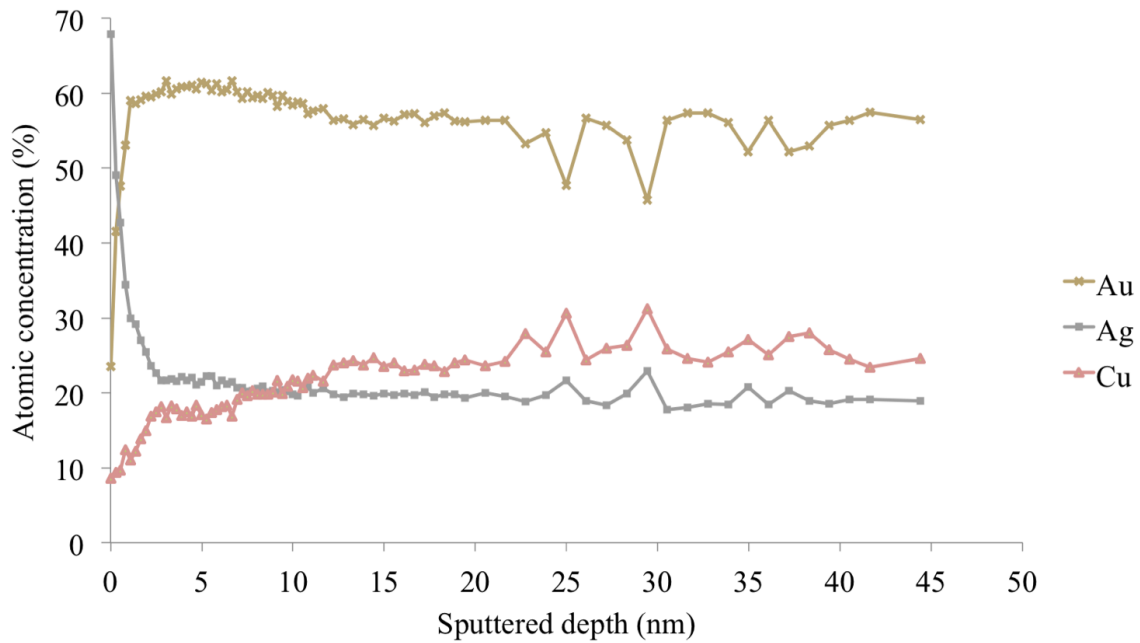
Figure 6.9: Signal intensities in AES analysis for the three alloying elements and carbon and oxygen that can be found on the surface as contaminants at a) location 1 and b) location 2 of the 3N dust cover.

Table 6.3: Calculated a^* and b^* based on compositions averaged in the first 5nm of the depth profiles at two locations on the watch dust cover

	a^*	b^*
Location 1 inside the defect	4.49	21.78
Location 2 outside the defect	4.68	21.83



(a)



(b)

Figure 6.10: In-depth atomic concentrations obtained by AES analysis a) at location 1 inside the defective zone and b) at location 2 of the 3N dust cover.

Using these a^* and b^* calculated based on chemical composition of the surface together with L^* values calculated based on surface roughness, the difference in color between defective and flawless area can be calculated according to the Equation 2.4 for ΔE^* . This value equals to 0.14 which is considered negligible for visual perception [39].

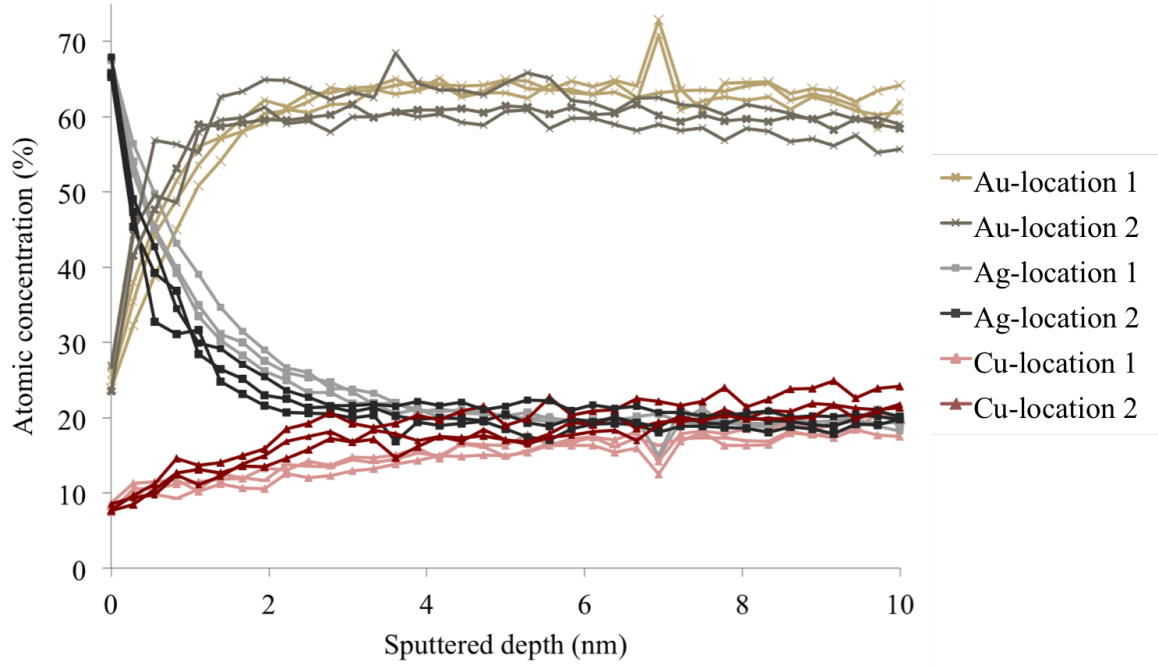


Figure 6.11: Three profiles obtained at each location are overlapped. It can be seen that the results are reproducible and the small differences observed between two locations in below surface composition are present in all measurements.

6.6 Summary and conclusions

Local reflectance measurement showed that defective pieces have more than three times higher radiance in the defective zone compared to a similar location on a flawless piece.

Calculation of a^* and b^* and L^* values based on chemical composition and surface roughness showed that the color difference between flawless and defective regions is negligibly small compared to typical sensitivity of a observer.

Calculation of total integrated scatter based on the developed model and using the measured roughness values showed that TIS is higher by 30% in the defective areas compared to flawless areas. This significant contrast in intensity of diffusely reflected light was also confirmed by local radiance measurements as shown in Figure 6.3.

Therefore, revisiting a defective watch piece and applying the methodology developed in this work showed that the aesthetic defect under study was the result of a contrast in diffuse reflection of light originated from long scale roughness (waviness).

Chapter 7

Conclusions and perspectives

The motivation behind this work was the industrial problem of presence of aesthetic flaws on polished surfaces of 18 karat gold jewelry and watch components. Notwithstanding the efficiency of these trained experts in detecting aesthetic imperfections, visual quality control in its essence has three main shortcomings: It involves individual judgment, it does not provide a link between the aesthetic flaw and the surface properties and finally it often does not reveal the origin of the aesthetic flaw in the fabrication process.

Based on this problematic, the current study was designed to answer four main questions. These questions and the pertinent findings of this research are listed below:

1) How can the aesthetic appearance of a surface be rationalized and linked to the properties of the surface?

The approach of this work to rationalization and quantification of visual perception of surfaces is to link defined and quantifiable surface properties to aspect of appearance as proposed by the British National Physics Laboratory (NPL). The NPL framework defines four parameters of color, gloss, translucency and texture as measurable surface properties that are correlated to appearance. Although this general framework is a reliable starting point in coupling surface features to the appearance, case specific definitions and measurement techniques need to be developed for it.

For determining these four parameters, a set of measurement techniques were selected and pertinent protocols developed. These techniques include:

- Color and gloss: spectrophotometry for total and diffuse reflectance measurement over the visible wavelength of light.
- Translucency: high resolution in-depth chemical analysis to include near surface properties together with the top surface.
- Texture: topography measurement techniques and roughness evaluations.

2) What are the surface features that control visual perception of mirror polished gold surfaces?

Industrial surfaces were studied and several features were found. Three main type of surface features were recognized to be surface roughness, near surface composition variations and holes. They all may affect the aesthetic appearance but the contrast in defective sample could not obviously be attributed to a single parameter because all these parameters vary over the surface. Therefore, assessing the role of each surface feature on visual appearance requires a quantitative approach that relates these features to visual appearance factors. Probably the effect is also the overlap of different features.

3) To which extent these features affect the appearance?

Surface features were correlated to aspects of appearance through CIELAB color metrics. L^* was found to quantitatively correlate to R_a and R_q roughness parameters for nearly Gaussian distribution of surface height profile. a^* and b^* color values were found to linearly change with averaged copper content and gold content at the first 5 nm of the surface respectively. The following three equations were drawn:

$$\begin{aligned}L^* &= -0.25R_q + 88.94 \\a^* &= 0.086 \text{ Cu at\%} + 3.36 \\b^* &= 0.12 \text{ Au at\%} + 15\end{aligned}$$

Considering the scatter in the data, roughnesses measured at higher length scale could be correlated to Total Integrated Scattering through the following relationship:

$$TIS = 0.0015R_q$$

The effect of holes at the extent found here was considered to be negligible on appearance of the concerned surfaces.

4) When are these features generated in the relevant process of fabricating a gold jewelry or watch component?

We found the origin of surface defects in the process of fabrication to be the following:

- Local deformation and heat treatment during steps of production induces inhomogeneity in microstructure that in turn causes non-uniform hardness. Inhomogeneity in local hardness of a single piece can cause faulty appearance of the final product through negatively affecting the outcome of polishing process.
- Polishing modifies near surface composition of 18 karat gold alloy and therefore alters the color. The extent of this modification depends on the process of polishing and chemistry of the polishing products.
- Holes can be induced on surface of these alloys by severe mechanical deformation followed by heat treatment.

7.1 Conclusions

Main conclusions that can be drawn from this work include:

- Main factors affecting the appearance of polished 18 karat gold alloy surfaces are roughness and surface composition.
- To determine the role of these two parameters in aspects of appearance, roughness should be considered at different length scales and composition should be studied over a certain nm-scale depth.
- For typical smooth mechanically polished 18 karat 4N alloy surfaces with Gaussian distribution of probability density function of surface heights, lightness can be linearly linked to R_q measured under specified conditions.
- a^* and b^* color values for the above mentioned surfaces can be also linearly correlated to average atomic concentration of copper and gold over a depth of 5 nm.
- The range of roughnesses that are found on the polished surface of a jewelry or watch piece induce little variation in lightness (L^*) but larger scattering in total integrated scattering.
- Polishing the surface of 18 karat gold alloys changes their color through modifying near surface composition. The extent of this modification depends on the polishing procedure and the chemicals used.
- Inhomogeneous microstructure and hardness that is induced in the watch or jewelry components during steps of manufacturing can impair the appearance of final product through non-uniform outcome of mechanical polishing.
- The methodology developed in this work allowed to identify waviness (large scale roughness) as the cause of an aesthetic defect on the surface of a industrial product.

Domains of visual perception and surface science are both extremely vast and truly rich. Exploring the interface where the two scientific fields meet can bring valuable insight to a variety of industries. The set of methodologies proposed by this study lay the groundwork for a general approach to the topic of assessing appearance of surfaces and particularly smooth metallic surfaces. Application to others systems than polished karat gold is in principle feasible but requires some further research aimed at validating and calibrating the different correlations between surface features and aspects of appearance developed here.

7.2 Perspectives

To complement this work for the specific case of appearance of polished 18 karat gold alloys, it would be interesting to:

- Expand the work with model surfaces to the study of higher ranges of surface roughnesses and wider range of compositions (other colored gold or copper alloys for example).
- To further explore roughness assessment techniques both in terms of choice of instrument (such as atomic force microscopy) and surface roughness parameters.
- Opt for local reflectance measurements and further study specular and diffuse components and their angle dependency.

Bibliography

- [1] Kurt Nassau. *The Physics and Chemistry of Color*. Wiley-Interscience, 2nd edition, 2001.
- [2] The international journal of newspaper technology, http://www.newsandtecharchives.com/issues/2002/02-02/ifra/02-02_greybalance.htm.
- [3] Cristian Cretu and Elma van der Lingen. Coloured gold alloys. *Gold Bulletin*, 32(4):115–126, 1999.
- [4] Otto Loebich. The optical properties of gold. *Gold Bulletin*, 5(1):2–10, 1972.
- [5] Michael R Pointer. Measuring visual appearance - a framework of the future, National Physical Laboratory report coam 19, 2003.
- [6] A. Welles and I. Le R. Strydom. Oxidation behaviour of some platinum and gold jewellery alloys at 150 ° c. *Journal of materials science letters* 5, (5):743–746, 1986.
- [7] Diffuse reflectance measurement (shimadzu corporation), https://www.shimadzu.com/an/molecular_spectro/uv/accessory/solid/sample/solid.html.
- [8] Paul William Palmberg. *Handbook of Auger Electron Spectroscopy: A Reference Book of Standard Data for Identification and Interpretation of Auger Electron Spectroscopy Data*. Physical Electronics Industries, 1972.
- [9] John F. Moulder. *Handbook of X-ray Photoelectron Spectroscopy: A Reference Book of Standard Spectra for Identification and Interpretation of XPS Data*. Physical Electronics Division, Perkin-Elmer Corporation, 1992.
- [10] Gary Hatfield and Sarah Allred. *Visual experience : sensation, cognition, and constancy*. Oxford University Press, 2012.
- [11] Ra Strehlow and Se Wright, editors. *Standardizing Terminology for Better Communication: Practice, Applied Theory, and Results*. ASTM International, 1993.
- [12] Christian Eugene. Measurement of “total visual appearance”: a CIE challenge of soft metrology. 12th IMEKO TC1 & TC7 Joint Symposium on Man, Science & Measurement, 2008.

- [13] T. Puntous, S. Pavan, D. Delafosse, M. Jourlin, and J. Rech. Ability of quality controllers to detect standard scratches on polished surfaces. *Precision Engineering*, 37(4):924–928, 2013.
- [14] Gabriel Spitz and Colin G. Drury. Inspection of sheet materials—test of model predictions. *Human Factors*, 20(5):521–528, 1978.
- [15] Judi E. See. Colour design, Sandia National Laboratories report, 2012.
- [16] N. Baudet, J. L. Maire, and M. Pillet. The visual inspection of product surfaces. *Food Quality and Preference*, 27(2):153 – 160, 2013.
- [17] N. Bruno, G. Garofalo, O. Daneyko, and L. Riggio. Visual similarity modulates visual size contrast. *Acta Psychologica*, 188:122–130, 2018.
- [18] Steven K Shevell and Jianping Wei. A central mechanism of chromatic contrast. *Vision Research*, 40(23):3173–3180, 2000.
- [19] J. Best. *Colour Design*. Woodhead Publishing, 2012.
- [20] Benjamin A. Graybeal, Brent M. Phares, Dennis D. Rolander, Mark Moore, and Glenn Washer. Visual inspection of highway bridges. *Journal of nondestructive evaluation*, 21(3):67–83, 2002.
- [21] E. D. Megaw. Factors affecting visual inspection accuracy. *Applied Ergonomics*, 10(1):27–32, 1979.
- [22] J. W. Schoonahd, J. D. Gould, and L. A. Miller. Studies of visual inspection. *Ergonomics*, 16(4):365–379, 1973.
- [23] Biswajit Sarkar and Sharmila Saren. Product inspection policy for an imperfect production system with inspection errors and warranty cost. *European journal of operational research*, 248(1):263–271, 2016.
- [24] Fion C. H. Lee and Alan H. S. Chan. Effects of magnification methods and magnifier shapes on visual inspection. *Applied Ergonomics*, 40(3):410–418, 2009.
- [25] Giuseppe Zamuner and Jacques Jacot. A system for the quality inspection of surfaces of watch parts. In Svetan Ratchev, editor, *Precision Assembly Technologies and Systems*, IFIP Advances in Information and Communication Technology, pages 134–143. Springer, 2012.
- [26] Franz Pernkopf and Paul O’Leary. Image acquisition techniques for automatic visual inspection of metallic surfaces. *NDT and E International*, 36(8):609–617, 2003.
- [27] Franz Pernkopf and Paul O’Leary. Visual inspection of machined metallic high-precision surfaces. *EURASIP Journal on Advances in Signal Processing*, 2002.
- [28] Tadhg Brosnan and Da-Wen Sun. Improving quality inspection of food products by computer vision—a review. *Journal of food engineering*, 61(1):3–16, 2004.
- [29] John B. Hutchings. *Food Colour and Appearance*. Springer US, 1999.
- [30] J. M. Alexander, R. D. Rawlings, J. C. Anderson, and K. D. Leaver. *Materials Science*. Springer US, 4 edition, 1990.

- [31] N. N. Nagib, N. A. Mahmoud, L. Z. Ismail, M. A. Amer, and Kh. Abd-El-Sabour. Effect of surface roughness on the optical constants of bulk polycrystalline gold samples. *Optik - International Journal for Light and Electron Optics*, 125(3):1085–1087, 2014.
- [32] R. T. Poole. The colour of the noble metals. *Physics Education*, 18(6):280, 1983.
- [33] Keming Ji, Yongqiang Xue, and Zixiang Cui. A new method for colors characterization of colored stainless steel using CIE and munsell color systems. *Optical Materials*, 47:180–184, 2015.
- [34] Rosangela Conrrado, Nerilso Bocchi, Romeu C Rocha-Filho, and Sonia R Biaggio. Corrosion resistance of colored films grown on stainless steel by the alternating potential pulse method. *Electrochimica Acta*, 48(17):2417–2424, 2003.
- [35] R. R. Seghi, W. M. Johnston, and W. J. O’Brien. Spectrophotometric analysis of color differences between porcelain systems. *The Journal of Prosthetic Dentistry*, 56(1):35–40, 1986.
- [36] Randall M. German, Matthew M. Guzowski, and David C. Wright. The colour of gold-silver-copper alloys. *Gold Bulletin*, 13(3):113–116, 1980.
- [37] M.R. Pointer AR. Robertson R. Seve J.D. Schanda K. Witt. E.C. Carter, Y. Ohno. Colorimetry, report from international commission on illumination, 3rd edition, 2004, 2004.
- [38] R.R. Seghi, E.R. Hewlett, and J. Kim. Visual and instrumental colorimetric assessments of small color differences on translucent dental porcelain. *Journal of Dental Research*, 68(12):1760–1764, 1989.
- [39] M. Mahy, L. Van Eycken, and A. Oosterlinck. Evaluation of uniform color spaces developed after the adoption of CIELAB and CIELUV. *Color Research and Application*, 19(2):105–121, 1994.
- [40] Richard S. Hunter. Methods of determining gloss. *Journal of research of the national bureau of standards*, 18:19–41, 1937.
- [41] A. C. Chadwick and R. W. Kentridge. The perception of gloss: A review. *Vision Research*, 109, Part B:221–235, 2015.
- [42] Asim Kumar and Choudhury, Roy. *Principles of Colour and Appearance Measurement*, volume 1. Woodhead Publishing, 2014.
- [43] Harold B. Westlund and Gary W. Meyer. Applying appearance standards to light reflection models. In *Proceedings of the 28th Annual Conference on Computer Graphics and Interactive Techniques*, pages 501–51. ACM, 2001.
- [44] Paul Mulvaney. Not all that’s gold does glitter. *MRS Bulletin*, 26(12):1009–1014, 2001.
- [45] Angela Furrer. Colours in thin metallic films based on precious metals and their intermetallic phases, PhD thesis, ETH Zurich, 2013.

- [46] Kristin J. Dana, Bram van Ginneken, Shree K. Nayar, and Jan J. Koenderink. Reflectance and texture of real-world surfaces. *ACM Transactions on Graphics*, 18(1):1–34, 1999.
- [47] Elena González, Francesco Bianconi, Marcos X. Álvarez, and Stefano A. Saetta. Automatic characterization of the visual appearance of industrial materials through colour and texture analysis: An overview of methods and applications. *Advances in Optical Technologies*, 2013.
- [48] *ASM handbook*, volume 18, Friction, lubrication and wear technology. ASM International, 1992.
- [49] Terry Jones. Electropolishing of precious metals. *Metal Finishing*, 102(7):45–57, 2004.
- [50] Ugur Erdemir, Esra Yildiz, Meltem Mert Eren, Alev Ozsoy, and Fulya Toksoy Topcu. Effects of polishing systems on the surface roughness of tooth-colored materials. *Journal of Dental Sciences*, 8(2):160–169, 2013.
- [51] James A. Ferwerda, Fabio Pellacini, and Donald P. Greenberg. Psychophysically based model of surface gloss perception, Proceedings of Photonics West 2001 - Electronic Imaging. pages 291–301, 2001.
- [52] H. E. Bennett and J. O. Porteus. Relation between surface roughness and specular reflectance at normal incidence. *Journal of the Optical Society of America*, 51(2):123–129, 1961.
- [53] Stephen O. Rice. Reflection of electromagnetic waves from slightly rough surfaces. *Communications on Pure and Applied Mathematics*, 4(2):351–378, 1951.
- [54] Petr Beckmann and Andre Spizzichino. *The Scattering of Electromagnetic Waves from Rough Surfaces*. Artech Print on Demand, 1987.
- [55] Lin Qi, Mike J. Chantler, J. Paul Siebert, and Junyu Dong. The joint effect of mesoscale and microscale roughness on perceived gloss. *Vision Research*, 115, Part B:209–217, 2015.
- [56] Barton L. Anderson. Visual perception of materials and surfaces. *Current Biology*, 21(24):R978–R983, 2011.
- [57] Stefano Padilla, Ondrej Drbohlav, Patrick R. Green, Andy Spence, and Mike J. Chantler. Perceived roughness of 1/f(beta) noise surfaces. *Vision Research*, 48(17):1791–1797, 2008.
- [58] Ronald G. Driggers. *Encyclopedia of Optical Engineering: Pho-Z, pages 2049-3050*. CRC Press, 2003.
- [59] James Harvey, Andrey Krywonos, and Cynthia L. Vernold. Modified beckmann-kirchhoff scattering model for rough surfaces with large incident and scattering angles. *Optical Engineering*, 46(7):078002, 2007.
- [60] L. H. Tanner and M. Fahoum. A study of the surface parameters of ground and lapped metal surfaces, using specular and diffuse reflection of laser light. *Wear*, 36(3):299–316, 1976.

- [61] Shree K. Nayar, Katsushi Ikeuchi, and Takeo Kanade. Surface reflection: Physical and geometrical perspectives. *IEEE Trans. Pattern Anal. Mach. Intell.*, 13:611–634, 1991.
- [62] Michael Bass, Casimer DeCusatis, Jay Enoch, Vasudevan Lakshminarayanan, Guifang Li, Carolyn Macdonald, Virendra Mahajan, and Eric Van Stryland. *Handbook of Optics, Third Edition Volume V: Atmospheric Optics, Modulators, Fiber Optics, X-Ray and Neutron Optics*. McGraw-Hill, Inc., 3rd edition, 2010.
- [63] James E. Harvey, Narak Choi, Sven Schroeder, and Angela Duparré. Total integrated scatter from surfaces with arbitrary roughness, correlation widths, and incident angles. *Optical Engineering*, 51(1):013402, 2012.
- [64] Sven Schröder, Angela Duparré, Luisa Coriand, Andreas Tünnermann, Dayana H. Penalver, and James E. Harvey. Modeling of light scattering in different regimes of surface roughness. *Optics Express*, 19(10):9820–9835, 2011.
- [65] G. A. Somorjai. Correlations between the structure and reactivity at solid-gas and solid-liquid interfaces. *Journal of the electrochemical society*, pages 205–214, 1977.
- [66] G. C. Nelson. Determination of the surface vs bulk composition of ag/au alloys by low-energy ion-scattering spectroscopy. *Journal of Vacuum Science and Technology*, 13(1):512–513, 1976.
- [67] Makiko Yonehara, Tsutomu Matsui, Koichiro Kihara, Hiroaki Isono, Akira Kijima, and Toshio Sugibayashi. Experimental relationships between surface roughness, glossiness and color of chromatic colored metals. *Materials Transactions*, 45(4):1027–1032, 2004.
- [68] Adrien Van Gorp, Maxence Bigerelle, and Denis Najjar. Relationship between brightness and roughness of polypropylene abraded surfaces. *Polymer Engineering and Science*, 56(1):103–117, 2016.
- [69] N. Fredj, J. S. Kolar, D. M. Prichard, and T. D. Burleigh. Study of relative color stability and corrosion resistance of commercial copper alloys exposed to hand contact and synthetic hand sweat. *Corrosion Science*, 76:415–423, 2013.
- [70] Keyence 3d laser scanning confocal microscope catalogue, VK-x series.
- [71] P. F Chauvy, C Madore, and D Landolt. Variable length scale analysis of surface topography: characterization of titanium surfaces for biomedical applications. *Surface and Coatings Technology*, 110(1):48–56, 1998.
- [72] Jacques Laurent. Modélisation de la dissolution sélective d’alliages binaires en dessous du potentiel critique, PhD thesis, École Polytechnique Fédérale de Lausanne, 1989.
- [73] Sandra Guadalupe Maldonado. Tribocorrosion in pressurized high temperature water : a mass flow model based on the third body approach, PhD thesis, École Polytechnique Fédérale de Lausanne, 2014.



Leili BATOOLI

Ch. de Veilloud 56
1024 Ecublens
Switzerland
+41 78 9133191
leili.batooli@gmail.com
inkedin.com/in/batooli

Languages

English: C1
European level
French: B1
European level
Persian: Native
language

Holder of Swiss B permit with the right to work

Strengths

Materials science	Surface science
Microfabrication	Precious metals
Aesthetics of surfaces	Tribology

Education

Ph.D. In Materials Science and Engineering EPFL, Tribology and Interfacial Chemistry group Topic: Correlation of physical properties to aesthetic aspects of jewelry gold alloy	2015-2019
M. Sc. In Materials Science and Engineering EPFL, Microsystems laboratory 4 Thesis: In-plane integration of a-Si photodiodes in microfluidic scintillation detectors	2011 –2014
B. Sc. In Metallurgy and Materials Engineering University of Tehran, Solidification laboratory Thesis: Effect of nucleating agents on microstructure and corrosion behavior of high strength aluminum alloys	2006 –2010

Experience

Ph.D Researcher Some of the skills I gathered during the course of this thesis work funded by Patek Philippe SA include: <ul style="list-style-type: none">❖ Expertise in the field of aesthetic appearance of surfaces❖ Extensive experience with jewelry gold alloys❖ Proficiency in large range of physical and chemical surface characterization methods❖ Know-how to design and perform tribological experiments❖ Experience in planning and execution of long term projects❖ Working autonomously and self driven	2015-Present
Researcher Feasibility study on surface characterization of watch components, Tribology and interfacial chemistry Group, EPFL In a project funded by Patek Philippe SA, I studied several surface properties of gold watch components. This work involved choosing relevant characterization techniques, performing measurements and interpreting the results.	Sep. 2014- Mar. 2015

Researcher

Jun. 2014-Sep. 2014

Fabrication of SU-8/Ionic Liquid Composite for Tribological coatings and MEMS, **Gersteltec SA** and **Tribology and Interfacial Chemistry Group**, EPFL

In this project, a novel SU-8/ionic liquid composite was developed for applications in coatings and MEMS. I tested tribological properties of the composite as well as its UV patternability and water affinity. The results have been published in an article.

Internship

Design and fabrication of Microfluidic channel for Electron Spin Resonance (ESR) spectroscopy, **Microsystems Laboratory 1**, EPFL

Oct. 2012–Jan 2013

During this internship and through the design of a microfluid system, I have followed intensive trainings in the cleanroom of EPFL and learned several microfabrication techniques.

Research Assistant

Sep. 2011 – Jun. 2012

Studying solidification behavior of Al-Zn alloys with respect to temperature gradient variation, **Computational Materials Laboratory**, EPFL

This work included molding samples in an oven under different temperature gradients and studying the effects on the microstructure of Al-Zn alloy.

Publications

Novel SU-8/ionic liquid composite for tribological coatings and MEMS

L. Batooli, S. Guadalupe, M. Judelewicy, S. Mischler, Micromachines, 2015

Elastic, dielectric and piezoelectric anomalies and Raman spectroscopy of $0.5\text{Ba}(\text{Ti}_{0.8}\text{Zr}_{0.2})\text{O}_3$ - $0.5\text{Ba}(\text{Ti}_{0.7}\text{Ca}_{0.3})\text{TiO}_3$

D. Damjanovic, A. Biancoli, L. Batooli, A. Vahabzadeh, J. Trodahi, Applied Physics Letters, 2012

Technical skills

- ❖ Scanning Electron Microscopy.
- ❖ Surface profilometry (light, laser).
- ❖ Color and reflection measurements.
- ❖ Chemical surface analysis: Auger Electron Spectroscopy and X-ray Photoelectron Spectroscopy.
- ❖ Instrumental hardness measurement.
- ❖ Large variety of cleanroom microfabrication technique (including but not limited to photolithography, DRI etching, wet etching, sputtering/evaporation tools, bonding equipment).
- ❖ Softwares: Origin, Image J, LaTeX, Photoshop, Mountains map, Clewin, Sketch up, Microsoft office.

Soft skills

- ❖ Teamwork skills in multicultural environments
- ❖ Presentation skills for large audiences
- ❖ Critical opinion and problem solving attitude
- ❖ Knowledge transfer skills

